

**Regulation of the subunit assembly and the
catalytic activity in heteromeric kinesin-2 from
*Caenorhabditis elegans***

Marija Vukajlovic

Dissertation der Fakultät für Biologie
der Ludwig-Maximilian-Universität München
zur Erlangung des akademischen Grades
„Doktor der Naturwissenschaften“
(Dr. rer. nat.)

vorgelegt von
Marija Vukajlovic
aus Kragujevac, Serbien

München, 2012

1. Gutachter: Prof. Dr. Manfred Schliwa
2. Gutachter: Prof. Dr. Angelika Böttger

Datum der Einreichung: 26. April 2012

Tag der mündlichen Prüfung: 20. Juli 2012

Ehrenwörtliche Versicherung

Ich versichere hiermit ehrenwörtlich, dass die vorgelegte Dissertation von mir selbständig und ohne unerlaubte Hilfe angefertigt ist.

München, den 26.04.2012

Marija Vukajlovic

Ort der Durchführung

Der experimentelle Teil dieser Dissertation wurde hauptsächlich durchgeführt im Labor von Prof. Dr. Manfred Schliwa am Institut für Anatomie und Zellbiologie der Ludwig-Maximilians-Universität München unter Betreuung von Dr. Zeynep Ökten und Prof. Dr. Manfred Schliwa. Ein Teil der Experimente wurde in Laboren von Prof. Dr. Michael Schleicher (Institut für Anatomie und Zellbiologie der Ludwig-Maximilians-Universität München), Prof. Dr. Peter Becker (Adolf-Butenandt-Institut der Ludwig-Maximilians-Universität München), Prof. Dr. Hendrik Dietz (Walter-Schottky-Institut der Technischen Universität München) und Prof. Dr. Matthias Rief (Department E22 für Biophysik der Technischen Universität München) durchgeführt.

Publications

Articles

Vukajlovic M., Dietz H., Schliwa M., Oekten Z. How kinesin-2 forms a stalk, *Mol. Biol. Cell.* vol 22 (2011), p4279

Poster Presentations

Vukajlovic M., Schliwa M., Oekten Z., *How kinesin-2 forms a stalk*, ASCB 50th int. meeting, 2010, Philadelphia, PA

Vukajlovic M., Schliwa M., Oekten Z., *Seeded motor dimerization in heteromeric kinesin-2*, Center for Integrated Protein Science Munich (CIPSM) annual meeting, 2010, Wildbad Kreuth, Germany

Vukajlovic M., Schliwa M., Oekten Z., *What brings them together? – Assembly of the three subunits in heteromeric kinesin-2*, EMBO annual meeting 2010, Barcelona, Spain

Vukajlovic M., Kösem S., Schliwa M., Oekten Z., *Autoregulation of heteromeric kinesin-2 from C. elegans*, DGZ annual meeting, 2010, Regensburg, Germany

Table of contents

Summary	1
Zusammenfassung	3
Introduction	5
1 Intracellular transport and molecular motors	5
2 Kinesin superfamily	7
2.1 Catalytic heads' role in kinesin movement	9
2.2 Role of the tail domain in kinesin regulation	11
3 Kinesin-2	12
3.1 Kinesin-2 function	12
3.2 Kinesin-2 structure	13
4 Goals of this thesis	15
Materials and methods	17
1 Materials	17
1.1 Reagents and laboratory consumables	17
1.2 DNA	17
1.2.1 Full length sequences of KLP11, KLP20 and KAP	17
1.2.2 Cyan and yellow fluorescent proteins (CFP and YFP)	17
1.2.3 Primers	17
1.2.4 Vectors	18
1.3 Cells	18
2 Methods	19
2.1 Molecular biological methods	19
2.1.1 Cloning	19
2.1.2 Generation and isolation of baculovirus shuttle vectors (bacmids)	20
2.1.3 Bacmid isolation	22
2.2 Cell biological methods	22
2.2.1 Cell culture	22
2.2.1 Bac-to-bac expression system	22
2.3 Biochemical methods	23
2.3.1 Protein purification via 6xHis affinity tag	23

Table of contents

2.3.2 Protein purification via Flag tag	24
2.3.3 Gel filtration.....	25
2.3.4 Co-immunoprecipitation assays	26
2.3.5 Tubulin preparation from pork brain and polymerization of purified tubulin	26
2.3.6 Microtubule affinity assay	27
2.3.7 Enzymatically coupled ATPase assay.....	27
2.4 Biophysical methods	30
2.4.1 Transmission electron microscopy	30
2.4.2 In solution Förster resonance energy transfer measurements.....	30
2.4.3 Circular dichroism spectroscopy.....	33
Results.....	36
1 Regulation of the catalytic activity.....	36
1.1 Tail domains are necessary for motor inhibition.....	36
1.2 Tail domains could anchor the inactive motor to microtubules	38
1.3 Inhibition requires dimeric state of the heads.....	39
1.4 Co-immunoprecipitation of inhibitors with motors.....	41
2 Domain assembly.....	43
2.1 Dimerization of truncated KLP11 and KLP20 constructs.....	43
2.1.1 The C-terminal half of the stalk is necessary and sufficient for heterodimerization of KLP11 and KLP20	43
2.1.2 Heterodimerization of KLP11/20 is triggered by a seed located at the C-terminal end of the stalk.....	47
2.1.3 Full-length partner cannot compensate for the C-terminal truncation in the other motor.....	51
2.1.4 Kinesin Associated Protein (KAP) binds only to KLP11	52
2.2 Transmission electron microscopy of the wild type kinesin-2 reveals an extended coiled-coil	54
2.3 FRET analysis confirms the close apposition of the two heads when the full-length stalk is present	56
2.4 Circular dichroism spectroscopy gauges the extent of stalk formation	59
2.4.1 Coiled-coil content grows with growing chain length.....	59
2.4.2 FL-KLP11/20 is not thermodynamically more stable than KLP11/20-C	61
2.4.3 KLP11 and KLP20 do not homodimerize	61
Discussion.....	65
1 Heterodimeric structure is required for autoinhibition.....	65
2 Co-factors in kinesin-2 kinetics	68
3 KAP on top of it.....	69

Table of contents

4 From seed to stalk	71
5 Only with the right partner	73
6 The stability issue	74
7 The seed as a common good	75
Outlook	76
References	78
List of constructs.....	89
Protein sequences.....	92
List of figures	94
Acknowledgements	96
Curriculum vitae	98

Summary

In highly compartmentalized and structurally complex eukaryotic cells cytoskeleton-associated motor proteins accomplish a significant part of logistic work and bring cellular components to their place of action.

The kinesin superfamily counts at least 14 different major classes whose members combine two motor domains necessary to move along a microtubule filament. Most kinesin motors are homodimers, so the heterotrimeric structure of kinesin-2 makes it a unique member of the kinesin superfamily. Molecular details of the oligomer assembly by two distinct motor domains and one accessory subunit of kinesin-2 are largely unknown, which to uncover was one of the objectives of this work.

A multifaceted approach combining biophysical and biochemical methods was applied to kinesin-2 from *Caenorhabditis elegans* to demonstrate how nature favours heterodimerization and prevents homodimerization of motor domains in a protein family in which preferentially homodimers are formed.

The C-terminal end of the stalk in both motor domains, kinesin like proteins 11 and 20 (KLP11 and KLP20), contains a “seed” sequence of two heptad repeats, which is necessary and sufficient to induce dimerization. Lack of the short seed makes dimerization impossible regardless of the provided stalk length. On the other hand, despite its short length the seed is sufficient for stable dimerization of the two interacting partners.

Once initiated by the seed, a coiled-coil is formed that spans the entire stalk in the KLP11/20 motor. However, results indicate that the N-terminal part of the stalk is able to uncoil providing some space between the motor heads and thus giving them certain flexibility, which may affect kinesin’s stepping behaviour. In addition to explaining the formation of the kinesin-2 stalk, the seed sequence identified here bears great potential for generating specific heterodimerization in other protein biochemical applications.

The third subunit of the heterotrimeric complex, kinesin associated protein (KAP), necessary for interaction with cargo, interacts only with the KLP11 motor. The interaction site was localized in the random coil tail of KLP11 and the middle segment of KAP, which consists of 9 Armadillo repeats.

Summary

The second objective of this work was to investigate how kinesin-2 is regulated by means of autoinhibition, a regulatory mechanism, which seems to have co-evolved with the kinesin family. Results indicate that the free KLP20 random coil tail interacts with the KLP11 head in the wild type motor, thus abolishing catalytic activity. Both tails are capable of inhibiting motor heads *in trans*. The heads must be in dimeric state in order to be inhibited and the most significant inhibition is achieved when the two different heads are combined.

This work provides comprehensive molecular insights into the subunit assembly and regulation of the catalytic activity in kinesin-2 from *C. elegans*. It further paves the way for detailed investigation of these processes in the future.

Zusammenfassung

In strukturell komplexen eukaryotischen Zellen, welche viele verschiedene Kompartimente enthalten, sind es die Zytoskelett-assoziierten Motorproteine, welche für die Logistik verantwortlich sind. Myosine, Dyneine und Kinesine transportieren Zellkomponenten zu den Zellloci, in welchen sie gebraucht werden.

Die Kinesin-Superfamilie zählt 14 Unterklassen, deren Mitglieder aus zwei Motorketten bestehen, was für den Langstreckentransport auf Mikrotubuli notwendig ist. Die meisten Kinesine sind Homodimere, daher ist die heterotrimere Struktur von Kinesin-2 einzigartig in der gesamten Kinesin-Superfamilie. Molekulare Details der Kombination von zwei verschiedenen Motorketten und einer akzessorischen Untereinheit sind weitestgehend unbekannt.

Eine interdisziplinäre Untersuchung von Kinesin-2 aus *C. elegans*, in welcher biochemische und biophysikalische Methoden kombiniert wurden, beschreibt den Oligomerisierungsmechanismus in diesem Motor. Erkenntnisse wurden darüber geliefert, wie die Natur die Heterodimerisierung der Homodimerisierung vorzieht in einer Proteinfamilie, welche hauptsächlich Homodimere hervorbringt.

Das C-terminale Ende der Schaft-Domäne (stalk) agiert als der „Dimerisierungskeim“. Dieser „Keim“ ist etwa zwei Heptaden groß und unbedingt notwendig, aber auch vollkommen ausreichend, um die Heterodimerisierung von KLP11 und KLP20 (Motor-Untereinheiten von Kinesin-2 in *C. elegans*) zu bewerkstelligen. Ist diese Sequenz nicht vorhanden, so kommt es zu keiner Dimerisierung von KLP11 und 20, ganz gleich welcher Anteil von dem α -helikalen Schaft noch zur Verfügung steht.

Ist die Dimerisierung einmal durch den Keim induziert, so wird ein coiled-coil ausgebildet, welches sich über den gesamten Schaft bis zu den Motorköpfen erstreckt. Ergebnisse deuten jedoch darauf hin, dass sich die N-terminale Hälfte des Schafts unter Umständen entwinden kann. Dieses würde sich auf die Flexibilität der Köpfe und ihr Schreitverhalten auswirken.

Die dritte Untereinheit des Komplexes, das Kinesin assoziierte Protein (KAP), welches den Kontakt zum Cargo herstellt, interagiert mit der KLP11 Motor-Untereinheit. KLP20 ist an der Interaktion nicht beteiligt. Für die Interaktion sind der

Zusammenfassung

unstrukturierte Schwanz von KLP11 und der mittlere Sequenzbereich von KAP notwendig. Der letztere besteht aus neun Armadillo-Motiven.

Ein weiteres Ziel dieser Arbeit war es die Regulation der katalytischen Aktivität von Kinesin-2 zu untersuchen. Der Mechanismus der Autoinhibierung scheint sich mit dieser Proteinfamilie entwickelt zu haben und auch auf das heterodimere Kinesin-2 zuzutreffen. Interaktionsuntersuchungen deuten darauf hin, dass der Schwanz von KLP20 mit dem Kopf von KLP11 interagiert und die katalytische Aktivität unterbindet. *In trans* scheinen jedoch beide Schwänze eine inhibierende Wirkung zu haben, solange die Köpfe im dimeren Zustand vorliegen. Am effektivsten ist die Inhibierung, wenn die zwei verschiedenen Köpfe kombiniert werden und sich an ihrer nativen Position befinden.

Diese Arbeit gewährt tiefe Einblicke in die Regulation der Domänenassemblierung, sowie in die Regulation der katalytischen Aktivität von Kinesin-2 und ist eine solide Grundlage für die weiterführenden Untersuchungen von diesen Prozessen.

Introduction

1 Intracellular transport and molecular motors

In eukaryotes intracellular transport systems have evolved to cope with increasing infrastructural demands of highly compartmentalized and polarized cells. Molecular motors bring cell components to their place of action, thus localizing organelles, proteins and RNA molecules, assembling mitotic spindles, moving chromosomes, specifying cleavage planes, and contributing to the assembly, stability and beating of cilia and flagella.

Molecular motors, kinesins, dyneins, and myosins are cytoskeleton-associated nano-machines, which harness chemical energy from ATP hydrolysis to carry out mechanical work. These three families of motors are responsible for virtually all biological movements. All eukaryotes including those with slimmed-down genomes (e. g. budding yeast) have multiple genes for kinesins, dyneins and myosins, which form real motor superfamilies. These many different motors in one family are responsible for the transport of different cargo and are expressed at different cell stages and in different tissues in more complex organisms.

All molecular motors use only polarized components of the cytoskeleton as tracks: Myosins move on actin filaments, while kinesins and dyneins use microtubules as tracks. Some of the motors are capable of undertaking many consecutive steps before falling off the track, thus accomplishing the challenging task of long-range transport.

The long-range transport is especially important in elongated structures such as axons in neurons and motile and immotile cilia. Depending on the cell type, cilium is a moving and/or sensory organelle that transduces a multitude of sensory stimuli and is a key participant in intercellular signalling (Marshall and Nonaka, 2006; Singla and Reiter, 2006). Impaired cilium assembly leads to severe disorders like polycystic kidney disease (Lin *et al.*, 2003), hydrocephalus, situs inversus (Nonaka *et al.*, 1998; Marszalek *et al.*, 1999; Takeda *et al.*, 1999) or retinal degeneration (Mukhopadhyay *et al.*, 2010).

Introduction

All these disorders involve mutations in kinesin-2, one of at least 14 members in the kinesin superfamily of microtubule associated motor proteins (Brown *et al.*, 1999; Miki *et al.*, 2001; Miki *et al.*, 2005), which is essential for proper assembly and maintenance of cilia and flagella (Cole *et al.*, 1998; Brown *et al.*, 1999; Signor *et al.*, 1999; Scholey, 2008), as well as for intraflagellar trafficking (Cole *et al.*, 1998; Orozco *et al.*, 1999) (Figure 1).

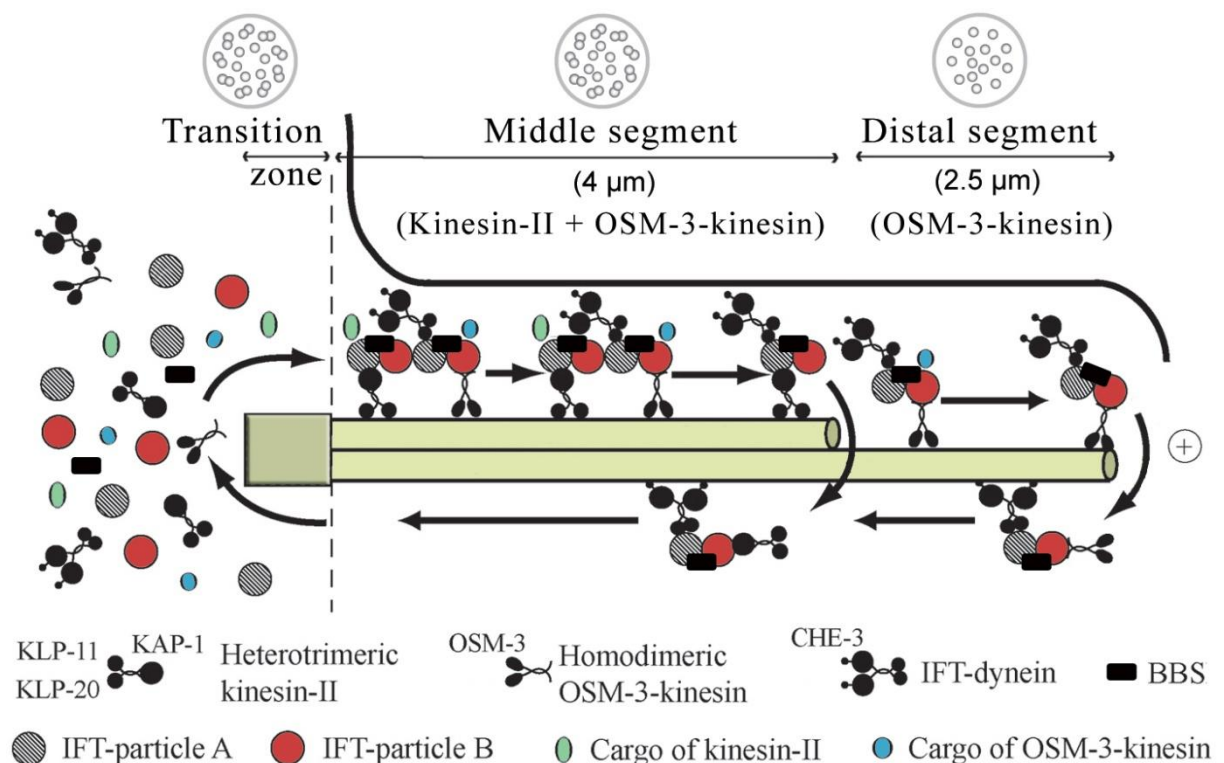


Figure 1: Intraflagellar transport (IFT) in *C. elegans*. Components of the IFT machinery and ciliary cargo assemble at or near the transition zone (basal body). Two kinesins, heterotrimeric kinesin-2 and homodimeric OSM-3-kinesin, bind IFT particles, ciliary precursors and dynein, and transport these along the middle segment in the anterograde (+) direction. BBS proteins act to stabilize the association between the motors and IFT particle subcomplexes A and B. In the distal segment, OSM-3-kinesin alone transports the IFT particles and dynein/cargo. At the distal tip of the cilium cargo unloading, motor switching and turnover occurs. Then kinesin-2, components of the IFT machinery and presumably other ciliary molecules are recycled back to the base of the cilium using the IFT-dynein molecular motor. The lengths of the transition zone (1 μm), middle segment (4 μm) and distal segment (2.5 μm) regions are shown (for amphid cilia) along with transverse view schematics of the microtubule arrangements (on top). Adapted from Inglis *et al.*, 2007.

2 Kinesin superfamily

Since their discovery (Brady, 1985; Scholey *et al.*, 1985; Vale *et al.*, 1985) kinesins have grown to a protein superfamily with continuously increasing number of members. Through gene duplication and recombination evolution produced at least 14 different major kinesin classes (Miki *et al.*, 2001; Miki *et al.*, 2005), which are universal from the bottom of the eukaryotic radiation. This large diversity explains why kinesins are capable of fulfilling many different tasks in the cell.

Although kinesins vary in shape, there are overarching principles concerning their molecular architecture, underlining their common origin. A detailed mechanistic inquiry into kinesins' overall architecture therefore is a prerequisite to the molecular understanding of how these motors accomplish their versatile cellular tasks. Three main domains are identified in all kinesins: Catalytic head, stalk and tail (Figure 2).

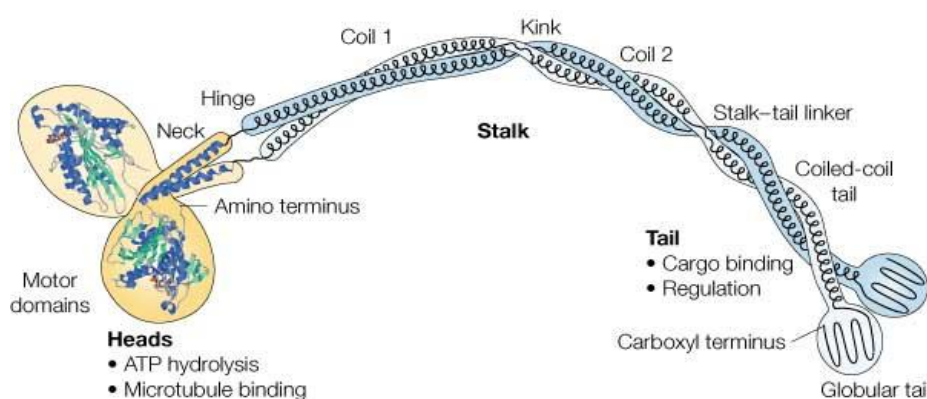


Figure 2: Structural organization of kinesins. All kinesins display modular morphology containing a head, stalk and tail domain. Structural organization of kinesins is depicted here on the example of kinesin-1 (adapted from Woehlke and Schliwa, 2000). The catalytic head is the motor domain where ATP-binding and hydrolysis take place. The motor head also contains the microtubule binding site and is the moving part of the motor. The stalk domain is responsible for dimerization and thus contains one or more α -helical stretches, which build a coiled-coil. These α -helical stretches can be separated by more flexible regions like kinks and hinges, the number and length of which is family dependent. The tail domain can be globular or unstructured and is the cargo or accessory subunit binding site. The tail further plays a role in regulation of catalytic activity in some kinesin families.

The catalytic head contains the microtubule interaction site as well as the ATP-binding pocket (Hirokawa *et al.*, 1989) and is the actual motor domain. It is 40% conserved among all kinesin classes (Vale and Fletterick, 1997; Hirokawa *et al.*,

Introduction

1998; Ogawa *et al.*, 2004), which demonstrates its essential role for the functioning of the motor. The motor domain is found at the N- or C-terminus or in the middle of the protein sequence (Figure 3). The head position seems to affect the direction of kinesin movement. While most kinesins with an N-terminal head move towards the plus-end of microtubules, the C-terminal head leads to a movement towards the minus-end (Endow and Waligora, 1998). Kinesins with the motor domain in the middle of the protein sequence accumulate at the ends of microtubules (Ogawa *et al.*, 2004).

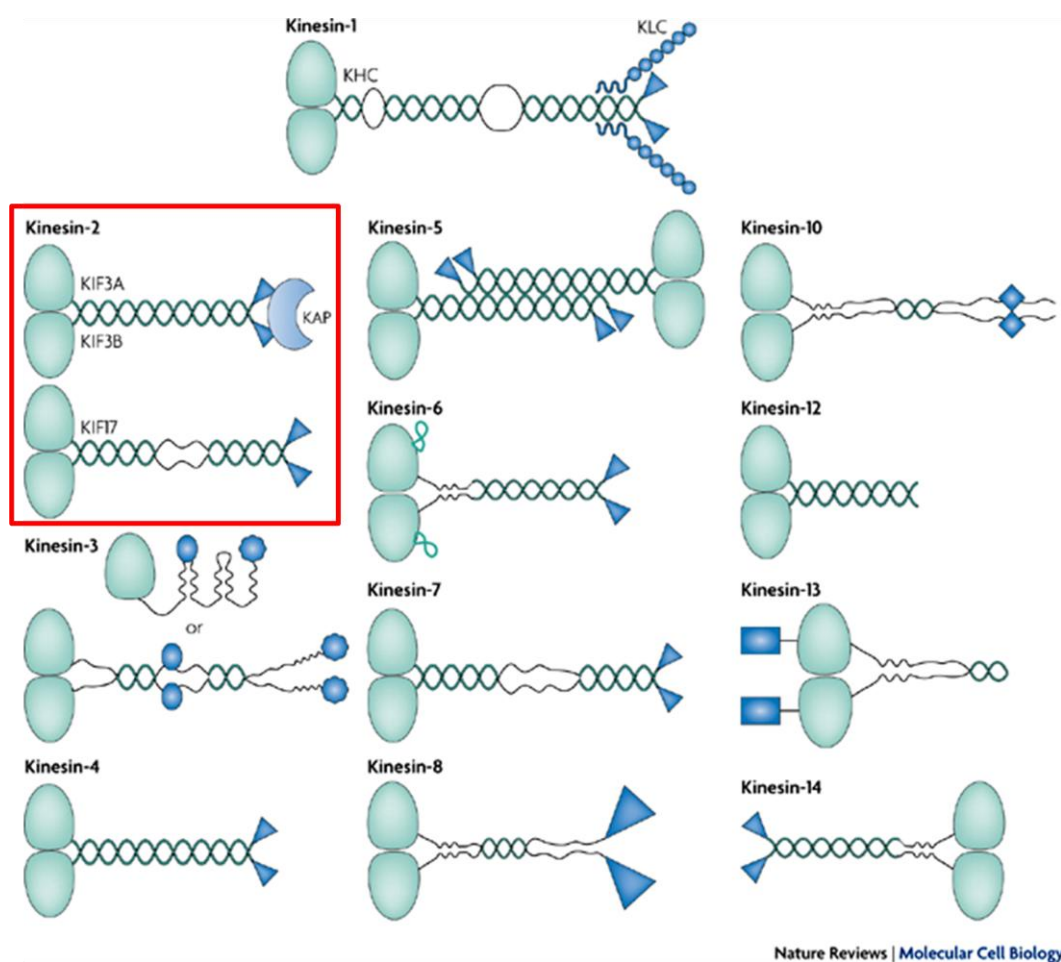


Figure 3: Diversity in the kinesin superfamily. Despite their common features in the structural organization kinesin families display morphological diversity. Kinesins can be monomers (kinesin-3), homodimers (most of the kinesin families), heterotrimers (one of the two members of the kinesin-2 family), and tetramers (kinesin-5). The motor domain can be placed at the N-terminus (most kinesins), C-terminus (kinesin-14) or in the middle of the sequence (kinesin-13). Kinesin-2 family with its mouse orthologues is high-lightened by a red square (adapted from Verhey and Hammond, 2009).

The neck linker and the neck domain connect the motor head to the stalk. The conformational change of these small domains (10 and 40 amino acids on average) during the ATPase cycle is essential for kinesin movement (Endow and Waligora, 1998). The stalk is an α -helical structure responsible for dimerization of two kinesin-chains via a coiled-coil. Most kinesins are dimers but there are also monomers, trimers and tetramers (Vale and Fletterick, 1997) (Figure 3).

The tail domain shows the greatest diversity among kinesin families, which explains the ability to bind to diverse cargoes and to fulfil many different tasks (Vale and Fletterick, 1997; Woehlke and Schliwa, 2000).

2.1 Catalytic heads' role in kinesin movement

Kinesins can move processively or unprocessively along microtubules. In processive movement motor undertakes many consecutive steps without falling off the track. To establish processive movement cooperation of two heads is required that ensures maintenance of physical contact with microtubules (Hancock and Howard, 1998). Nevertheless, there are also processive monomeric (Okada and Hirokawa, 1999) and unprocessive dimeric kinesins (Sablin *et al.*, 1998). Both modes of movement represent adaptations to the required physiological function.

Processively moving kinesins undertake discrete 8 nm steps, which is the distance between β -tubulin subunits in a microtubule (Svoboda *et al.*, 1993). Stepping is directly coupled to ATP hydrolysis: one mechanical step requires the hydrolysis of one ATP molecule. The catalytic heads of unbound kinesins contain ADP, which is rapidly released upon interaction with microtubules. The ADP release increases the heads affinity for the microtubule. In the next step ATP is bound inducing conformational changes of the head and the neck-linker. The neck-linker associates with the catalytic head leading to a power-stroke that brings the rear head to the next β -tubulin subunit in front of the leading head (Gilbert *et al.*, 1995; Johnson and Gilbert, 1995; Farrell *et al.*, 2002) (Figure 4). While the new leading head releases its ADP and binds tightly to the microtubule, the new rear head is hydrolyzing its ATP causing the unzipping of the neck linker and dissociation of the head from the microtubule due to reduction in microtubule affinity. The new rear head can now be brought forward by a new power-stroke induced by the neck-linker association with

Introduction

the new leading head (head-over-head stepping, (Yildiz *et al.*, 2004) (Figure 4). In order to walk processively, the two heads must perform biphasic kinetics, i. e. their ATPase cycles must be coupled and out of phase (Hackney, 1994; Ma and Taylor, 1997; Gilbert *et al.*, 1998), so that at any time-point at least one head is attached to a microtubule. Thus processivity in principle requires two heads (Hancock and Howard, 1998).

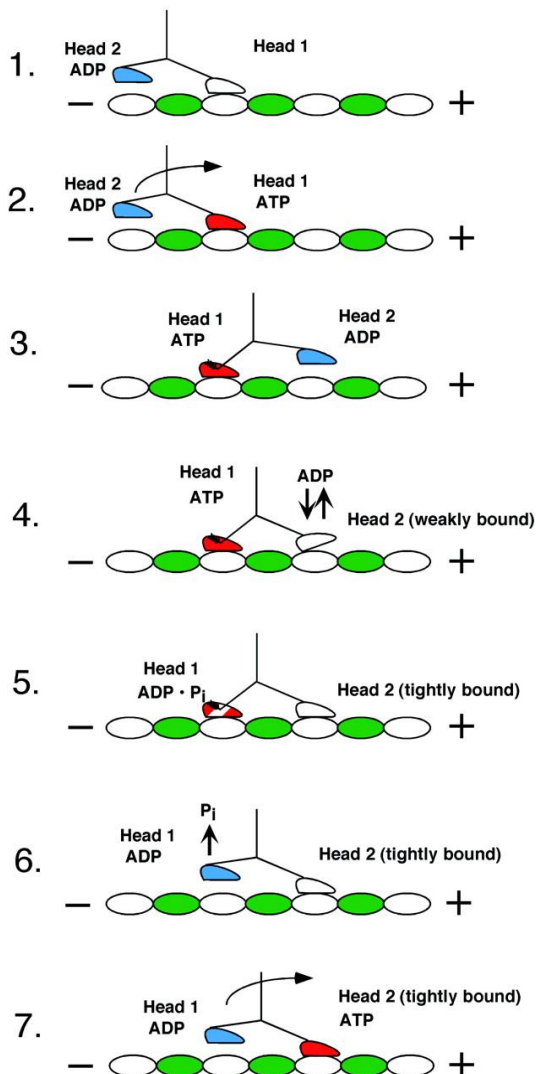


Figure 4: Processive kinesins move head-over-head. The ATPase cycles of the two heads are biphasic, thus preventing detachment of the two heads at the same time. Keeping the ATPase cycles out of phase ensures the processive movement. Upon microtubule binding the catalytic head loses its ADP (white head 1 in panel 1.). In the next step the same head binds ATP (red head 1 in panel 2.) causing the head 2 (blue) with its bound ADP (panel 2.) to swap to the next β -tubulin subunit (white) in front of the head 1 (panel 3.). Now the head 2 loses its ADP (panel 4.) and tightly associates with the microtubule (panel 5.) while the head 1 hydrolyzes its ATP (panel 5.) and its ADP-bound state lowers its affinity for microtubules (panel 6.). Upon ATP-binding by head 2 head 1 swaps to the next β -tubulin subunit in front of the head 2 and the cycle starts again (adapted from Farrell *et al.*, 2002).

2.2 Role of the tail domain in kinesin regulation

Hydrolyzing one ATP molecule per step makes processive kinesins large energy consumers. Because kinesins are activated upon contact with microtubules independently of carrying cargo or not, a mechanism must exist, which prevents kinesins from walking when they do not have cargo to transport and thus prevent the waste of ATP.

The mechanism of catalytic regulation is very well studied in the case of kinesin-1. The catalytic activity is regulated by means of autoinhibition (Figure 5). During this process the motor folds at the flexible hinge in the middle of the stalk region thus allowing the tail region to interact with the motor heads (Hackney *et al.*, 1992; Coy *et al.*, 1999; Friedman and Vale, 1999; Stock *et al.*, 1999; Seiler *et al.*, 2000; Yonekura *et al.*, 2006; Cai *et al.*, 2007; Dietrich *et al.*, 2008; Hackney *et al.*, 2009). This interaction leads to slowed ADP release and thus to significant reduction in the stepping rate, while the affinity for microtubules remains unchanged (Coy *et al.*, 1999; Stock *et al.*, 1999; Hackney and Stock, 2000, 2008; Wong *et al.*, 2009). Meanwhile the exact interaction site was revealed by the crystal structure, which showed that the microtubule-binding site remains exposed, while the head-tail-interaction acts as a “lock down” preventing the movement of the motor domains that is needed to undock the neck linker and release ADP (Kaan *et al.*, 2011). Tails are even capable of inhibition when added *in trans* to active motor heads (Coy *et al.*, 1999; Stock *et al.*, 1999; Yonekura *et al.*, 2006; Dietrich *et al.*, 2008; Hackney and Stock, 2008; Wong *et al.*, 2009). A similar mechanism was demonstrated for the monomeric kinesin-3 (Lee *et al.*, 2004; Yamada *et al.*, 2007; Hammond *et al.*, 2009) and there are strong indications that autoinhibition also regulates the catalytic activity of the homodimeric kinesin-2 (Imanishi *et al.*, 2006; Hammond *et al.*, 2010).

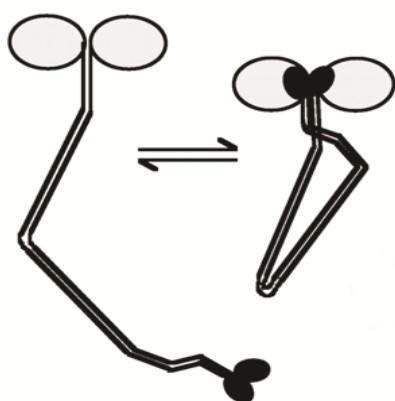


Figure 5: Tail domain regulates the catalytic activity in some kinesin families. Some kinesin motors have flexible regions (kinks or hinges) in their stalk domain. This feature allows the motor to fold and bring the tail domain in the proximity of the heads, thus enabling their interaction. For some kinesin families this interaction was shown to inhibit motor's activity.

3 Kinesin-2

Kinesin-2 is a heterogeneous kinesin class of processive, plus-end directed motors (Cole *et al.*, 1993). It includes homodimeric and heterotrimeric members (Figure 3), which both seem to have co-evolved with cilia and flagella, since these motors are essential for proper assembly and maintenance (Cole *et al.*, 1998; Brown *et al.*, 1999; Signor *et al.*, 1999; Scholey, 2008), as well as for the function of these structures throughout eukaryotic phyla (Morris and Scholey, 1997; Cole *et al.*, 1998; Orozco *et al.*, 1999; Pan and Snell, 2002; Rosenbaum and Witman, 2002; Lin *et al.*, 2003; Scholey and Anderson, 2006; Scholey, 2008).

After its discovery in sea urchin eggs (Cole *et al.*, 1993) kinesin-2 orthologues have been found in many different organisms from green algae, ciliated protozoa, nematodes to vertebrates including mammals and humans.

3.1 Kinesin-2 function

The homo- and the heterodimeric kinesin-2 are together responsible for the intraflagellar transport (IFT), a mechanism by which cilia are built and maintained (Lin *et al.*, 2003) (Figure 1). Besides transporting building blocks, proper IFT and cilium functioning are also essential for processes like sensory transduction during mating in *Chlamydomonas* (Pan and Snell, 2002), vision (Pazour *et al.*, 2002) and chemosensory behaviour in metazoans (Perkins *et al.*, 1986; Starich *et al.*, 1995). This points to the vital role of motile and immotile cilia in all forms of eukaryotic life. Motile cilia move fluid past cells, e. g. mucus in the airway, while immotile cilia are sensory organelles essential for e. g. proper kidney functioning and are key players in transducing a multitude of sensory stimuli, like chemical concentration of growth factors, hormones, odorants and developmental morphogens and are thus inevitable for sight, smell, and mechanosensation (Marshall and Nonaka, 2006; Singla and Reiter, 2006).

During the course of evolution kinesin-2 has adopted various different and cell type dependent functions also outside the cilium. These include vital roles in development especially of elongated structures like axons, spermatids and photoreceptors (Yamazaki *et al.*, 1995; Miller *et al.*, 1999; Takeda *et al.*, 2000; Mukhopadhyay *et al.*,

2010; Wang *et al.*, 2010), organelle sorting and anterograde transport in axons (Coy and Howard, 1994; Kondo *et al.*, 1994; Yamazaki *et al.*, 1995), endoplasmic reticulum and Golgi membrane transport (Le Bot *et al.*, 1998), dispersion of melanosomes (Tuma *et al.*, 1998), localization of RNA molecules (Heinrich and Deshler, 2009), participation in embryonic development (Morris and Scholey, 1997; Nonaka *et al.*, 1998; Marszalek *et al.*, 1999; Takeda *et al.*, 1999), signal transduction (Kolpakova-Hart *et al.*, 2007; Corbit *et al.*, 2008; Ocbina and Anderson, 2008), as well as in mitotic spindle assembly (Haraguchi *et al.*, 2006), chromosome segregation (Miller *et al.*, 2005) and cytokinesis (Fan and Beck, 2004). Because of the large diversity of intracellular tasks and involvement in some tumors like Hippel-Lindau tumor (Mans *et al.*, 2008) and breast cancer (Lukong and Richard, 2008), it is important to better understand this motor protein.

3.2 Kinesin-2 structure

Unlike other processive kinesins predestined for long-range transport, which are homodimers (Hancock and Howard, 1998), some members of the kinesin-2 family consist of two distinct motor domains and an accessory cargo binding subunit (Cole *et al.*, 1998). In *C. elegans* the two motor domains are named kinesin like protein 11 and 20 (KLP11 and 20) and the cargo-binding domain is called kinesin associated protein (KAP) (Figure 6). This heterotrimeric structure is unique in the kinesin superfamily.

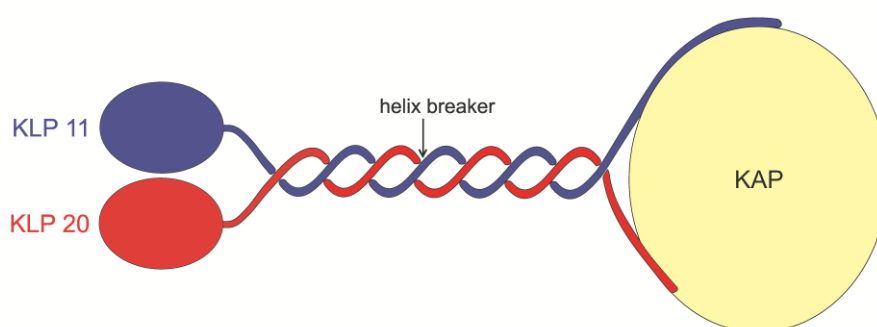
Both motor domains consist of an N-terminal globular catalytic head, a central stalk, and a C-terminal unstructured tail (Rashid *et al.*, 1995; Yamazaki *et al.*, 1995; Cole, 1999). Whereas the extended stalk with its α -helical structure represents the site of motor subunit heterodimerization (Rashid *et al.*, 1995; Cole, 1999), the proline-rich unstructured tail is thought to interact with the accessory subunit (Wedaman *et al.*, 1996; Yamazaki *et al.*, 1996). KAP is a globular protein with a high α -helical content not predicted to form coiled-coils (Wedaman *et al.*, 1996; Sarpal and Ray, 2002).

An evolutionarily conserved helix breaker site, situated in the middle of the stalk region, is present in all kinesin-2 sequences ($G^{450}S^{451}$ in KLP11 and $G^{444}G^{445}$ in KLP20). This helix breaker may allow the motor dimer to fold (Imanishi *et al.*, 2006; Dietrich *et al.*, 2008; Hackney *et al.*, 2009; Wong *et al.*, 2009) and has been shown to

Introduction

influence the activity of the kinesin-2 motors from *C. elegans* (Imanishi *et al.*, 2006; Brunnbauer *et al.*, 2010) and mouse (Hammond *et al.*, 2010). However, a detailed molecular mechanism of how the kinesin-2 motors are autoinhibited still remains elusive. From a mechanistic point of view, this question is especially intriguing in the case of the heterodimeric kinesin-2. Are both tails required for efficient autoregulation or is one subunit enough to inhibit the activities of the catalytic heads?

A



B

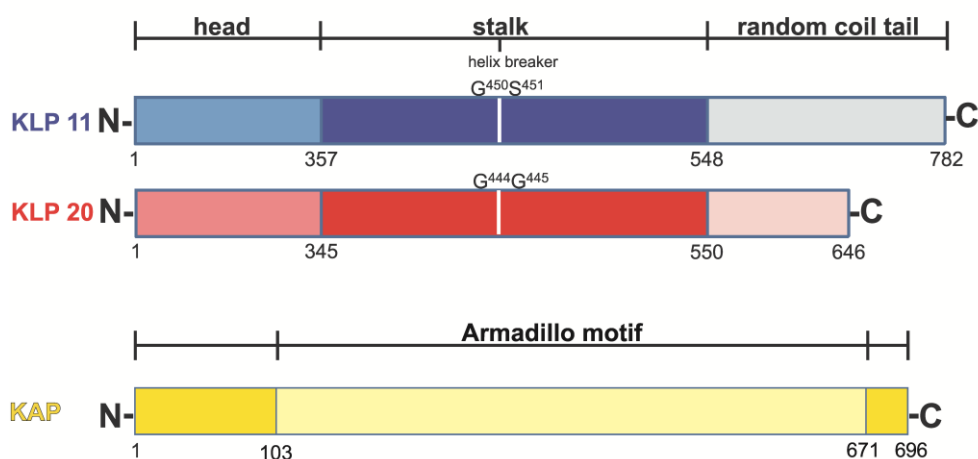


Figure 6: Kinesin-2 architecture. (A) Schematic overview of the *C. elegans* heterotrimeric kinesin-2. KLP (kinesin like protein) 11 and 20 have N-terminal motor domains and form a heterodimer that C-terminally associates with the cargo binding subunit, Kinesin Associated Protein (KAP). (B) Linear maps of the two motor subunits and KAP. For the motor subunits the head, coiled-coil stalk and random coil tail domains are shown together with the amino acid positions that delimit their borders. The helix breaker positions are indicated in both motor domains; they allow folding of the tail onto the head domains to auto-regulate catalytic activity. For KAP the conserved part containing Armadillo repeats is depicted.

Astonishingly, none of the kinesin-2 motor domains seems to be able to form stable homodimers, neither *in vitro*, nor *in vivo* (Rashid *et al.*, 1995; Yamazaki *et al.*, 1995; De Marco *et al.*, 2003). This strong preference for heterodimerization suggests its functional importance, but the evolutionary advantage of combining three different subunits into a functional entity is not yet understood (Brunnbauer *et al.*, 2010). Although a significant amount of work has been done to provide insights into the mechanisms underlying kinesin-2 complex assembly (De Marco *et al.*, 2001; Chana *et al.*, 2002; De Marco *et al.*, 2003; Chana *et al.*, 2005), it is still not clear which regions are sufficient and which are necessary for heterodimer formation. A particularly conspicuous region is the highly charged stretch at the beginning of the stalk found in heterodimeric pairs of KRP85/95 from sea urchin, Xklp3A/B from *Xenopus laevis*, and Kif3A/3B from mouse (Rashid *et al.*, 1995; De Marco *et al.*, 2001; Chana *et al.*, 2002). Intriguingly, the two distinct polypeptide chains have complementary charges, which intuitively suggest a role in heterodimerization. However, the contribution of these charged regions to heterodimerization in kinesin-2 is ambiguous (De Marco *et al.*, 2001; Chana *et al.*, 2002; Chana *et al.*, 2005).

4 Goals of this thesis

Not only its diverse cellular roles but also its unique morphology make kinesin-2 a valuable object for investigation. What is the evolutionary advantage of combining three different subunits and what is the molecular basis of kinesin-2 complex assembly? It is intriguing how nature ensures heterodimerization in a protein family whose members are mostly homodimers. Which regions are necessary and sufficient for heterodimerization? How does the accessory subunit associate with the motor? What are the consequences of this complex assembly for the motor's activity?

To offer answers to those questions this work has focused on the heterodimeric kinesin-2 motor from *C. elegans*. To find out which regions in its motor subunits, KLP11 and KLP20, are necessary and sufficient for dimerization, a number of N- and C-terminally truncated constructs of different lengths were generated. In a multifaceted approach using co-immunoprecipitation assays (co-IP), transmission electron microscopy (TEM), Förster (fluorescence) energy transfer (FRET) and

Introduction

circular dichroism spectroscopy (CD) this work elucidates the mechanistic principles of kinesin-2 heterodimerization.

Previous work in our laboratory demonstrated that the catalytic activity of the KLP11/20 motor is regulated via the universally conserved helix breaker position (Brunnbauer *et al.*, 2010). Such helix breakers are found in other kinesins and the prevalent model states that the folding of the distal tails onto the catalytic head domains is responsible for the motor's autoregulation. To provide a detailed mechanistic framework of how the heterodimeric tail affects the motor's catalytic activity, ATPase assays were performed in which isolated tails were added *in trans* to monomeric and dimeric kinesin-2 motor variants to dissect the effects of tail-mediated inhibition. In addition, the distal tails were removed in the wild type heterodimer to narrow down the region responsible for the observed autoinhibition. By determining the ATP turnover (k_{cat}) and the affinity for microtubules (K_m) first insights were obtained how autoinhibition is achieved in the KLP11/20 heterodimer.

Materials and methods

1 Materials

All instruments, computer programs, and buffers used are named in the methods.

1.1 Reagents and laboratory consumables

Standard laboratory chemicals were purchased from BioMol, Biorad, Fluka, Invitrogen, Merck, PeqLab, Roche, Roth, Serva or Sigma and had the degree of purity "p.a." unless otherwise mentioned. Media and buffers used in this study were prepared with de-ionised water (Millipore), sterilized either by autoclaving or passing through a micro-filter (pore size 0.2 µm).

Laboratory consumables were predominantly purchased from Grainer, Nunc, Peske and Sarstedt.

1.2 DNA

1.2.1 Full-length sequences of KLP11, KLP20 and KAP

The full-length DNA sequences of KLP11, KLP20 and KAP were a kind gift from Prof. Jonathan M. Scholey (University of California, Davis) and were provided as cDNA cloned into the pDest8 plasmid (Invitrogen).

1.2.2 Cyan and yellow fluorescent proteins (CFP and YFP)

CFP and YFP DNA sequences were synthesized by GenScript.

1.2.3 Primers

All cloning primers used in this study were designed manually to include desired tags and restriction sites and were synthesized by Biomers (Ulm). Sequencing primers were designed with the help of *GenScript DNA Sequencing Primers Design Tool* (http://www.genscript.com/cgi-bin/tools/sequencing_primer_design) to align every 400bp and were also synthesized by Biomers (Ulm).

Materials and methods

1.2.4 Vectors

All constructs were cloned into pFastBac1TM (Invitrogen) as a donor plasmid for generating bacmids in MAX Efficiency[®] DH10BacTM competent *E. coli* cells (see methods).

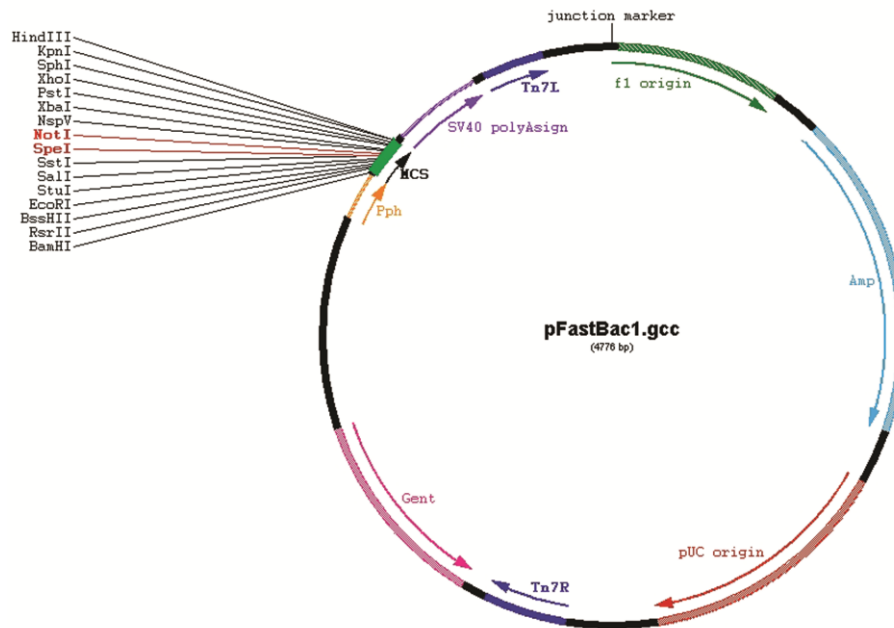


Figure 7: Plasmid map of pFastBac1. All KLP11, KLP20 and KAP constructs used in this work were cloned into pFastBac1 plasmid using SpeI and NotI restriction sites (red) in the multiple cloning site (MCS). Ampicillin resistance (Amp, light blue) was the selection marker during amplification of the recombinant plasmid in *E. coli* XL1 blue, which is then used for recombinant bacmid generation in *E. coli* DH10 cells. *E. coli* DH10 cells further contain a helper plasmid encoding a transposase that uses Tn7 sites (dark blue) to translocate the gene of interest into the bacmid, where it disrupts the *lacZ* gene.

1.3 Cells

Chemically competent *E. coli* XL1-blue strain (Stratagene) was used for plasmid amplification.

Chemically competent MAX Efficiency[®] DH10BacTM competent *E. coli* cells (Invitrogen) served for bacmid (baculovirus shuttle vector) generation (see methods).

All proteins were expressed in *Spodoptera frugiperda* Sf9 cells (Invitrogen) as part of the Bac-to-BacTM eukaryotic expression system (Invitrogen).

2 Methods

2.1 Molecular biological methods

All constructs were generated using standard molecular biological methods.

2.1.1 Cloning

Truncations were introduced by PCR on the original full-length cDNA in linearized pDest8 vector (1.2.1). Primers were designed not only to align the start and the end of the desired sequence, but also to contain restriction sites and to encode desired tags. The forward primers contain the *SpeI* and the reverse primers the *NotI* restriction site. Two different restriction sites ensure insertion of the PCR product in the correct orientation into the pFastBac1TM plasmid. Depending on the construct the tag is located either at 5' or at 3' end of the sequence. PCR was performed with the high fidelity *Pfx50TM* DNA polymerase (5 U/μl, Invitrogen) in a thermo block (MWG Biotech, Primus 96^{plus}) using provided polymerase buffer (10X *Pfx50TM* PCR mix) and 10 mM dNTP mix.

PCR products were *SpeI/NotI* digested according to enzymes' manufacturer's recommendation (New England Biolabs, NEB).

Digested DNA was purified by electrophoresis in an analytical agarose gel of high purity (1 % in TAE buffer) from which the DNA was then eluted using Qiagen Gel Extraction Kit.

Digested and purified PCR products were cloned into the *SpeI/NotI* digested and dephosphorylated (Antarctic phosphatase, NEB) pFastBac1 vector (Invitrogen) with T4 ligase (NEB) in a ligase buffer and with ATP provided by the manufacturer with the ligase.

Some truncated motor constructs were fused to fluorophores for Förster resonance energy transfer (FRET) measurements. Cyan and yellow fluorescent proteins were custom synthesized by GenScript as cDNA with desired cloning sites at both ends. The fluorophores were then fused to the motor subunits by applying restriction/ligation strategy. The fusion products were then ligated into pFastBac1 vector as described above.

Materials and methods

Recombinant pFastBac1 was then used to generate the construct coding baculovirus by described and established method (Baculovirus-Sf9 expression system described by O'Reilly *et al.* (1992), Invitrogen).

TAE buffer: 24.2 % Tris base, 5.7 % glacial acetic acid, 50 mM EDTA (pH 7.0)

2.1.2 Generation and isolation of baculovirus shuttle vectors (bacmids)

Recombinant pFastBac1 vectors were amplified by heat shock transformation into chemically competent *E. coli* XL1-blue cells. After the heat shock at 42 °C cells were recovered in S.O.C medium before they were plated onto LB-ampicillin agar plates. Four to six ampicillin-resistant colonies were inoculated in 4 ml LB-ampicillin medium for further growth in shaking culture. Amplified pFastBac1 vector was isolated using Qiagen Mini-Preparation kit. All amplified pFastBac1 vectors were *SpeI/NotI* digested and separated on an agarose gel to check for the correct size of the insert.

Before performing any experiments all vectors to be used for recombinant bacmid generation were sequenced by the DNA sequencing facility of the LMU, Munich (biology faculty, genetics department), and the insert sequence accurately checked for its correctness.

After amplification recombinant pFastBac1 was transformed into chemically competent MAX Efficiency® DH10Bac™ competent *E. coli* cells (Invitrogen). This specific *E. coli* strain contains a transposase coding helper plasmid, as well as a *Autographa californica* nuclear polyhedrosis virus (AcNPV) bacmid containing the low-copy-number mini-F replicon, a kanamycin resistance marker, and a segment of DNA encoding the *lacZ* α peptide. By site-specific transposition of the mini-Tn7 element containing the gene of interest from the pFastBac1 donor plasmid to the mini-*attTn7* attachment site on the bacmid, the *lacZ* α gene compensating for the chromosomal deletion of *lacZ* is disrupted (Figure 8 and Invitrogen instruction manual). Transposition functions are provided *in trans* by the helper plasmid, which further confers resistance to tetracycline.

Materials and methods

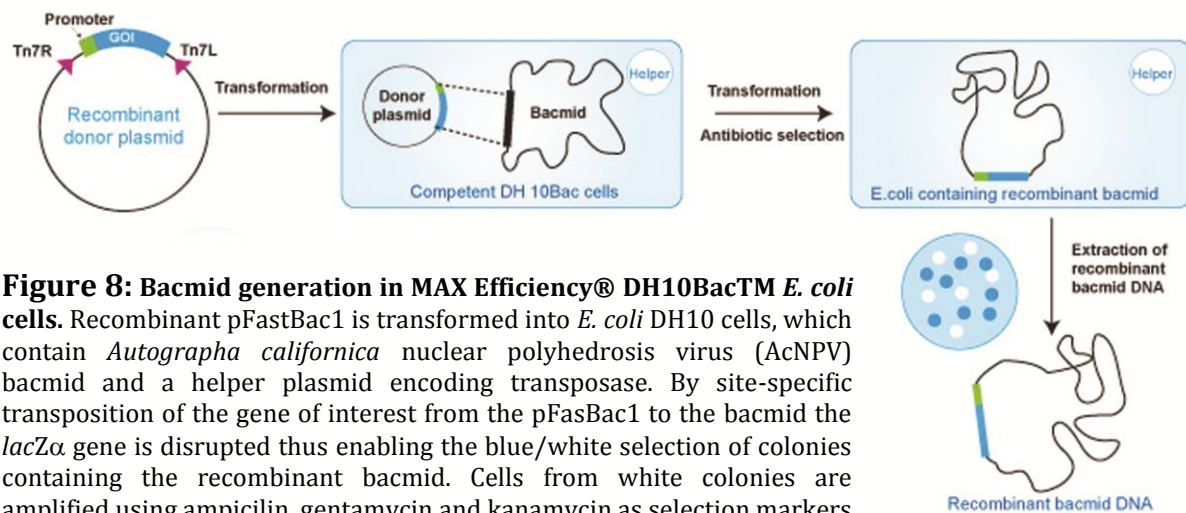


Figure 8: Bacmid generation in MAX Efficiency® DH10Bac™ *E. coli* cells. Recombinant pFastBac1 is transformed into *E. coli* DH10 cells, which contain *Autographa californica* nuclear polyhedrosis virus (AcNPV) bacmid and a helper plasmid encoding transposase. By site-specific transposition of the gene of interest from the pFasBac1 to the bacmid the *lacZα* gene is disrupted thus enabling the blue/white selection of colonies containing the recombinant bacmid. Cells from white colonies are amplified using ampicilin, gentamycin and kanamycin as selection markers and the bacmid is isolated (adapted from BacuVance™ Baculovirus Expression System (GenScript)).

Transformed MAX Efficiency® DH10Bac™ cells were plated on Bluo-Gal LB agar plates for blue-white selection. White colonies were once again spread on Bluo-Gal supplemented LB agar plates to exclude false positive results. Colonies growing white both times were then inoculated in 6 ml LB DH10 selection medium and bacmids isolated using reagents from the Qiagen DNA Mini-Preparation Kit (see 2.1.3 Bacmid isolation).

S.O.C medium: 2 % Tryptone, 0.5 % yeast extract, 10 mM NaCl, 2.5 mM KCl, 10 mM MgCl₂, 2 % 1 M Glucose

LB-ampicillin medium/agar: 1 % Tryptone, 0.5 % yeast extract, 0.5 % NaCl, 100 µg/ml Amicilin, (1.5 % agar)

Bluo-Gal LB: 1 % Tryptone, 0.5 % yeast extract, 1 % NaCl, 50 µl/ml kanamycin, 7 µg/ml gentamycin, 10 µg/ml tetracycline, 100 µg/ml Bluo-Gal, 40 µg/ml IPTG

DH10 selection medium: LB, 50 µl/ml kanamycin, 7 µg/ml gentamycin, 10 µg/ml tetracycline

2.1.3 Bacmid isolation

The first steps up to the centrifugation after adding P3 buffer from Qiagen Plasmid Purification Mini Kit are performed as described in the Qiagen handbook. The supernatant was then mixed with equivalent volume of isopropanol and centrifuged again at room temperature and 14000 rpm for 30 min. Pellet was washed in 250 μ l ethanol and centrifuged again for 10 min at room temperature and 14000 rpm. After discarding the supernatant the pellet dried completely and was then resuspended in 70 μ l TE buffer. For better dissolving the sample was kept at 37 °C for 10 min.

TE buffer: 10 mM Tris-HCl; 1 mM EDTA; pH 8

2.2 Cell biological methods

2.2.1 Cell culture

Sf9 cells were cultivated for the protein expression purposes. The Sf9 cell line was developed from ovaries of the fall army worm (*Spodoptera frugiperda*) (Vaughn *et al.*, 1977) and is a specific host for the baculovirus.

Cells were grown in shaking culture at 28-30°C and 110rpm and kept at densities between 1 and 5×10^6 cells per millilitre. Cells are kept and diluted in Sf-900 serum free medium (SFM) (Invitrogen) supplemented with 10 % FBS and 0.1 mg/ml gentamycin (PAA).

Cell density was checked daily by diluting cells in trypan blue (Sigma) solution (0.4 % in PBS) and counting the cells in a Neubauer counting chamber (Brand) in a Leitz Labovert microscope.

PBS: 140 mM NaCl, 2.7 mM KCl, 1.8 mM KH_2PO_4 , 10 mM Na_2HPO_4 , pH 7.4

2.2.1 Bac-to-bac expression system

The next step from isolated bacmid to a construct coding baculovirus is the bacmid transfection into Sf9 cells.

The DNA was coated with Cellfectin reagent (Invitrogen) and added to adherent Sf9 cells washed in serum free medium at a density of 0.5×10^6 cells/ml in a 6-well culture

plate (Cellstar, Greiner). The samples are incubated for 5 h and then washed with serum free medium. Transfected cells are incubated in supplemented medium 4-7 days. During this time the bacmid DNA is translated and virus particles are formed leading to cell lysis. These processes are visible as cell swelling and holes in the cell lawn.

The so called P0 virus generation is harvested in that the medium (2 ml) is taken up into a syringe and pressed through a micro filter with 0.2 μm pore size. Virus was amplified by infecting larger volume (20-30 ml) of cells at 10^6 cells per ml with the virus and incubating again for 4-7 days. Intact cells and cell debris are separated from the virus (P1 generation) containing medium by centrifugation at 3500rpm for 10 minutes in a 50 ml tube (Greiner). Pellets were used for test purification of the protein (see 2.3.1 and 2.3.2). The size was checked via SDS-PAGE and Coomassie staining of the polyacrylamide (PAA) gel. The respective gel bands were cut out and analyzed by mass spectrometry (Zentrallabor für Proteinanalytik, LMU Munich).

For protein expression cells were grown to $2 \cdot 10^6$ cells per ml and infected with the amount of virus required for decent protein concentration. The amount was unique for every virus and virus generation and dependent on the volume of the cell culture. Infected cells were incubated for 48-72 h and harvested before virus particles formed and cell lysis occurred by centrifugation at 3500 rpm for 10 min.

2.3 Biochemical methods

2.3.1 Protein purification via 6xHis affinity tag

Depending on the experiments proteins were purified either in PIPES or sodium phosphate buffer.

Harvested cells were lysed in the lysis buffer (4 ml for 100 ml cells) and centrifuged in an ultracentrifuge (Beckmann L8-M, rotors 70.1 Ti, 50.2 Ti, or Beckmann Optima TL, rotor TLA 100.3) at 30000 rpm for 10 min to separate the cell debris from the lysate. The lysate was then incubated with washed Ni-NTA coated sepharose beads (Ni-NTA agarose, Qiagen) for 1h (500 μl Ni-NTA beads for 4ml cell lysate). The beads were washed twice with 2.5x volume Ni-NTA washing buffer. Depending on the volume used, the sepharose incubated with the cell lysate was either poured onto a

Materials and methods

column (Poly-Prep[®] chromatography column, pore size 30 μ m, Biorad) or washed in the batch in an Eppendorf reaction tube.

Column purification (beads volume > 100 μ l):

The fluid phase was let to flow through before the beads were extensively washed with the washing buffer to discard all unbound protein. Bound protein was eluted by 300-500 mM imidazole in the elution buffer with which the beads were incubated for 30 min on the column.

Batch purification (beads volume < 100 μ l):

After incubation the sample was centrifuged and the supernatant removed. Six washing steps were performed of resuspending the Ni-NTA agarose pellet with bound protein in washing buffer and a following centrifugation step. Protein was eluted by incubating the washed beads in the elution buffer for 30 min.

Purified protein was either used immediately or shock-frozen in liquid nitrogen and stored at -70 °C.

PIPES basic buffer: 80 mM PIPES, 200 mM KAc, 1 mM MgCl₂, 1 mM DTT and 100 μ M ATP, when constructs containing the catalytic head domain were purified.

Na-phosphate basic buffer: 50 mM NaH₂PO₄+Na₂HPO₄, 200 mM KAc, 1 mM MgCl₂, 1 mM DTT and 100 μ M ATP, when constructs containing the catalytic head domain were purified.

Ni-NTA washing buffer: basic buffer, 10 mM β -mercaptoethanol

Lysis buffer: basic buffer, 1 % Triton-X 100, protease inhibitor cocktail (c0mplete, Roche), 20 mM imidazole, pH 8

Washing buffer: basic buffer, 40 mM imidazole, pH 6.3

Elution buffer: basic buffer, 500 mM imidazole, pH 7.2

2.3.2 Protein purification via Flag tag

Affinity purification of the proteins via Flag-tag was performed analogous to the 6xHis-tag affinity purification.

Materials and methods

The cell lysate was incubated with agarose beads coated with anti-Flag antibody (ANTI-FLAG[®] M2 Affinity Gel, Sigma) for 90 min. For washing the beads were either poured onto the column, or washed in a batch, again depending on the volume of the medium. Anti-Flag beads were washed with washing buffer and subsequently with the same amount of basic buffer. Protein elution happened by incubating the beads with the elution buffer, containing a large excess of FLAG-peptide (Sigma), once or twice for 30 min.

PIPES basic buffer: 80 mM Pipes, 200 mM KAc, 1 mM MgCl₂, and 1 mM DTT (For purification of constructs containing the catalytic head domain 100 μM ATP were added.)

Na-phosphate basic buffer: 50 mM NaH₂PO₄+Na₂HPO₄, 200 mM KAc, 1mM MgCl₂, and 1 mM DTT (For purification of constructs containing the catalytic head domain 100 μM ATP were added.)

Lysis buffer: basic buffer, 1 % Triton-X 100 and protease inhibitor cocktail (c0mplete, Roche)

Washing buffer: basic buffer with 500 mM KAc, 1 mM EGTA and 0.02 % Tween

Elution buffer: basic buffer with 100 μg/ml FLAG-peptide (Sigma)

2.3.3 Gel filtration

Gel filtration was performed with the Äkta purifier 100 (GE Healthcare) and the Superdex 200 10/300 GL gel filtration column (GE Healthcare). Gel filtration was the second instance purification step after the affinity purification and was done to verify the integrity of kinesin-2 complexes with truncated subunits, like KLP11-C and KLP20-C (see the construct list on page 89 and results section 2.1.1). When required, samples were concentrated by centrifugation in an Amicon[®] Ultra centrifugal filter unit (10 kDa exclusion size, Millipore) before loading onto the column. The sample volume was 150 μl (1.5x V of the sample loop of 100μl)

Gel filtration buffer: 80 mM PIPES, 200 mM KAc, 1 mM MgCl₂, 1 mM DTT, 1 mM EGTA

2.3.4 Co-immunoprecipitation assays

Sf9 cells were co-infected with two Baculoviruses, one coding for a Flag-tagged and one for untagged or 6xHis-tagged interaction partner. Overexpressed protein was affinity-purified via the Flag-tag. Elution was checked for the content of untagged/6xHis-tagged protein via SDS-PAGE and Coomassie-staining of the gel. Depending on the size of purified proteins 10-15 % PAA gels were used (Rotiphorese[®] Gel 30, Roth). Prospective gel bands were analyzed by mass spectrometry (ZfP, LMU Munich).

When no co-precipitation of the 6xHis-tagged partner with its Flag-tagged partner was observed, Ni-NTA purification was performed to ensure that the 6xHis-tagged protein was indeed expressed.

2.3.5 Tubulin preparation from pork brain and polymerization of purified tubulin

Tubulin used in this work was isolated from pork brain. On the day of preparation five brains from freshly slaughtered pigs were collected at the local slaughterhouse and transported on ice. Tubulin was isolated according to Mandelkow *et al.* (1985) in a one-day process.

For polymerization of microtubules the tubulin solution was centrifuged for 10 min at 4 °C and 80000 rpm (Beckman ultracentrifuge Optima TL, rotor TLA 100.3 or 120.1) to remove denaturated and aggregated tubulin, which cannot polymerize anymore. 1 mM GTP was added to the supernatant, which was then incubated for at least 30 min at 35 °C. Polymerized filaments were stabilized by adding 20 µM Taxol and incubating for another 30 min at 35 °C.

For the ATPase assay (2.3.6) microtubules were purified from unpolymerized tubulin by a spin-down (15 min, 80000 rpm, 25 °C) over a sucrose cushion. The pellet was then washed and resuspended in 12A25 buffer containing 20 µM Taxol.

The tubulin concentration was determined photometrically after denaturing microtubules in tubulin dimers with guanidinium hydrochloride according to Huang and Hackney, 1994. The concentration was calculated applying the law of Lambert-Beer:

Materials and methods

$$E = \varepsilon * c * d$$

$$c \text{ (tubulin dimmers in g/l)} = E_{280} / 1.03 * \text{dilution factor}$$

where E is the extinction of the solution measured at $\lambda=280\text{nm}$, ε is the extinction coefficient of tubulin at 280nm ($\varepsilon_{280}=1.03$), c is the tubulin concentration in g/l and d the path length (=1 cm).

With the tubulin dimer size of 100 000 g/mol molar concentration of tubulin in solution could be determined:

$$c \text{ (mol/l)} = c \text{ (g/l)} / \text{molecular weight (g/mol)}$$

GTP: 100mM in H₂O

12A25 buffer: 12 mM Aces-KOH, 25 mM KAc, 2 mM MgAc, 0.5 mM EGTA, pH 6.8

Sucrose cushion: 40 % Sucrose in 12A25 buffer

2.3.6 Microtubule affinity assay

Polymerized microtubules were incubated with Flag-tag purified (Methods 2.3.2) tail monomers and the tail dimer for 30 min at room temperature. The samples were then centrifuged over a 40 % sucrose cushion for 10 min at 80000 rpm and 25 °C. The supernatant on the sucrose cushion was carefully removed and the cushion discarded. The pellet was resuspended in 12A25 buffer containing 250 mM NaCl and incubated for 20 min at room temperature before it was centrifuged again as described above. The supernatant on the sucrose cushion was carefully removed and the cushion discarded. The pellet was resuspended in 12A25 buffer containing 250 mM NaCl. Both supernatants and both pellets were analyzed for tail content by SDS-PAGE.

2.3.7 Enzymatically coupled ATPase assay

The microtubule-stimulated ATPase activity of different kinesin-2 constructs was measured in an assay in which the ATP hydrolysis by kinesin-2 was coupled to NADH oxidation by an ATP regeneration system (Figure 9).

Materials and methods

The pyruvate kinase (PK) in the ATP regeneration system regenerates the hydrolyzed ATP so that the ATP concentration remains unchanged during the whole assay. Simultaneously, PK oxidizes phosphoenolpyruvate (PEP), another component of the regeneration system, to pyruvate, which is then reduced to lactate by lactate dehydrogenase (LDH), also a part of the regeneration system. NADH in the regeneration system acts as proton donor in this last reaction and gets oxidized to NAD^+ , so that hydrolysis of one ATP molecule by kinesin-2 is coupled to oxidation of one NADH molecule.

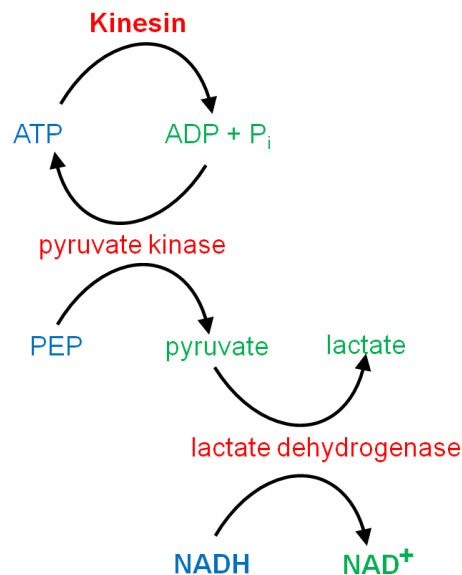


Figure 9: Enzymatic coupling during the ATPase assay. Enzymes are depicted in red, substrates in blue and reaction products in green. Pyruvate kinase (PK), lactate dehydrogenase (LDH), PEP and NADH are contained in the regeneration system. The diagram shows how the hydrolysis of one ATP molecule by a kinesin catalytic head is coupled to oxidation of one NADH molecule by LDH. While the hydrolyzed ATP is regenerated by PK the decrease in NADH concentration is followed photometrically at $\lambda=340\text{nm}$.

The decrease of NADH concentration over time is followed photometrically at 340 nm and calculated applying the law of Lambert-Beer (2.3.5):

$$\Delta E/t = \varepsilon \cdot \Delta c(\text{NADH}) \cdot d/t$$

with $\Delta E/t$ being the over time changing extinction (corresponds to maximal reaction velocity v_{max}), ε being the extinction coefficient of NADH ($\varepsilon_{280}=6.22$) and d being the

Materials and methods

path length. The assay is performed in 96-well PS-microplate, flat bottom, half area (Greiner) with an area size $A=0.15 \text{ cm}^2/\text{well}$. The reaction volume is $50 \mu\text{l}$ corresponding to 0.05 cm^3 . The path length is thus $d=0.333 \text{ cm}$ ($d=V/A$).

The coupling of hydrolysis of one ATP molecule to oxidation of one NADH molecule and v_{max} being $\Delta E/t$ gives:

$$\Delta c[\text{ATP}]_{\text{max}}/s=(v_{\text{max}}/6.22*0.333) \text{ mM/s}$$

To determine kinesin-2 Michaelis-Menten enzyme kinetics the motor was stimulated with increasing microtubule concentration ($c[\text{MT}]=1-80 \mu\text{M}$) at constant ATP concentration (1mM) and the ATPase-rate ($\Delta c[\text{ATP}]_{\text{max}}/c[\text{kinesin-2}]$) determined. Setting the ATPase rate in relation to $c[\text{MT}]$, the k_{cat} (the maximal number of hydrolyzed ATP molecules per kinesin head and second) and K_m ($c[\text{MT}]$ at which $1/2v_{\text{max}}$ is reached) were determined.

$$\text{ATPase-rate}=(k_{\text{cat}} * c[\text{MT}])/(K_m+ c[\text{MT}])$$

ΔE_{340} was recorded at $27 \text{ }^\circ\text{C}$ over 30 min with a spectrophotometer (Bio Tek). $50 \mu\text{l}$ reaction volume was composed of $37 \mu\text{l}$ microtubule dilution in 12A25 with $20 \mu\text{M}$ Taxol, $10 \mu\text{l}$ protein dilution with defined protein concentration ($7.7 \mu\text{l}$) and regeneration system ($2.3 \mu\text{l}$) in 12A25, as well as $3 \mu\text{l}$ of 15 mM Mg*ATP in 12A25 mixed in this order. ATP starts the reaction and was therefore added just before the measurement. For the background measurement, either MT dilution, or ATP was substituted by buffer (12A25 with $20 \mu\text{M}$ Taxol).

Depending on the construct, kinesin-2 concentration used was 50, 80 or 100 nM.

12A25 buffer: 12 mM Aces-KOH, 25 mM KAc, 2 mM MgAc, 0.5 mM EGTA, pH 6.8

ATP regeneration system: 1.5 mM NADH in 100 mM HEPES, 3 mM PEP in 12A25, 1.6 U/ml PK, 2.2 U/ml LDH

Taxol: 4 mM in DMSO

Mg*ATP: 100 mM ATP in H_2O , 100 mM MgCl_2

2.4 Biophysical methods

To assess the length and integrity of the heterologous coiled-coil between the stalks of KLP11 and KLP20 a number of biophysical methods was applied. Transmission electron microscopy (TEM) should provide a global picture of the kinesin-2 heterotrimer. Förster resonance energy transfer (FRET) should give confidence in the coiled-coil length and circular dichroism (CD) spectroscopy should determine the number of amino acids involved in coiled-coil formation.

2.4.1 Transmission electron microscopy

For imaging of the kinesin-2 heterotrimer, purified protein particles were adsorbed onto glow-discharged formvar- and carbon-coated Cu400-TEM grids and then stained immediately using a 2 % aqueous uranyl formate solution containing 25 mM NaOH. Imaging was performed using a Philips CM100 operated at 100 kV.

Particles were collected from the micrographs using “boxer” application of the EMAN 1.9 software (<http://blake.bcm.edu>, National Center for Macromolecular Imaging, Baylor College of medicine). Particle length and distance between globular domains were determined using ImageJ 1.45 software (Wayne Rasband).

2.4.2 In solution Förster resonance energy transfer measurements

FRET allows detection of molecule-molecule interactions in nanometer range and is therefore used as molecular nanoscale. The quantitative theory on molecular resonance transfer was first described by Förster (Förster, 1946, 1948) and finds a very broad application field especially with fluorophores and is therefore also called fluorescence resonance energy transfer. FRET is a non-radiative transfer of energy from an excited donor molecule to a suitable acceptor molecule in a very close proximity (<10 nm). The donor and acceptor molecules are different fluorophores with spectral overlap. It is necessary that the emission spectrum of the donor fluorophore overlaps with the excitation spectrum of the acceptor fluorophore (Figure 10). Ideally, the maxima of these two spectra overlap and the emission spectra of the two fluorophores are separated. In the case that FRET occurs, the excitation of the donor fluorophore results in emission characteristic for the acceptor fluorophore. In addition to spectral overlap, FRET efficiency (E) also depends on the distance between two

fluorophores of the FRET pair. Decreasing efficiency with the sixth power of the fluorophore distance makes FRET a very sensitive method resolving in nanometer range.

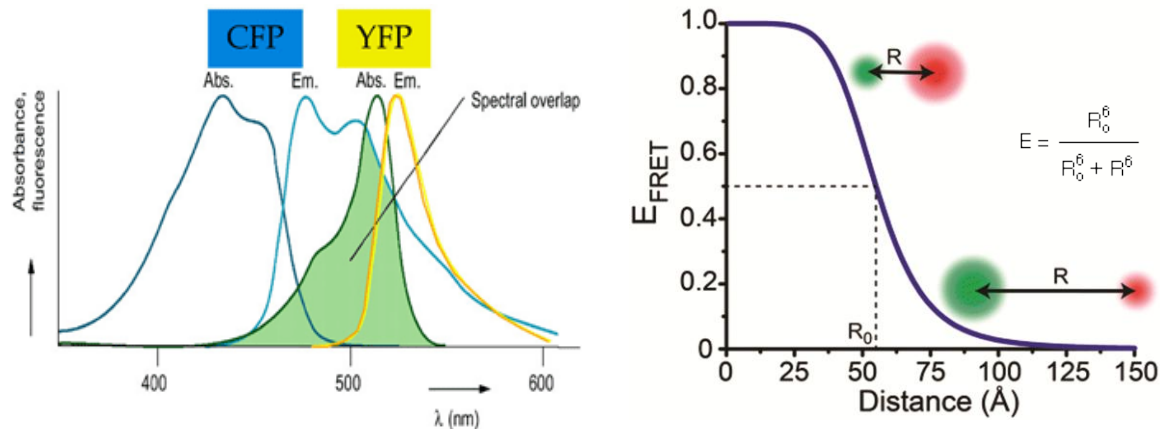


Figure 10: Donor-acceptor pairs and FRET efficiency. *Left panel:* CFP and YFP are a widely used FRET pair because the emission spectrum of CFP overlaps with the absorption spectrum of YFP (green area). On the other hand, the absorption spectrum of CFP overlaps only slightly with the absorption spectrum of YFP. This means that YFP will to the greatest extent be excited by the CFP emission caused by CFP excitation at certain wavelength. Such YFP excitation can, however, only occur if CFP and YFP are close enough, i. e. closer than 8nm (Kalab and Soderholm). *Right panel:* The solid curve represents the relationship between the efficiency of FRET and the distance separating the donor and the acceptor. The equation describes this relationship accurately and shows that the efficiency (E) decreases with the sixth exponential of the distance between the two probes (R). R₀ is the Förster distance, that is, the distance between the donor and acceptor probe at which the energy transfer is (on average) 50% efficient.

CFP and YFP (cyan and yellow fluorescent protein) is the most commonly used fluorescent protein FRET pair in which the energy is transferred from CFP to YFP (Figure 10). All KLP11 constructs used were Flag-tagged and fused to YFP, whereas all KLP20 constructs contained a 6xHis-tag and were fused to CFP. To ensure the greatest possible heterodimer content in the protein solution the co-expressed FRET pair was purified via the Flag-tag in the first instance and successively the elution was purified again via the 6xHis-tag.

For the FRET measurements KLP11-YFP/ KLP20-CFP dimers were used at a concentration of 50 nM. The optimal protein concentration was determined by successive dilution of the protein solution until optimal fluorescence intensities were reached. For the calculation of the net FRET signal heterodimers containing only one fluorophore, KLP11-YFP/ KLP20 and KLP11/ KLP20-CFP, were measured in the YFP and the CFP channel at a concentration of 50 nM. These constructs were also

Materials and methods

used to determine the ideal excitation wavelength, which turned out to be 435 nm for CFP and 505 nm for YFP. While the measurement in the YFP channel was a mere quality control, the spectra of dimers containing only one fluorophore measured in the CFP channel were subtracted from the actual FRET measurement (heterodimers with both fluorophores) to obtain the net FRET signal.

$$\text{Net FRET} = (\text{KLP 11-YFP/ KLP 20-CFP})_{\text{CFP channel}} - (\text{KLP 11-YFP/ KLP 20})_{\text{CFP channel}} - (\text{KLP 11/ KLP 20-CFP})_{\text{CFP channel}}$$

Subtracting the emission of KLP11-YFP/ KLP20 excited in the CFP channel eliminates the “bleed-through” of YFP into the CFP channel, i. e. the emission of YFP that occurs by direct 435 nm excitation. Subtracting the emission of KLP11/ KLP20-CFP excited in the CFP channel removes residual CFP emission remaining after FRET and leaves the clean FRET signal, i. e. YFP emission after excitation by CFP emission.

In the YFP channel 505 nm was the excitation wavelength and the emission was scanned between 500 and 550 nm with the YFP emission maximum at 530 nm. For the CFP channel, the emission of the fluorophores excited with 435 nm was scanned in the range between 470 nm and 550 nm. The CFP emission maximum lies at 490 nm. The CFP channel is at the same time the FRET channel. For each measurement 10 spectra were recorded and averaged at a scanning speed of 10 nm/min with PerkinElmer LS55 fluorescence spectrometer.

To calculate FRET efficiency following equation was applied:

$$E=1-(F_{da}/F_d)$$

E is FRET efficiency, F_{da} is the fluorescence intensity of the donor in the presence of acceptor, F_d is the fluorescence intensity of the donor in the absence of acceptor.

Approximate distances between fluorophores were calculated by:

$$r=R_0*(1/E-1)^{1/6} \text{ (from } E=R_0^6/R_0^6-r^6)$$

where r is the distance between fluorophores, R_0 is the Förster radius for CFP and YFP (4,92nm (Patterson *et al.*, 2000)). Förster radius is the distance at which $E=0.5$.

2.4.3 Circular dichroism spectroscopy

Chiral structures, such as amino acids, are optically active, meaning they rotate the plane of monochromatic linearly polarized light. The benzene ring in the aromatic amino acids phenylalanine, tryptophan and tyrosine acts as a chromophore and absorbs left and right circular polarized light unequally in the chiral environment, which results in elliptical polarization of light that passes through the sample.

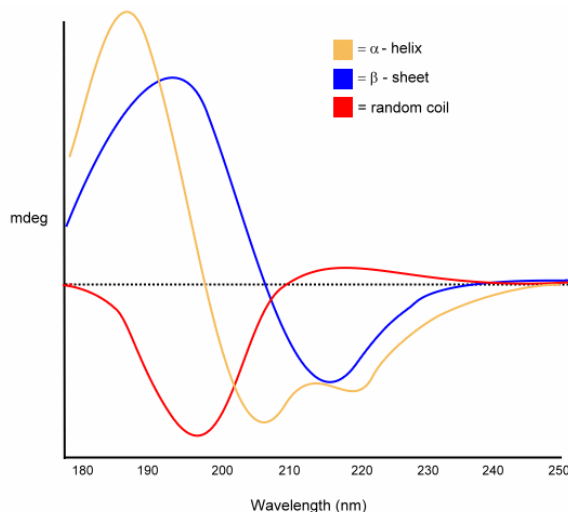


Figure 11: Far UV CD spectra of protein secondary structures. Protein secondary structures α -helix, β -sheet and random coil all display characteristic far UV (250-180 nm) spectra. The α -helix and coiled-coil spectrum (yellow) is characterized by two minima at 208 nm and 222 nm and a maximum at 190 nm.

By circular dichroism spectroscopy the difference in absorption for left and right handed components can be measured, which is then expressed as θ in millidegrees (mdeg), which is the ellipticity of the beam outgoing from the sample. Circular dichroism is an excellent method for analyzing the protein secondary structure in solution and is also useful for following the changes in folding as a function of temperature. Protein secondary structures α -helix, β -sheet and random coil display characteristic far UV (250-180 nm) spectra (Figure 11). α -helix and coiled-coil spectrum typically have two negative bands at 222 nm and 208 nm and one positive band at 190 nm (Chen *et al.*, 1974). Using θ at 222 nm and 208 nm from the recorded far UV spectrum the number of amino acids involved in coiled-coil formation in the construct measured can be determined by applying following equations:

Materials and methods

Molar ellipticity $[\theta]$:

$$[\theta] = \theta / (10 * C * l)$$

where θ is measured ellipticity in mdeg, C is the molar concentration (mol/l) of the protein and l is the cell path in cm. $[\theta]$ is expressed in $\text{deg} * \text{cm}^2 * \text{decimole}^{-1}$.

For proteins the **mean residue molar ellipticity** is used $[\theta]_{\text{MRW}}$:

$$[\theta]_{\text{MRW}} = \theta / (10 * C_r * l)$$

Formula is still the same, but C_r is the mean residue molar concentration:

$$C_r = (n * 1000 * c_g) / \text{MW}$$

where n is the number of peptide bonds (residues), c_g is the protein concentration in g/ml and MW is the molecular weight of the species in g/mol.

Mean residue molar ellipticity at 222 nm of a 100 % α -helical protein with a certain number of residues is predicted to be:

$$[\theta]_{222} = -40 \times 10^3 \times (1 - 4.6/n) \text{ (Chen } et al., 1974; \text{ Gans } et al., 1991)$$

where n is the number of residues in the protein.

The helical content in % of the protein measured was calculated from the observed $[\theta]_{222}$ value and the predicted mean residue molar ellipticity:

$$\alpha\text{-helix (\%)} = [\theta]_{222 \text{ observed}} / [\theta]_{222 \text{ predicted}} * 100$$

The number of helical residues in analyzed protein was calculated by multiplying the % of helical content with chain length.

Proteins for CD spectroscopy were purified in sodium-phosphate buffer (2.3.1 and 2.3.2) and subsequently dialyzed in pure 50 mM sodium-phosphate buffer (sample:dialysis buffer=1:2000) to remove FLAG-peptides, imidazole, DTT and salt because of their absorbing properties in the UV range. Dialysis was performed in Slide-A-Lyzer dialysis cassettes (Thermo scientific) twice for one hour.

Far UV spectra

To determine the number of residues involved in coiled-coil formation in kinesin-2 heterodimer, circular dichroism spectra were recorded between 250 and 190 nm in a JASCO 815 spectrometer in a thermostatically controlled (20 °C) quartz cell of 0.1 cm path length. Accumulation and averaging of 10 spectra was performed with a scanning speed of 20 nm/min, response time 4 s and band width 1 nm. Spectra were normalized to their mean residue molar ellipticity $[\theta]_{MRW}$ (deg*cm²*dmol⁻¹).

Temperature-dependent CD spectroscopy

To analyze dimer stabilities and helix-coil transitions, temperature-dependent spectrum measurements were performed. Temperature was raised from 10 °C to 80 °C with 2 °C/min. Spectra were recorded every 5 °C (50 nm/min, 5 accumulations) 5 minutes after the temperature was reached between 250 nm and 190 nm. Spectra were normalized to their mean residue molar ellipticity $[\theta]_{MRW}$ (deg*cm²*dmol⁻¹) and analyzed for isodichroic point.

Melting curves

To determine the melting temperature of coiled-coils melting curves were recorded by following the change of $[\theta]_{222}$ between 20 °C and 80 °C with a temperature slope of 2 °C/min, a response of 16 s and band width of 1 nm. Fraction of folded protein at a given temperature was calculated by equation:

$$f_f = ([\theta] - [\theta]_u) / ([\theta]_n - [\theta]_u)$$

$[\theta]_n$ and $[\theta]_u$ represent the ellipticity values for the fully folded and fully unfolded species, respectively. $[\theta]$ is the observed ellipticity at 222 nm at any temperature. Melting temperature is at $f_f = 0.5$ (Greenfield, 2006).

All spectra were deconvoluted manually using equations above, as well as by using Dichroweb (Provencher and Glockner, 1981; van Stokkum *et al.*, 1990; Whitmore and Wallace, 2004, 2008). Both methods delivered the same results.

Results

1 Regulation of the catalytic activity

To prevent ATP waste in the cell a mechanism must exist that regulates kinesin's catalytic activity when the motor is not engaged in active transport of cargo. While the autoinhibition mechanism is well studied for the kinesin-1 family, only little is known how the regulation is accomplished in kinesin-2. The homodimeric family member seems also to be regulated by autoinhibition like kinesin-1, a process in which the tail domains play essential role (Imanishi *et al.*, 2006; Hammond *et al.*, 2010).

There are only few indications that the tail domains may be a part of regulation mechanism in heteromeric kinesin-2. Brunnbauer *et al.* (2010) showed that replacing the two glycine residues at the helix breaker position by glutamates in both motor chains leads to a constitutively active motor. In line with results obtained from kinesin-1, this result suggests that preventing folding of the tail domains onto the catalytic heads serves as an activating switch in kinesin-2 as well. Furthermore, this study demonstrated that solely switching the head positions also abolishes the ability of autoinhibition. These results together not only emphasize a potential role of the tails in the regulation of catalytic activity, but they also indicate that the different tails might have distinct tasks in this process. It can be speculated that specific interaction sites between the heads and the tails exist, and that the heads and the tails must be in their proper position for autoinhibition to work.

Comparing the catalytic properties of a number of different mutations and truncations of KLP11 and KLP20 in monomeric and dimeric state in ATPase assays (Methods 2.3.6) promises mechanistic insights into this regulation process.

1.1 Tail domains are necessary for motor inhibition

To test the tails' potential role in inhibiting the ATPase activity of the motor heads of KLP11 and KLP20, the catalytic activity of the wild type motor was not only compared to the EE-mutant, but also to that of a truncated motor dimer lacking the tail domains at the C-terminus (Figure 12).

Results

In the EE-mutant the helix-breaker residues, G⁴⁵⁰S⁴⁵¹ in KLP11 and G⁴⁴⁴G⁴⁴⁵ in KLP20 (Figure 6), were replaced by glutamates. If the heterodimer is indeed able to fold at the helix-breaker position, replacing the flexible residues by glutamates should prevent the potential interaction of heads and tails. Figure 12 shows that removal of the flexible residues in the stalk abolishes the capability of the motor to autoinhibit its catalytic activity (blue line). To directly demonstrate the involvement of the distal tails in autoinhibition, a C-terminally truncated motor that contains the wild type stalk was tested. This construct is potentially able to perform autoinhibitory folding but lacks the putative inhibitory tail regions.

Figure 12 depicts the average activities of the three motor variants in the form of Michaelis-Menten kinetics. The k_{cat} of the motor lacking the tail domains (green line) is indistinguishable from the previously described EE-mutant, demonstrating that the absence of the C-terminus prevents autoinhibition and confining the inhibitory domain to the distal tails. Taken together, these results demonstrate that preventing folding and/or eliminating the tails abolish inhibition in the KLP11/20 motor.

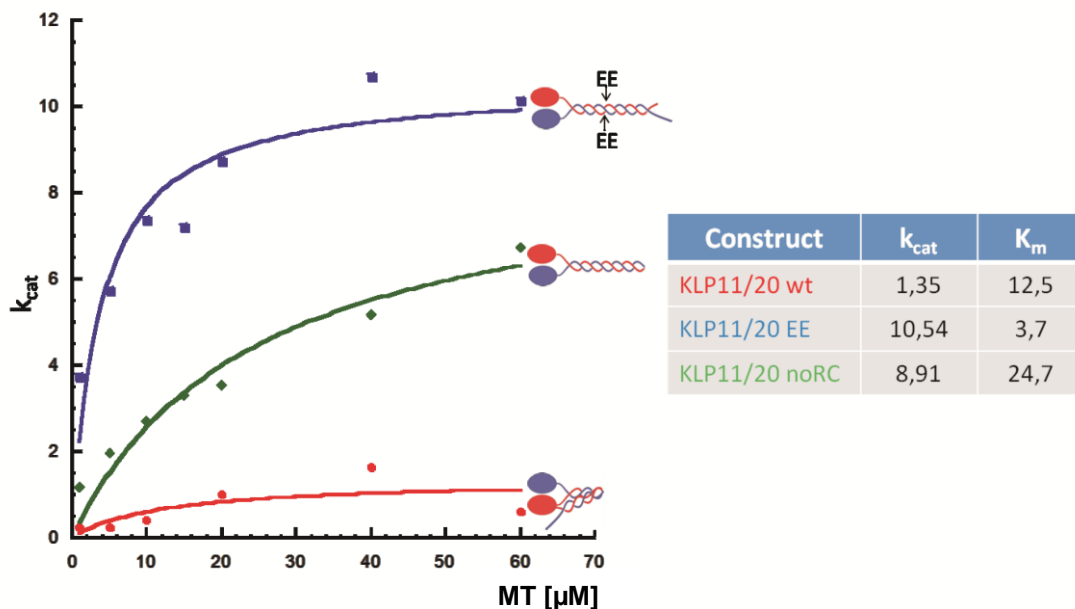


Figure 12: Influence of the tail domain and the helix breaker on the catalytic activity of kinesin-2. The wild type full-length motor displays almost no activity (red). Mutating the helix breaker and thus abolishing the flexibility of this position leads to a robust motor activity (blue). Almost the same activity is achieved by deleting the random coil (RC) tail (green). This result confirms the role of the helix breaker and the tail region in regulation of motor activity. Furthermore, the decreased affinity for microtubules (K_m) of KLP11/20noRC indicates a new role of the tail domain in MT binding. k_{cat} is the catalytic constant giving the number of hydrolyzed ATP molecules per kinesin head and second.

Results

1.2 Tail domains could anchor the inactive motor to microtubules

Interestingly, the motor without the tails shows considerably lower affinity for microtubules compared to the EE-mutant (K_m in Figure 12), which points to an additional role of this domain. The tail's affinity for microtubules was already described in the case of kinesin-1 (Dietrich *et al.*, 2008) along with its additional role as an anchor, so that inactive motor does not diffuse from the track but is ready for a new transport event.

Whether kinesin-2 tail domains show affinity for microtubules for themselves was tested in the microtubule affinity assay (Methods 2.3.6). Figure 13 demonstrates that both tails (KLP11-C and KLP20-C, constructs 31 and 32, page 91) indeed interact with the filaments, as they co-pellet through a 40 % sucrose cushion. If no interaction between the tails and the filaments occurred, the tails would stay in the supernatant on the cushion.

Figure 13 further shows that this interaction, if of ionic nature requires salt concentrations higher than 250 mM to be reversed, which points to a rather stable binding of the interaction partners. Thus, the tail domains of kinesin-2 could, as well as in kinesin-1, serve as an anchor of the inactive motor.

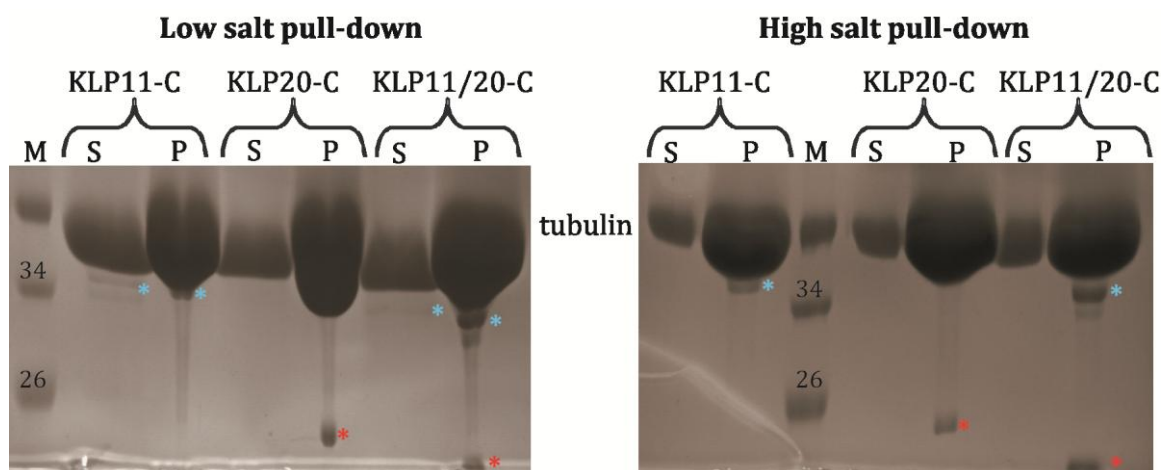


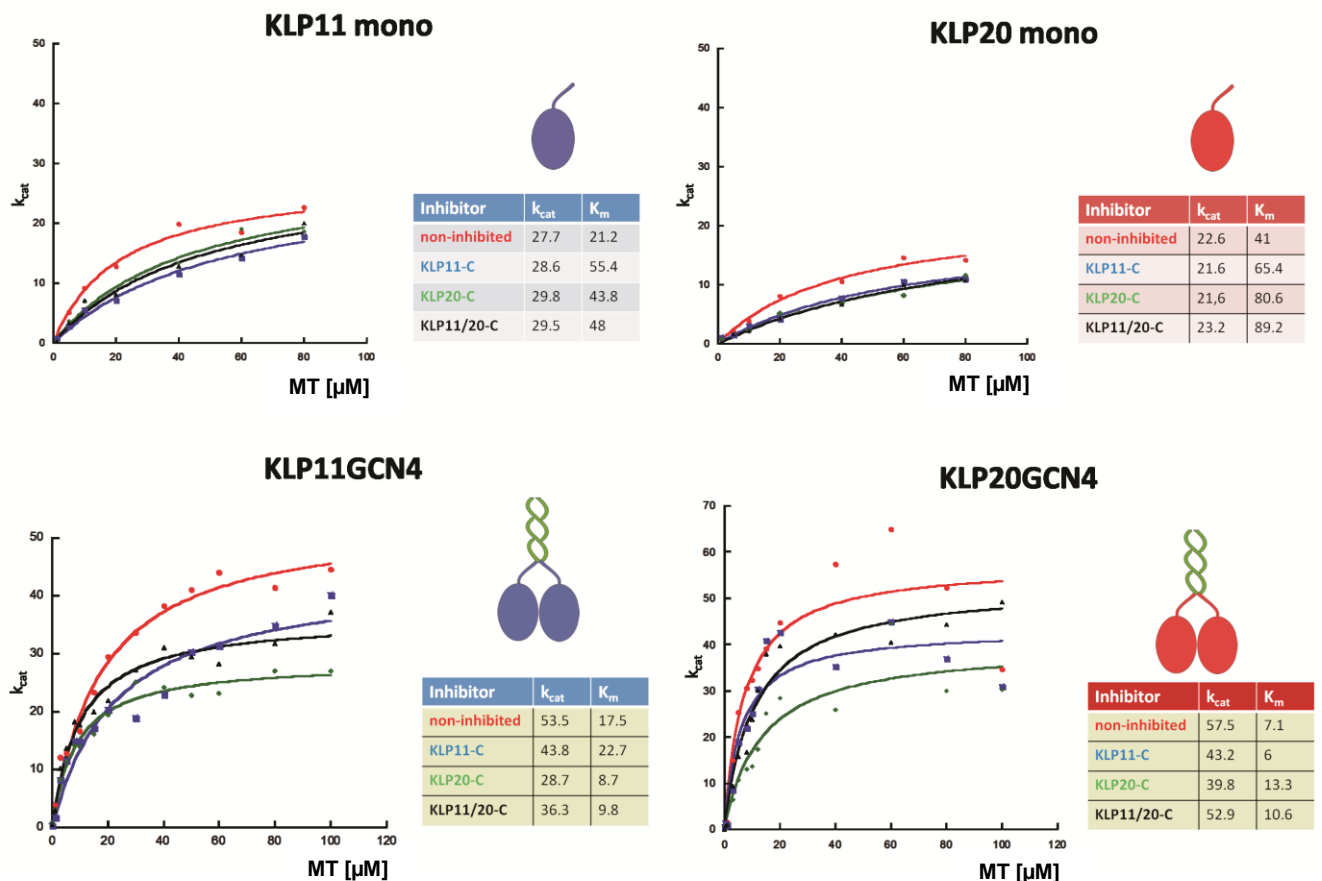
Figure 13: Both kinesin-2 tails bind to microtubules. The mixture of tails and microtubules contains 50 mM KAc. After the first centrifugation step (gel on the left) both tails, as well as the tail dimer are found in the pellet (P) with microtubules. In the case of KLP11 tail a small portion is also found unbound in the supernatant (S, blue asterisk) along with unpolymerized tubulin. The same is probably true for KLP20 tail but due to its smaller size it is not visible after Coomassie-staining at this concentration. The pellet was resuspended in buffer now containing 250 mM KAc. After the second centrifugation step (gel on the right) tails were still found associated with the microtubules. This time no unbound tail was detected in the supernatant. KLP11 tail is depicted by a blue and KLP20 by a red asterisk. S=supernatant, P=pellet, M=protein marker (sizes in kDa).

Results

1.3 Inhibition requires dimeric state of the heads

To test which tail influences which head, truncated monomeric motors were used that include only the catalytic head domain and the neck linker. Purified C-terminal tails of KLP11 and KLP20 along with the tail heterodimer were added *in trans* to the monomeric motor in motor to tail molar ratio of 1:20.

Non-inhibited heads were both robustly active showing even higher k_{cat} values than the EE-mutant (Table 1). This truncation effect is also observed for kinesin-1 (Coy *et al.*, 1999; Hackney and Stock, 2008; Adio *et al.*, 2009) and indicates the necessity of regions further C-terminal for motor regulation. Surprisingly, none of the tail combinations added *in trans* had an inhibitory effect on the monomeric KLP11 and KLP20 head compared to the non-inhibited control (Figure 14, Table 1). Interestingly, previous experiments with kinesin-1 demonstrated that the tail domain of only one chain interacts with both heads of the dimeric molecule whereas the monomeric heads showed no significant inhibition (Hackney *et al.*, 2009). To test if this also applies to the kinesin-2 motor, the KLP11 and KLP20 head domains were homodimerized by the GCN4 leucine zipper. Homodimerization was necessary to distinguish which tail influences which head's kinetics (Figure 14).



Results

Figure 14: Kinesin-2 motor heads must be in dimeric state to be inhibited. While homodimerized kinesin-2 heads, KLP11 GCN4 and KLP 20 GCN4, could be partially inhibited by adding tail constructs *in trans*, no such effect was observed with monomeric heads excluding the possibility that the inhibition is due to crowding effects caused by the presence of excess of tail constructs. Red line: non-inhibited motor, blue line: KLP11 tail added, green line: KLP20 tail added, black line: KLP11/20 tail dimer added.

Again non-inhibited motor was compared with samples where tails were added *in trans* (1:20 molar ratio of heads and tails). The activities of the artificially dimerized motors were reduced to 80 % compared to the control (Table 2). KLP11 GCN4 homodimer could be most effectively inhibited by the tail dimer (residual activity 79.5 %), followed by the KLP20 tail (87 %) and the KLP11 tail (88.4 %). KLP20 GCN4 homodimer was most effectively inhibited by the KLP20 tail (80.5 %) followed by the KLP11 tail (86 %). The tail dimer could reduce the ATPase activity of KLP20 GCN4 head dimer only to 93 %.

Table 1. Comparison of the catalytic activity of different kinesin-2 motor variants

Inhibitor ¹	non-inhibited	KLP11-C	KLP20-C	KLP11/20-C
Motor	k_{cat}			
KLP11 mono	32.4	31.5	31.1	35.0
KLP20 mono	24.4	30.4	30.4	24.6
KLP11 GCN4	46.7	41.2	40.6	37.7
KLP20 GCN4	50.3	43.3	40.5	46.9
KLP11/20 EE	22.6	12.2	14.1	14.3

¹Inhibitors were added in 20fold molar excess

Unfortunately, the KLP11/20 GCN4 head heterodimer could not be purified in amounts needed for the ATPase assay, nor did the tandem protein purification result in the required 1:1 molar ratio for the heterodimer.

Taken together, the homodimeric heads could be partly inhibited *in trans*. However, the extent of the observed inhibition is rather low. It is conceivable that the inhibition *in trans* requires higher concentrations of the tail domains to take greater effect. Or, more likely, the artificially dimerized motors via the GCN4 leucine zipper may not represent a close enough mimic for the kinesin-2 dimeric state.

In fact, Brunnbauer *et al.* (2010) demonstrated that the heads in the KLP11/20 heterodimer must be in their wild type positions for the motor to be autoinhibited.

Results

Swapping the positions of the head domains leads to a constitutively active motor. In line with these results, a significant reduction of ATPase activity was observed with the EE-mutant when the tails were added *in trans*. The EE-mutant was most effectively inhibited by the KLP11 tail where the ATPase activity was reduced to 54 %. KLP20 tail and the tail dimer showed the comparable effects of reducing the motor activity to 62 %.

Table 2. Inhibitory potential of the tails on the kinesin-2 motor constructs

Motor	Residual ATPase rate ¹		
	inhibitor		
KLP11 GCN4	79.8 %	87%	8,4%
	KLP11/20-C	KLP20-C	KLP11-C
KLP20 GCN4	80.5%	86%	93%
	KLP20-C	KLP11-C	KLP11/20-C
KLP11/20 EE	54%	62%	
	KLP11-C	KLP20-C and KLP11/20-C	

¹compared to the motor activity without inhibitor added

1.4 Co-immunoprecipitation of inhibitors with motors

Although it was possible to inhibit the motor constructs *in trans* by adding different tails, these experiments failed to identify which tail affects which head. The KLP11 and 20 GCN4 head homodimers as well as the EE-mutant all display different inhibition patterns (Table 2). To show direct interactions between the tails and motor domains, tails were co-expressed with monomeric and homodimeric head constructs and their interaction analyzed by pull-down experiments (co-IP). Co-expression with the EE-mutant made no sense because asymmetric dimers would have formed (Results 2.1.3) leading to false positive results. For the co-IPs the salt concentration in all buffers (Methods 2.3.2) was reduced to 50 mM KAc to stabilize the possibly weak head-tail interaction as seen with kinesin-1.

None of the monomeric heads pulled down any of the tails (Figure 15), which is consistent with the lack of inhibitory effect on these motor constructs. Also KLP20 GCN4 failed to show co-precipitation with the tail constructs. Only KLP11 GCN4

Results

seems to form a stable interaction with the KLP20 tail (Figure 15). This result underlines the requirement of a dimeric state of the heads to interact with the tail, as the monomeric KLP11 head does not interact with KLP20 tail.

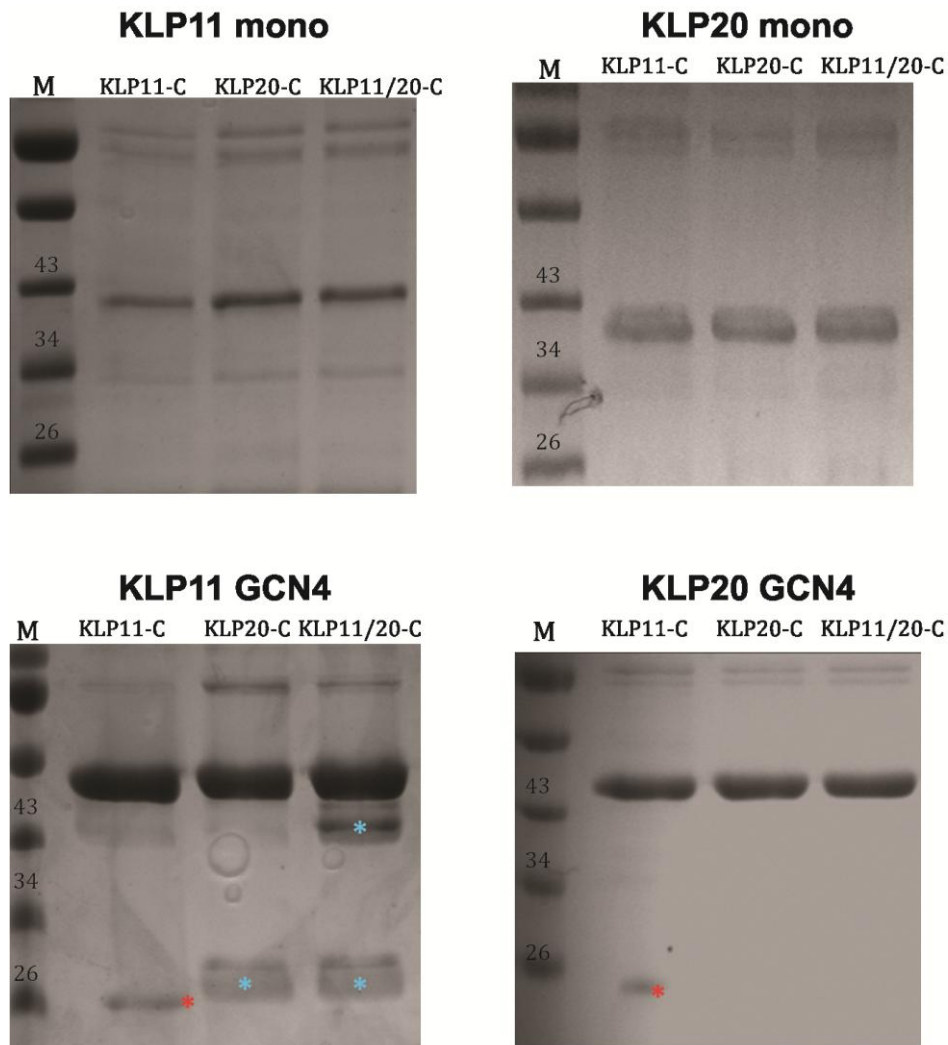


Figure 15: KLP20 tail stably binds to KLP11 head. 6xHis-tagged tails in monomeric and dimeric state were co-expressed with Flag-tagged kinesin-2 head monomers and GCN4 homodimers. Tails were only co-purified with KLP11 GCN4 and this only in presence of KLP20 tail (blue asterisks). KLP11 tail alone was not co-precipitated. Protein bands indicated by red asterisks were identified as mouse IgG, which originates from the Anti-Flag resin. This result indicates a stable interaction between KLP11 head and KLP20 head. The head must, however, be in a dimeric state. Identities of the protein bands were confirmed by LC-MS/MS. Marker (M) protein sizes are in kDa.

2 Domain assembly

Kinesin-2 is so far the only double-headed motor which combines two distinct catalytic subunits along with a non-catalytic accessory subunit to one functional heterotrimeric entity. To reveal how the two motor domains dimerize and where the accessory subunit (KAP) binds to the motor dimer, truncated KLP11 and KLP20 constructs were generated to be tested in different biochemical and biophysical assays. All truncation constructs used in this study are listed in the construct list on page 89.

2.1 Dimerization of truncated KLP11 and KLP20 constructs

To test the dimerization properties of different motor truncations differently tagged KLP11 and KLP20 constructs were co-expressed in Sf9 cells and then purified. Since the affinity tag purification aims only at one binding partner, obtaining both motors by co-immunoprecipitation (co-IP) indicates a stable interaction of KLP11 and KLP20.

2.1.1 The C-terminal half of the stalk is necessary and sufficient for heterodimerization of KLP11 and KLP20

In the first step the wild-type KLP11 and KLP20 motors were cut in half at the predicted helix breaker positions G⁴⁵¹/S⁴⁵² in KLP11 and G⁴⁴⁴/G⁴⁴⁵ in KLP20 (Figure 6). The helix breaker separates the stalk in two halves of the same length and functions as a hinge-joint whose flexibility is important for autoregulation in kinesins (Results 1.1) (Hammond *et al.*; Imanishi *et al.*, 2006; Brunnbauer *et al.*, 2010; Hammond *et al.*, 2010). The N-terminal halves, KLP11-N¹⁻⁴⁴⁹ and KLP20-N¹⁻⁴⁴³, comprise the head and the stalk up to the helix breaker position (Figure 17), whereas the C-terminal halves, KLP11-C⁴⁵⁰⁻⁷⁸² and KLP20-C⁴⁴⁴⁻⁶⁴⁶, include the helix breaker, the C-terminal half of the stalk, and the C-terminal tail that is predicted to be a random coil (Figures 16 and 20). Both halves of the stalk are predicted to form a coiled-coil (Figure 16) (Lupas *et al.*, 1991).

Results

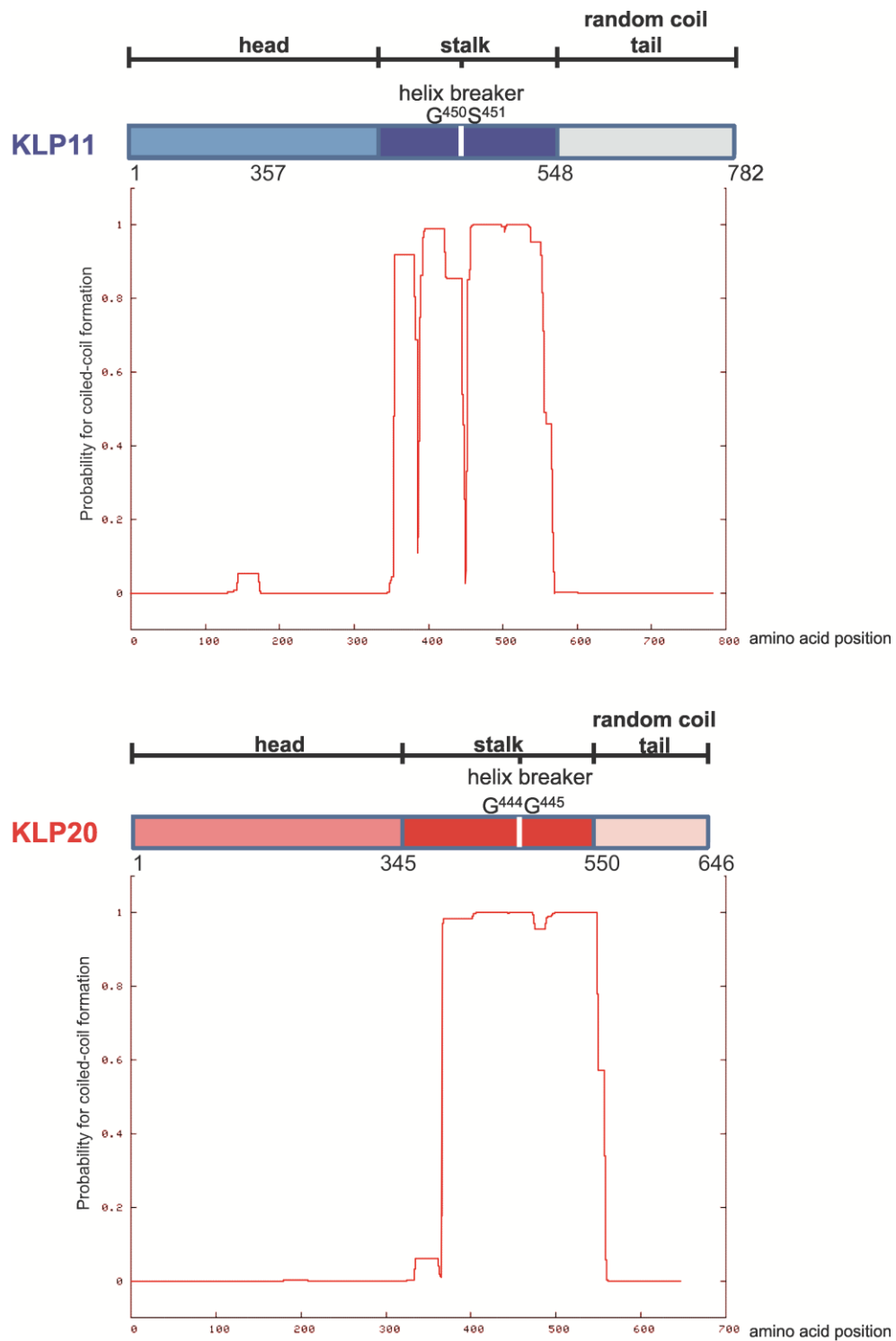
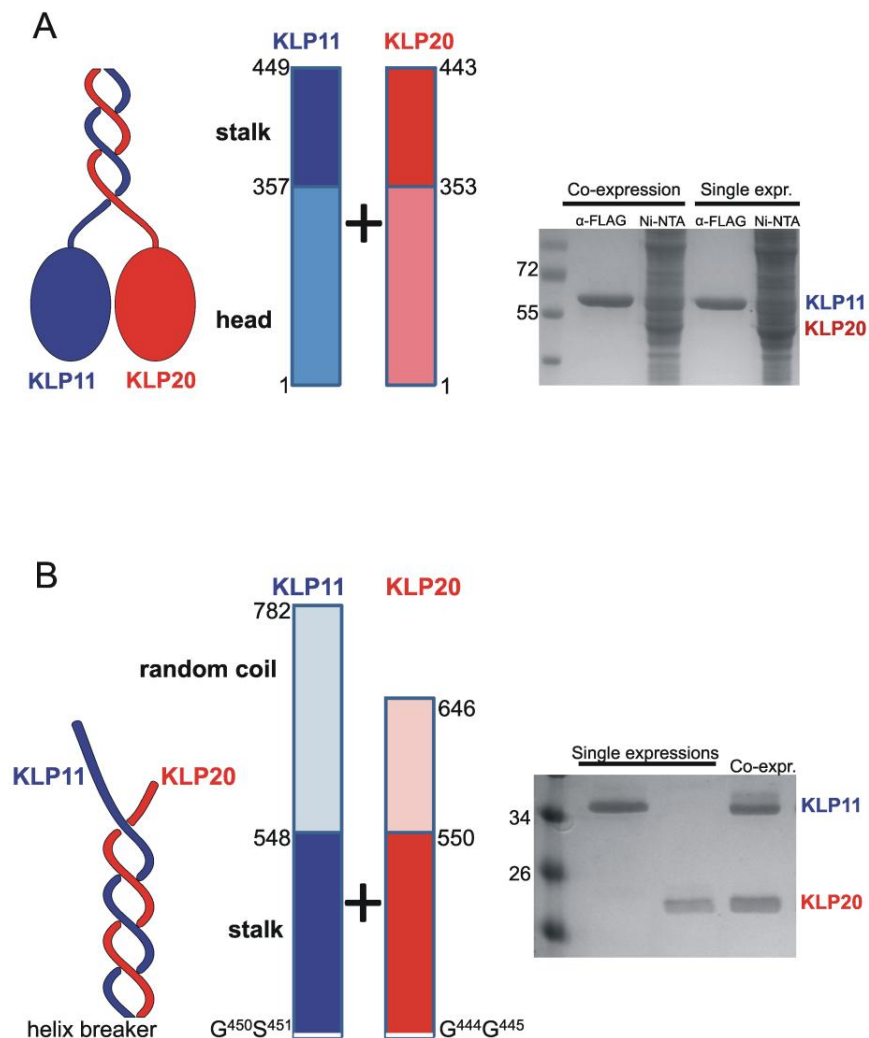


Figure 16: Coiled-coil predictions for KLP11 and KLP20. Virtually the entire stalk region in KLP11 and KLP20 is predicted to form a coiled-coil (Lupas *et al.*, 1991). The predictions are, however, limited to homodimeric coiled-coil formation.

Results

Using the Baculovirus expression system (Methods 2.2.1) N-terminally Flag-tagged KLP11-N¹⁻⁴⁴⁹ was co-expressed with N-terminally 6xHis-tagged KLP20-N¹⁻⁴⁴³. Likewise, the N-terminally 6xHis-tagged KLP11-C⁴⁵⁰⁻⁷⁸² was co-expressed with N-terminally Flag-tagged KLP20-C⁴⁴⁴⁻⁶⁴⁶. Unexpectedly, despite its 13 predicted heptad repeats, attempts to co-purify the truncated KLP20-N with its Flag-tagged KLP11-N counterpart were not successful (Figure 17A). This is not due to failed expression of KLP20-N¹⁻⁴⁴³, as pull down experiments with Ni-NTA confirmed the presence of 6xHis-KLP20-N¹⁻⁴⁴³ in the cell lysate (Figure 17A).



Results

Figure 17: The C-terminal half of the stalk is necessary and sufficient for motor dimerization.

The motor was cut at the helix breaker position. (A) Pull-down experiments of the N-terminal halves. The cell lysate was split for two different purification procedures, via anti-Flag and Ni-NTA, respectively, to ensure that both proteins are expressed successfully. The co-expression did not pull down the corresponding partner and was indistinguishable from the single expressions (single expr.). (B) Pull-down experiments of the C-terminal halves. Single expressions were performed with KLP11-Flag and KLP20-Flag. For co-expressions (co-expr.) KLP11-6xHis and KLP20-Flag constructs were used. Co-purification of KLP11-6xHis along with KLP20-Flag via anti-Flag showed heterodimerization of these two polypeptides. Proteins were analyzed by SDS PAGE. The identities of all protein bands were confirmed by mass spectrometry (LC-MS/MS). Marker protein sizes are shown in kDa.

In corresponding experiments with Flag-tagged KLP20-C⁴⁴⁴⁻⁶⁴⁶, its 6xHis- KLP11-C⁴⁵⁰⁻⁷⁸² counterpart faithfully co-purified (Figure 17B). According to these results only the C-terminal half of the stalk is capable of forming a stable coiled-coil by itself and is not only sufficient but also necessary for dimerization.

To test the specificity and stability of this C-terminal heterodimer size-exclusion chromatography was employed. The protein eluted as a mono-disperse population in a 1:1 molar ratio, as SDS-PAGE analysis shows, ruling out a possible dissociation into monomers (Figure 18). Theoretically, the heterodimer could dissociate into monomers and subsequently form homodimers, which would not be separated using size-exclusion chromatography owing to their similar sizes. To rule out this possibility, the heterodimeric complex was re-co-precipitated from the eluted fractions using the Flag-tag at the KLP20 subunit in a 1:1 ratio (Figure 18, gel on the right). Taken together, the protein is faithfully purified as a specific heterodimer and remains as such after the size exclusion chromatography. These results underline that the C-terminal halves of the KLP11 and KLP20 polypeptides form a specific and stable heterodimer, as does the full length KLP11/20 (Brunnbauer *et al.*, 2010).

Results

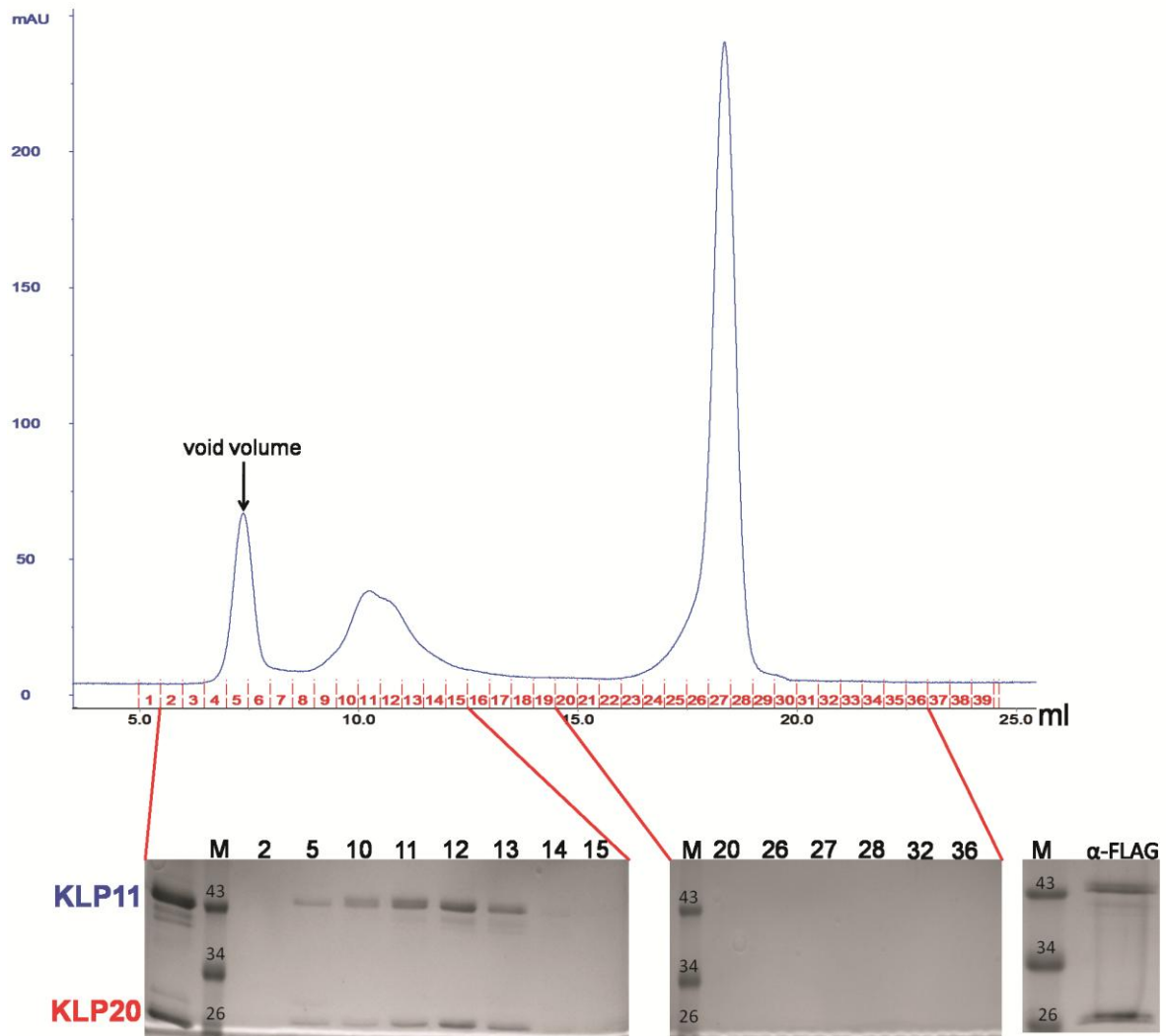


Figure 18: Size exclusion chromatography of KLP11/20-C reveals its heterodimeric state. Both interacting partners are always present in a 1:1 molar ratio. Presence of monomeric or even homodimeric KLP11 or KLP20 could not be detected. The same result was published for wild type KLP11/20 (Brunnbauer et al., 2010) demonstrating the high specificity of heterodimerization. Purifying pooled fractions 11 and 12 via FLAG-tag (Flag-KLP20-C; 6xHis-KLP11-C) after gel filtration again delivered a heterodimer with 1:1 molar ratio of interacting partners, thus further underlining the stability and specificity of the heterodimer.

2.1.2 Heterodimerization of KLP11/20 is triggered by a seed located at the C-terminal end of the stalk

Is the N-terminal half of the stalk sequence only an unstable coiled-coil, which can be stabilized by including regions further C-terminal, or is a region in the C-terminal half of the stalk necessary to induce dimerization?

To test possible stabilizing properties of the C-terminal half of the stalk the N-terminal pair of KLP11-N¹⁻⁴⁴⁹ and KLP20-N¹⁻⁴⁴³ was systematically extended

Results

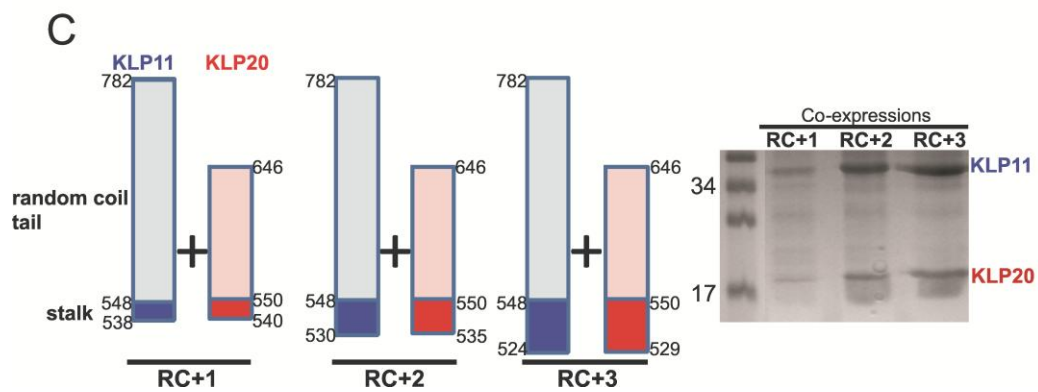
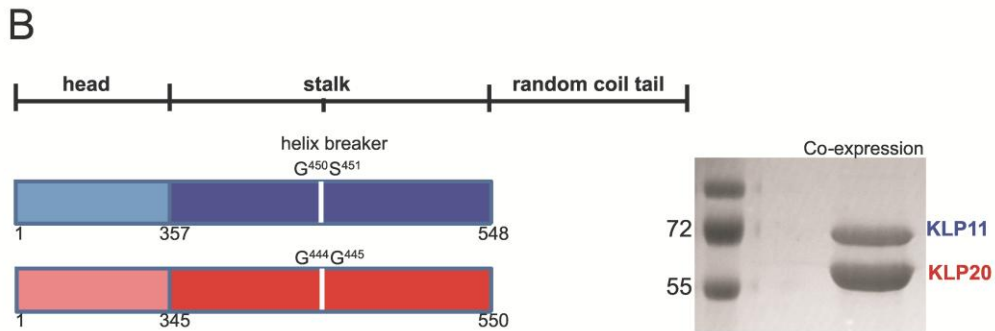
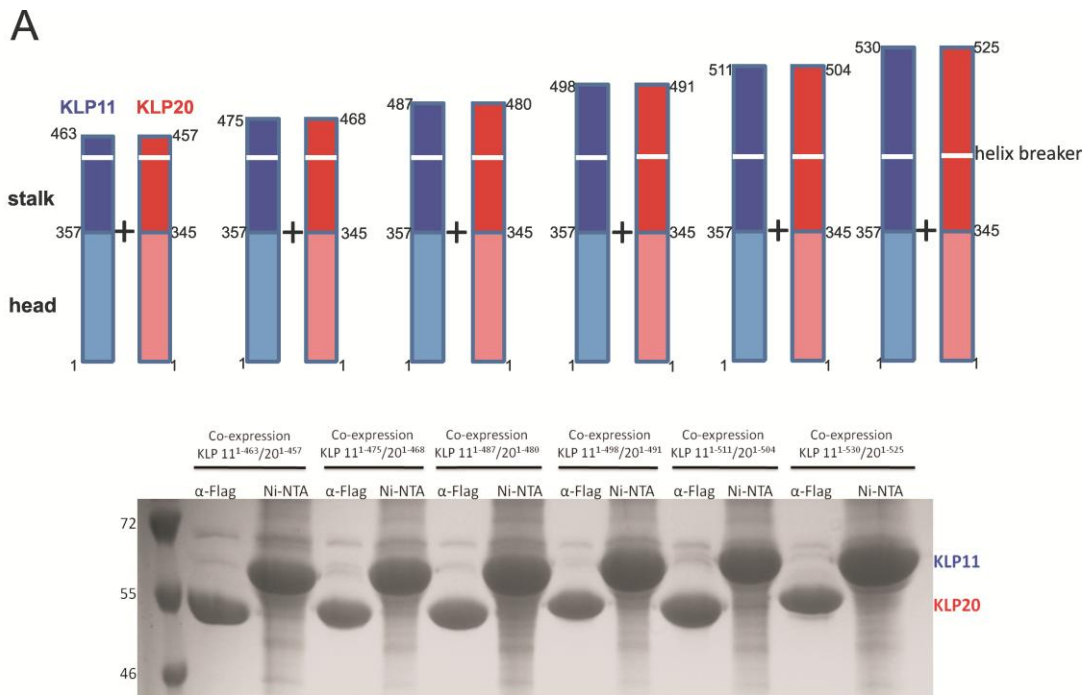
towards the C-terminus. In six consecutive steps these constructs were elongated by adding sets of at least 12 amino acids up to a chain length of KLP11-N¹⁻⁵³⁰ and KLP20-N¹⁻⁵²⁵ (Figure 19A). The longest constructs KLP11-N¹⁻⁵³⁰ and KLP20-N¹⁻⁵²⁵ lack just three predicted heptads of the C-terminal end of the stalk (Figures 6 and 16). Again, none of the extensions led to co-purification (Figure 19A, gel). These findings predict a distant, C-terminal region to be necessary for heterodimer formation.

Including this C-terminal portion of the stalk (amino acids 531-548 yielding KLP11¹⁻⁵⁴⁸ and amino acids 526-550 yielding KLP20¹⁻⁵⁵⁰) led to successful co-purification of both polypeptide chains (Figure 19B). This result demonstrates that the C-terminal tails (KLP11-RC⁵⁴⁸⁻⁷⁸² and KLP20-RC⁵⁵⁰⁻⁶⁴⁶), both predicted to be random coils (RC) (Lupas *et al.*, 1991; Tripet *et al.*, 2000), are not required for heterodimerization. Indeed, co-expressed random coil tails KLP11-RC and KLP20-RC did not form dimers (Figure 20). This leads to the conclusion that the C-terminal end of the stalk (i.e., KLP11⁵³⁰⁻⁵⁴⁸ and KLP20⁵²⁵⁻⁵⁵⁰) includes a trigger without which heterodimer formation of the full-length KLP11/KLP20 motor is not possible.

To test whether this C-terminal region of the stalk is sufficient to form dimers on its own, and in an attempt to define the shortest sequence that is sufficient for dimerization, the random coil tails KLP11-RC⁵⁴⁸⁻⁷⁸² and KLP20-RC⁵⁵⁰⁻⁶⁴⁶ were elongated by, respectively, 10, 18, and 24 amino acids of the stalk towards the N-terminus (Figure 19C). These roughly correspond to the last one, two or three heptads of the stalk. Accordingly, these constructs were named RC+1, RC+2, and RC+3.

While KLP11-RC⁵⁴⁸⁻⁷⁸² and KLP20-RC⁵⁵⁰⁻⁶⁴⁶ did not dimerize (Figure 20), their elongation by merely 10 amino acids towards the N-terminus (RC+1) already led to co-purification, as did RC+2 and RC+3 (Figure 19C). Thus, surprisingly, merely 10 amino acids of the C-terminal end of the stalk are sufficient to act as a seed for heterodimerization, requiring neither the preceding nor the following amino acids.

Results



Results

Figure 19: The C-terminal end of the stalk is essential for KLP11/20 dimerization. (A) The N-terminal halves of KLP11 and KLP20 in Figure 17A were elongated in six steps to include increasing numbers of residues from the stalk region. None of these extensions resulted in co-purification of the co-expressed partners (gel). To exclude the possibility that lack of protein expression is responsible for the obtained results, for each case the cell lysate was divided in two equal parts for Ni-NTA and α -Flag purification, respectively, to demonstrate that both polypeptides were expressed properly. Marker protein sizes are shown in kDa. (B) Dimerization takes place only if the entire stalk region is included as shown schematically on the left panel. The right panel shows the successful co-purification of KLP11-6xHis with KLP20-Flag via anti-Flag. (C) An elongation of the random coil tails (RC) towards the N-terminus by merely 10 residues is sufficient for co-purification via anti-flag. Numbers correspond to the amino acid positions in the full-length chain. The identities of all protein bands were confirmed by mass spectrometry (LC-MS/MS). Marker protein sizes are shown in kDa.

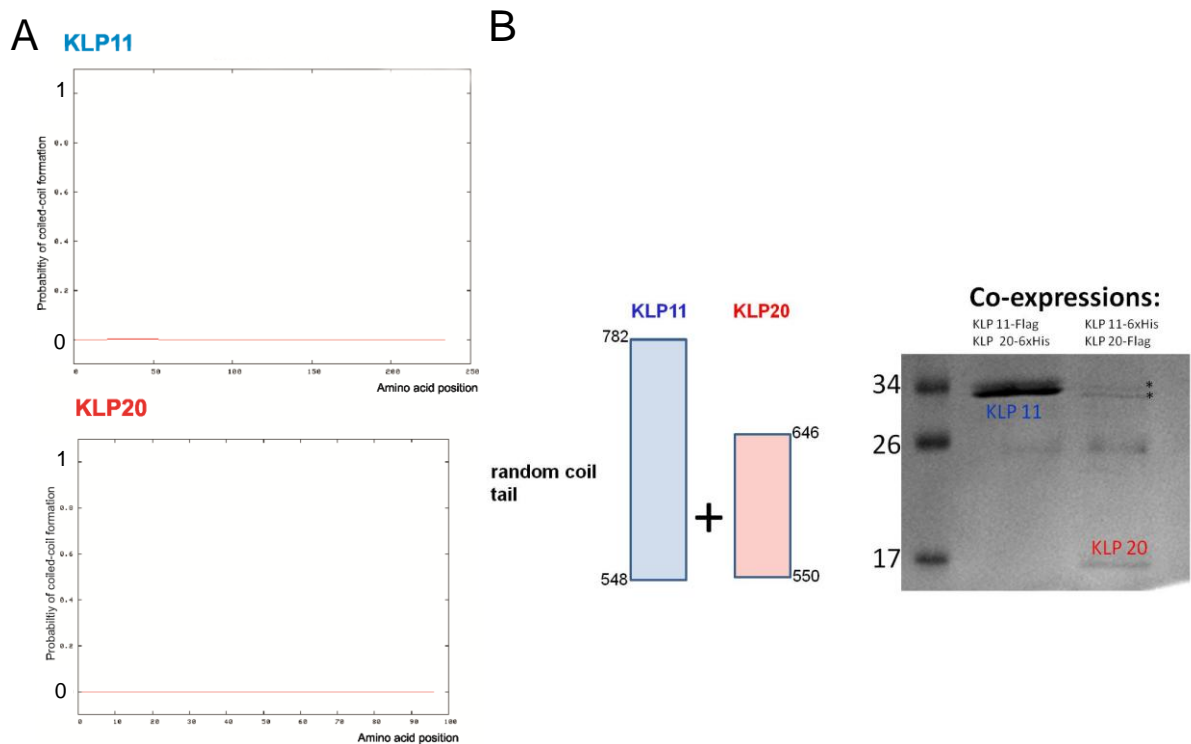
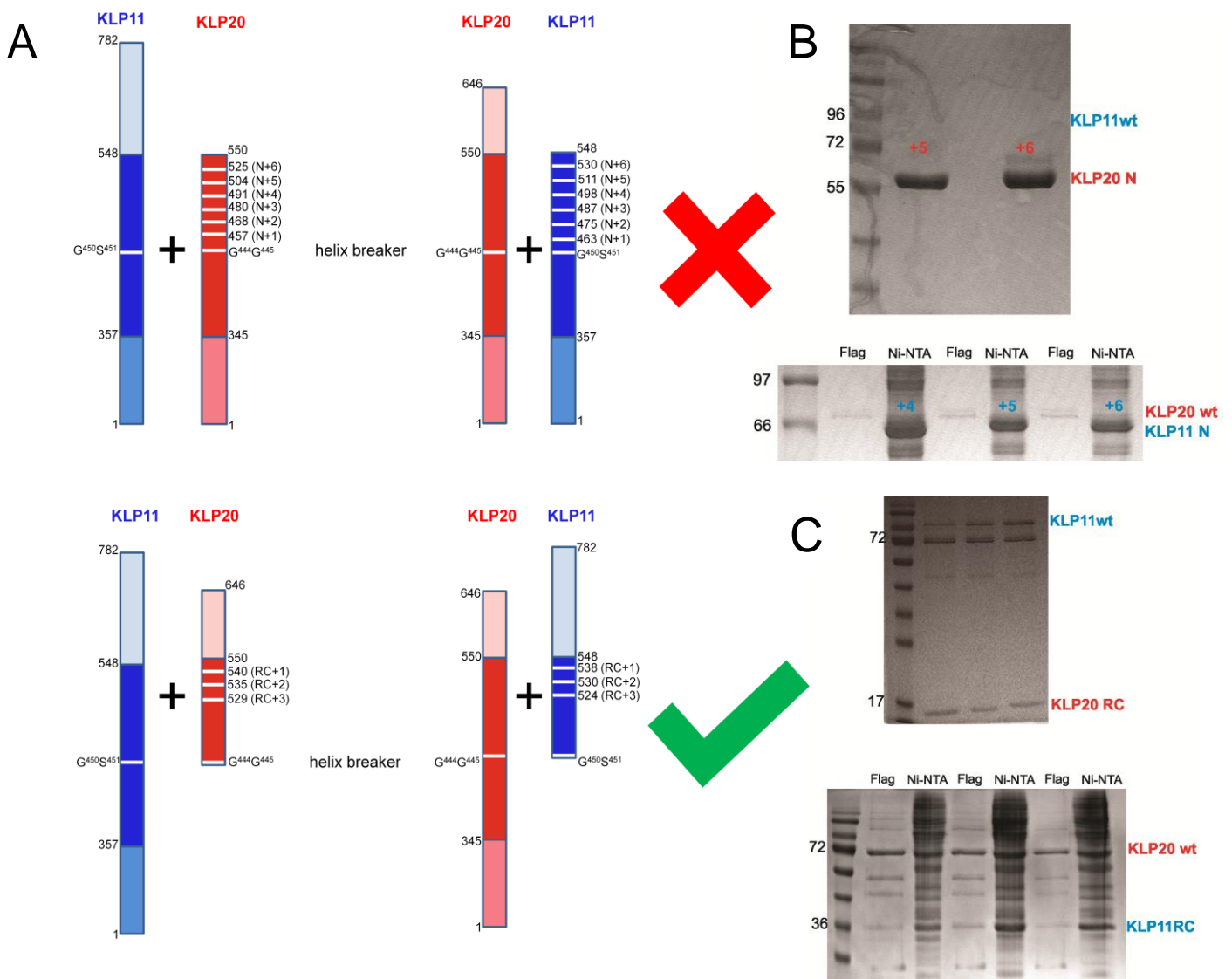


Figure 20: Random coil tails do not dimerize. (A) The probability of the C-termini of KLP11 (upper panel) and KLP20 (lower panel) to form a coiled-coil is predicted to be zero (COILS, Lupas *et al.*, 1991). (B) According to the coiled-coil predictions none of the attempts to co-purify the co-expressed random coil tails from the cell lysate were successful. The identity of all protein bands was confirmed by LC-MS/MS (*=keratin). Marker protein sizes are shown in kDa.

Results

2.1.3 Full-length partner cannot compensate for the C-terminal truncation in the other motor

All truncated constructs were combined with their respective full-length (FL) partner in asymmetric co-expression and co-precipitation experiments (Figure 21A). Again, all N-terminally truncated constructs still containing the C-terminal end of the stalk dimerized with their FL partner despite different length of the interacting partners (Figure 21C). None of the C-terminally truncated constructs formed an asymmetric dimer with their FL partner (Figure 21B), confirming the necessity of the C-terminal end of the stalk for dimerization. It must be provided in both interacting partners since no length of the partner stalk can compensate the missing end. This short sequence of only 10 amino acids is thus the seed for heterodimerization of KLP11 and KLP20, and is absolutely necessary to induce coiled-coil formation.



Results

Figure 21: Asymmetric co-expressions of kinesin-2 variants. A wild-type motor chain was co-expressed with each truncation variant of the partner chain. (A) Full-length wild type motors are depicted separately as linear maps with indicated domains and the helix breaker position. In the upper panel all C-terminal truncations are presented in one linear map each for KLP 11 (blue) and KLP 20 (red). The elongations of KLP11/20-N are shown as white lines with the ending amino acid position and named N+1 to 6. None of these co-expressions led to co-precipitation of the partner (red cross and gels in (B)). The lower panel depicts the elongations of the random coil tail in a single linear map. Starting positions are represented by a white line and named RC+1 to 3. Each of the N-terminally truncated variant was successfully co-precipitated with its full-length partner (green sign and gels in (C)). (B) The upper gel shows representative co-purifications of full-length wild type 6xHis-KLP11 with the two longest variants of C-terminally truncated Flag-KLP20 (N+5 (+5) and N+6 (+6)). Flag-purification delivered KLP20 bands but no KLP11 band, the expected position of which is depicted by “KLP11 wt” next to the gel. The lower gel shows representative co-purifications of full-length wild type Flag-KLP20 with the longest variants of C-terminally truncated 6xHis-KLP 11 (N+4 to 6). Tandem purification again shows that no heterodimer formation occurs. (C) The upper gel shows the co-immunoprecipitation of the full-length wild type KLP11 with RC-elongations of KLP20. In the lower gel the tandem purification (Flag and Ni-NTA) of the full-length wild type KLP20 with RC-elongations of KLP11 is depicted. In both cases heterodimers could be isolated underlining the importance of the end of the stalk and that the dimerization seed consists of this part of the chain in both interacting partners. In (B) and (C) numbers on the left edge of the gels represent protein marker sizes in kDa.

2.1.4 Kinesin Associated Protein (KAP) binds only to KLP11

The C-terminal part of the motor is not only necessary for dimerization, but is also supposed to be the binding site of the third subunit of the complex, kinesin associated protein (KAP). Co-immunoprecipitation experiment with Flag-tagged KLP20 and 6xHis-tagged KLP11 and KAP revealed that the KLP11/20 C-terminal dimer was sufficient for KAP binding (Figure 22A). To test whether the dimerized state of motor tails is a prerequisite for interaction with KAP, KAP was co-expressed with differently tagged KLP11-C and KLP20-C, respectively. The pull-down of Flag-tagged motor tail and 6xHis-tagged KAP revealed that not only no dimerization of tail domains is required, but also that KAP solely binds to KLP11-C (Figure 22B), which is 100 amino acids longer at the C-terminus than KLP20-C (Figure 6).

Results

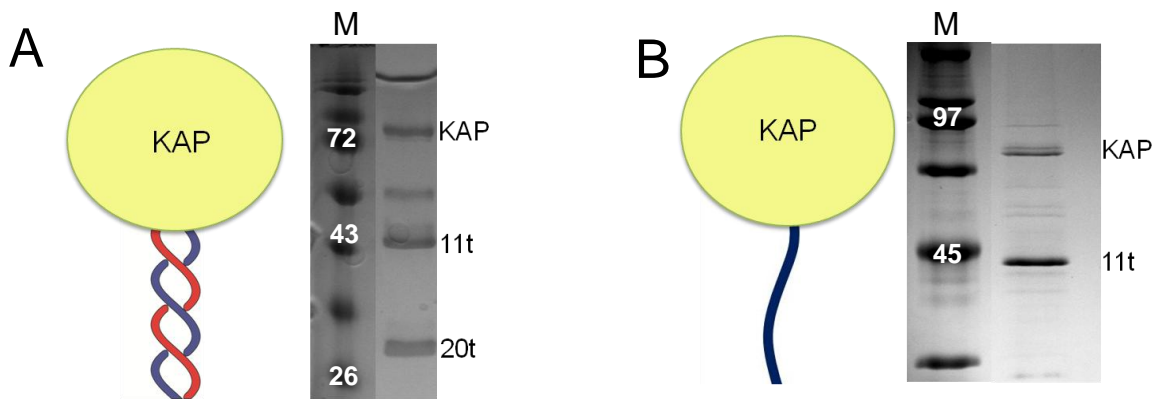


Figure 22: KAP binds to the C-terminal half of KLP11. (A) Co-expression of KAP with the C-terminal half of kinesin-2 led to successful trimer formation. The complex was isolated by Flag-purification using Flag-KLP20-C and 6xHis-KLP11-C and 6xHis-KAP. (B) Co-expressing 6xHis-KAP with each motor chain half (Flag-tagged) separately showed that KAP binds only to KLP11-C. Protein marker sizes (M) are in kDa.

To further investigate if KAP binds to the random coil tail or the C-terminal half of the stalk in KLP11, KAP was co-purified with the KLP11 random coil (RC) tail (construct nr. 23 in the list of constructs, page 89) and the C-terminally truncated motor lacking the random coil KLP11¹⁻⁵⁴⁸ (construct nr. 5), respectively. Figure 23 shows KAP interaction only with the RC tail. Binding of KAP to this domain of KLP11 can be an explanation for its larger size compared to the corresponding region of its partner motor KLP20.

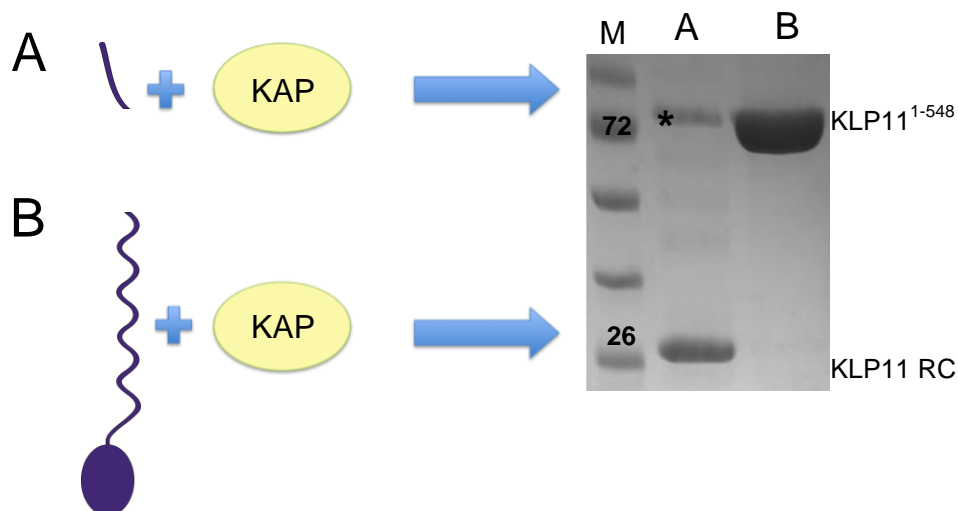


Figure 23: KAP binds to the random coil tail of KLP11. To determine whether KAP binds to the random coil tail or to the C-terminal part of the stalk KAP was co-expressed with KLP11-RC (A) and KLP11 no RC (KLP11¹⁻⁵⁴⁸, (B)), respectively. Whereas 6xHis-KAP was pulled down by Flag-KLP11-RC (lane A in the gel, KAP indicated by an asterisk), no co-purification of 6xHis-KAP occurred with Flag-KLP11¹⁻⁵⁴⁸ (lane B in the gel). Because of the similar sizes of KAP and KLP11¹⁻⁵⁴⁸ the upper border of the protein band was analyzed by LC-MS/MS but no KAP was detected. Protein marker sizes are in kDa.

Results

Looking at KLP11 RC tail more closely and comparing it with kinesin-2 orthologues from *Chlamydomonas*, sea urchin and mouse, a short motif in the middle of the random coil tail appeared to be somewhat conserved among species (T-Coffee 8.93). It was intriguing to test whether this short sequence (construct nr. 39) was the actual interaction site with KAP. Furthermore, KAP was also truncated to include only the Armadillo-repeats (Figure 6, construct nr. 38). Successful co-immunoprecipitation showed that the small region from the KLP11 RC tail and the Armadillo-motif in KAP are indeed sufficient for interaction of these two binding partners (Figure 24). Neither the N-terminal, nor the C-terminal end of KAP is necessary for the interaction with the motor.

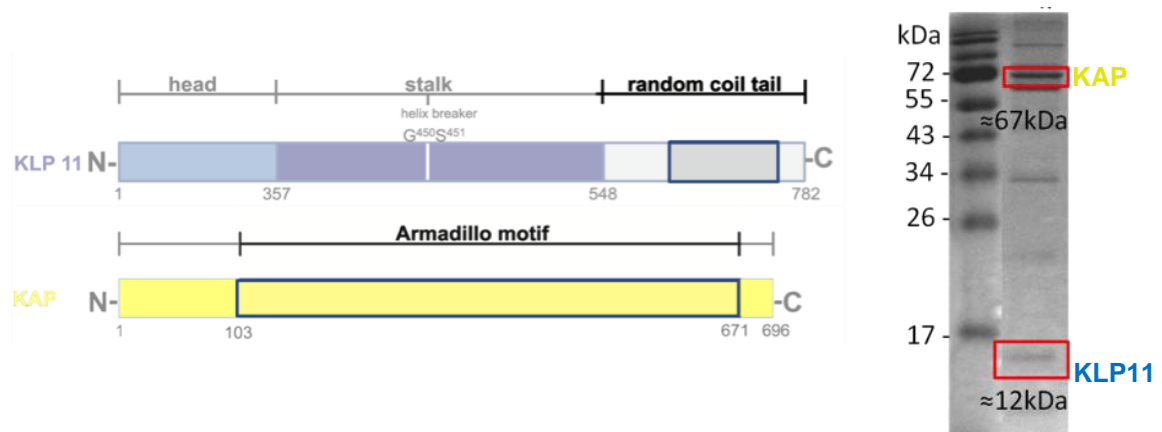


Figure 24: Small conserved region in the random coil of KLP11 and the Armadillo-motif in KAP are sufficient for interaction. The identity of protein bands from the gel was confirmed by LC-MS/MS.

2.2 Transmission electron microscopy of the wild type kinesin-2 reveals an extended coiled-coil

The pull-down experiments demonstrated the necessity of the C-terminal end of the stalk to induce coiled-coil formation between KLP11 and KLP20. Moreover, the N-terminal halves of the prospective dimerization domains of these two heterodimer partners cannot form a complex on their own. These results raise questions about the extent of coiled-coil formation in the wild-type KLP11/KLP20 heterodimer and its consequences for the structural organization of kinesin-2. Is the seed the sole dimerization site, leaving the heads hanging on the undimerized N-terminal portions of the stalk? This is a tempting speculation considering the inability of C-terminally

Results

truncated constructs to dimerize. Or does the seed trigger the formation of a coiled-coil along the entire stalk, bringing the heads into close proximity? Completely dimerized stalks are generally considered characteristic for kinesins. The coiled-coil length and the degree of flexibility of the heads would certainly affect the stepping behavior of the motor, therefore transmission electron microscopy (TEM) should clarify the molecular structure of the KLP11/KLP20/KAP heterotrimer. If the entire stalk dimerizes, the two heads are expected to be found in close proximity to each other.

For this experiment all three wild type protein subunits, KLP11, KLP20 and the accessory subunit, KAP, were co-expressed in Sf9 cells. A Flag-tag at the C-terminus of KLP20 was used to pull down a trimeric complex from the cell lysate in the subunit ratio of 1:1:1 and very high purity (Figure 25, right panel).

TEM shows two globular domains at one end of a rod-shaped structure and a single globular domain at the other (Figure 25, left panel). The calculated (Image J) overall length is $56.31 \text{ nm} \pm 5.9 \text{ nm}$ ($n=183$), which is in good agreement with values of other orthologues (Kondo *et al.*, 1994; Yamazaki *et al.*, 1995; Wedaman *et al.*, 1996). The two globular subunits and the single globular domain appear to be connected by a single thin shaft that possesses a certain degree of flexibility. Our micrographs thus indicate the presence of a coiled-coil structure along a significant portion of the stalk, which brings the two globular domains into proximity of $10.9 \text{ nm} \pm 1.79 \text{ nm}$ as measured between the centers of the globular domains.

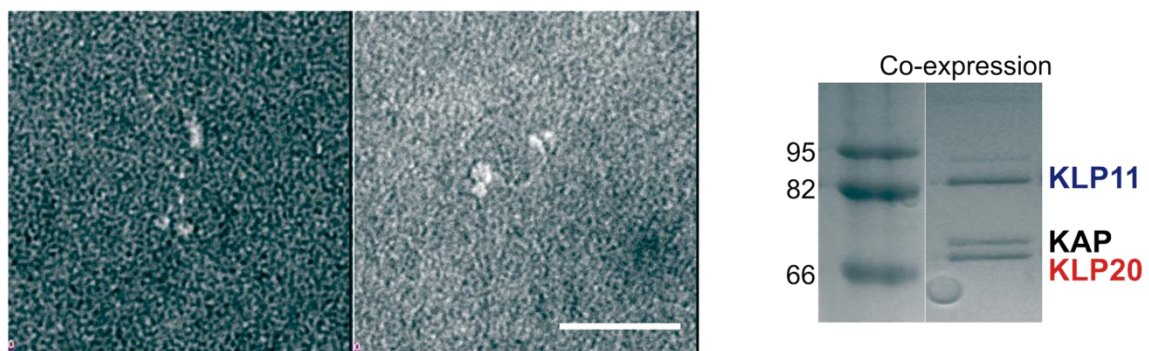


Figure 25: Transmission electron microscopy indicates a long stalk and motor heads in close proximity. The micrograph shows representative images of the KLP11/20/KAP trimeric complex ($n=183$). Quantification of recorded particles delivered a motor length of $56.31 \text{ nm} \pm 5.9 \text{ nm}$ and an average distance between the centers of the motor domains of $10.9 \text{ nm} \pm 1.79 \text{ nm}$. Bar, 50 nm. Right panel shows the pull-down of the heterotrimeric complex used for TEM recordings via the Flag-tagged KLP20 polypeptide chain.

Results

However, TEM is a relatively low-resolution method to assess the integrity of a coiled-coil and surface interactions may affect the overall integrity of the protein. Therefore a sensitive, solution-based spectroscopy was next applied to interrogate the molecular anatomy of the KLP11/20 stalk.

2.3 FRET analysis confirms the close apposition of the two heads when the full-length stalk is present

Förster resonance energy transfer (FRET) was used as a molecular nanoscale to determine whether the heads are indeed brought into close proximity by stalk dimerization over the whole length, as suggested by TEM. To this end, the wild type motor domains were replaced by either cyan (donor) or yellow (acceptor) fluorescent protein (CFP or YFP) (Figure 27). This FRET pair is ideal for two reasons. First, an efficient FRET signal is obtained if the fluorophores are less than 10 nm apart (Wu and Brand, 1994; Lakowicz, 1999; Shaner *et al.*, 2005; Shaner *et al.*, 2007), which is the expected distance of the two heads if the stalk forms an extended coiled-coil (see TEM results 2.2). Second, the dimensions of the fluorophores are similar to the actual size of the kinesin heads. The KLP11 head was replaced by YFP (KLP11-YFP) and the KLP20 head by CFP (KLP20-CFP) (Figure 27). The presence of two different affinity purification tags on the two polypeptide chains (KLP20-CFP-6xHis-tag and KLP11-Flag-tag) allowed the purification of heterodimers in a 1:1 ratio (Figure 26).

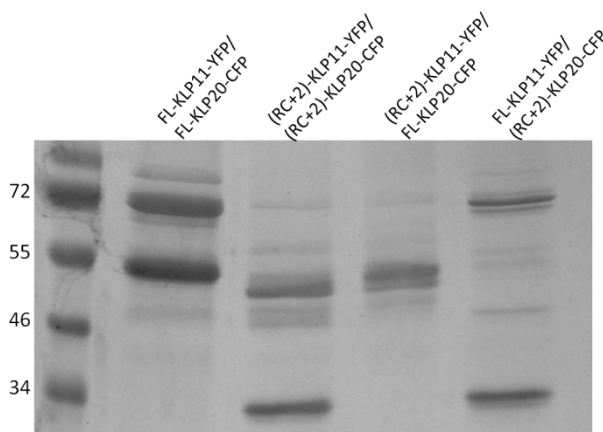


Figure 26: Co-expression of the FRET constructs. Differentially tagging KLP11 and KLP20 FRET-constructs (Flag-tag and 6xHis-tag, respectively) enabled dimer purification in a 1:1 molar ratio. FL-KLP11-YFP/FL-KLP20-CFP comprises the entire stalk; (RC+2)-KLP11-YFP/(RC+2)-KLP20-CFP serves as a positive control; (RC+2)-KLP11-YFP/FL-KLP20-CFP and FL-KLP11-YFP/(RC+2)-KLP20-CFP serve as negative controls. Marker protein sizes are shown in kDa.

Results

Depending on the extent of the coiled-coil, the following predictions can be made: If the coiled-coil starts at the C-terminal end and zips up the entire stalk, the two fluorophores at the N-terminus will be placed in close proximity, allowing FRET to occur. If however, coiled-coil only forms at the C-terminal end of the stalk, FRET will be highly unlikely. Indeed, a clear FRET signal for full-length KLP11/20 could be obtained (Figure 26, bottom panel).

As a positive control served a fusion construct of the fluorophores with the RC+2 pair, where due to its short dimerization sequence of 18 amino acids (Figure 19C) the fluorophores must be within FRET distance. RC+2 was used rather than RC+1 because of its greater stability and greater yield after purification. This construct also displays an unambiguous FRET signal (Figure 26, middle panel).

For generating a negative control the ability of asymmetric dimerization of full-length and an N-terminally truncated partner was exploited (Results 2.1.3, figure 21). The negative control was a dimer consisting of full-length KLP11-YFP and KLP20-RC+2 linked to CFP. This pair dimerizes via the seed sequence at the C-terminal end of the stalk, but the two fluorophores are placed too far apart (> 20 nm) for FRET to occur (Figure 26, top panel).

After determining FRET efficiencies, approximate FRET distances were calculated (Methods 2.4.2) to be 4.6 nm in the positive control and 4.95 nm in the full-length construct. No distance information for the negative control could be calculated due to the lack of a FRET signal. The lack of a positive FRET signal is explicable given the motor's overall length of 50 nm. With a fluorophore size of 5 nm (Shaner *et al.*, 2007) the distance between the two fluorophores is expected to be over 20 nm. Taken together, these findings demonstrate that the coiled-coil must encompass a stalk domain large enough to place the motor heads within a distance of between 3 nm and 8 nm, a distance range for sensitive FRET measurements with CFP and YFP (Kalab and Soderholm). These results confirm the conclusions drawn from the TEM analysis, which suggested close proximity of the head domains in the full length KLP11/20 heterodimer (Figure 25).

Results

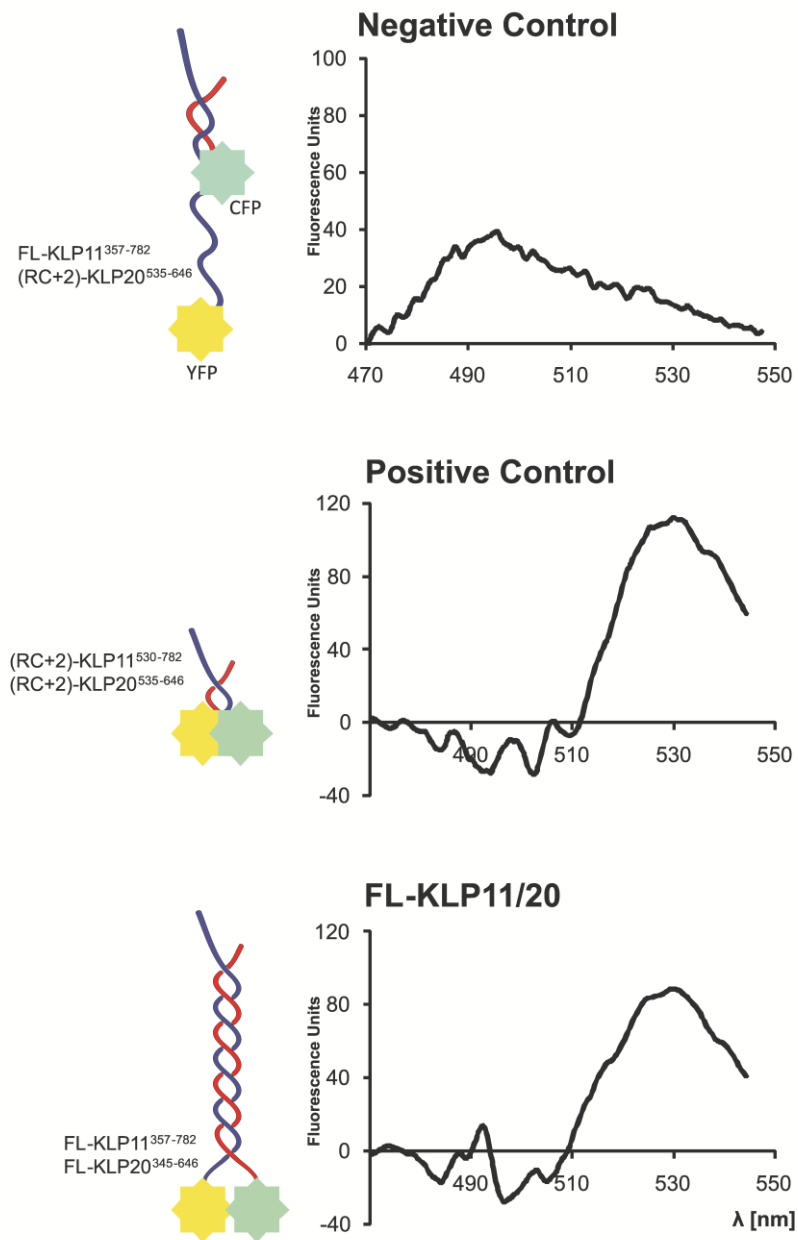


Figure 27: FRET analysis confirms the close proximity of the motor heads in wild type kinesin-2. Curves represent net FRET signal obtained after subtracting signals obtained with only one fluorophore (YFP or CFP) in the CFP channel (which is also the FRET channel) from the signal obtained with the FRET-pair (KLP11-YFP/KLP20-CFP) in the CFP channel. When excited with 435nm CFP transfers energy to YFP (excitation wavelength 505nm), which then emits with a maximum at 530nm. FRET signal is thus visible as a peak at 530nm. Due to the large separation of the fluorophores in the negative control (FL-KLP11/(RC+2)-KLP20) the curve represents only the remainder of the CFP emission spectrum and no maximum at 530nm. Positive control (RC+2)-KLP11/20 and FL-KLP11/20 both display FRET signals at 530nm. After determining FRET efficiencies, distances between CFP and YFP were calculated to be 4.6 nm in the positive control (RC+2)-KLP11/20 and 4.9 nm in FL-KLP11/20. FL=full length, RC=random coil tail.

2.4 Circular dichroism spectroscopy gauges the extent of stalk formation

2.4.1 Coiled-coil content grows with growing chain length

To quantify the α -helical content in the stalk, constructs of different lengths were examined by circular dichroism (CD) spectroscopy. For measurements of the full-length dimer the globular motor domains were removed, leaving the stalk and the RC tail (constructs nr. 7 and 8, page 89). Other constructs analyzed were KLP11/20-C and RC+1 and RC+2 dimers (Figure 28).

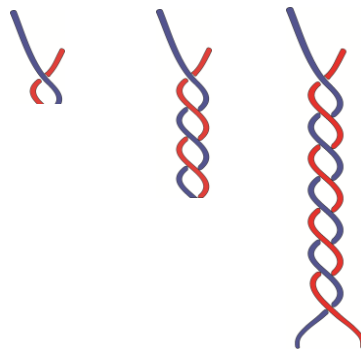


Figure 28: Constructs for CD analysis. Analyzing kinesin-2 constructs of increasing length in monomeric and dimeric state by circular dichroism spectroscopy shall quantify the part of the stalk involved in coiled-coil formation, as well as give answers whether homodimers can form. (RC+1)-KLP11/20 and (RC+2)-KLP11/20 are both represented by the shortest dimer since they differ in length only slightly (by 8 amino acids). KLP11/20-C (dimer in the middle) is expected to show significantly more secondary structure than the RC-constructs because of its increase in chain length. Further increase of signal in the case of the longest dimer would confirm the TEM and FRET results. Heads were removed to avoid dilution of the coiled-coil signal.

The CD spectra were evaluated for double minima at 208 nm and 222 nm and a maximum at 190 nm, features characteristic of an α -helix (Chen *et al.*, 1972; Chen *et al.*, 1974; Cooper and Woody, 1990). Interestingly, despite more than 90 % of random coil, the small percentage of α -helical content in the RC+1 and RC+2 heterodimers was still detectable, and the predicted α -helical content (in percent and amino acid residues) from the CD spectra closely matched the prediction based on sequence analysis (Figure 29A, Table 3). More importantly, the comparison of the absorption characteristics between the RC+1 to RC+2 constructs shows a

Results

significant increase in the stability of the coiled-coil, a result that corroborates the pull-down experiments (Figure 19C). Not only the minimum at the shorter wavelength shifts towards 208 nm, indicating a transition from a random coil (negative band minimum at 197 nm) to an α -helix, but also the value at 222 nm decreases significantly (Chen *et al.*, 1974). This suggests once more that although a certain length is necessary for stable dimerization, it is not more than approximately two heptads.

Comparison of the CD spectra of full-length KLP11/20 and KLP11/20-C offers interesting insights into the stability of the coiled-coil in the N-terminal half of the stalk. If this region forms a stable coiled-coil higher amplitudes are expected (indicative of more secondary structure) of the extrema in the full-length KLP11/20 spectrum, because the coiled-coil in this dimer is twice as long as that of KLP11/20-C. Strikingly, however, there is no apparent difference in the α -helical content in these two dimers (Figure 29B), although full-length KLP11/20 is 100 amino acids longer than KLP11/20-C (Table 3). The number of predicted α -helical residues calculated from CD spectra is identical for both dimers (Table 3). However, in the KLP11/20-C pair the prediction (in percent and number of residues) exceeds the actual number of residues of its stalk portion by 70 amino acids (Table 3). Conversely, the CD spectrum of KLP11/20 predicts a coiled-coil that is shorter by 30 amino acids than the actual stalk sequence. Also the $[\theta]_{222}/[\theta]_{208}$ ratio, which is indicative of coiled-coil content (Zhou *et al.*, 1992; Muhle-Goll *et al.*, 1994), is higher for the KLP11/20-C pair than for full-length KLP11/20 (Table 3). However, FL-KLP11/20 delivered a FRET signal, meaning that the N-terminal half of the stalk must form a coiled-coil at least transiently in order to bring the fluorophores within the 5 nm distance. Furthermore, the missing 30 amino acids correspond in the coiled-coil prediction (Figure 16) prediction to approximately half of the N-terminal part of the stalk. Considering the FRET and CD results together, it is tempting to speculate that transitions between the coiled and uncoiled state happen in this part of the stalk.

Results

2.4.2 FL-KLP11/20 is not thermodynamically more stable than KLP11/20-C

If the N-terminal half of the stalk forms a stable coiled-coil, then FL-KLP11/20 is supposed to be more thermally stable than KLP11/20-C. To test the thermal stability of the two dimers melting curves were recorded by following the change of $[\theta]_{222}$. The melting temperature, T_m , is comparable for both constructs (FL-KLP11/20 $T_m=39.6$ °C; KLP11/20-C $T_m=39.14$ °C) (Figure 29C), indicating no substantial gain in thermal stability in the full-length dimer and again suggesting that the N-terminal half of the stalk forms a somewhat less stable or a transient coiled-coil.

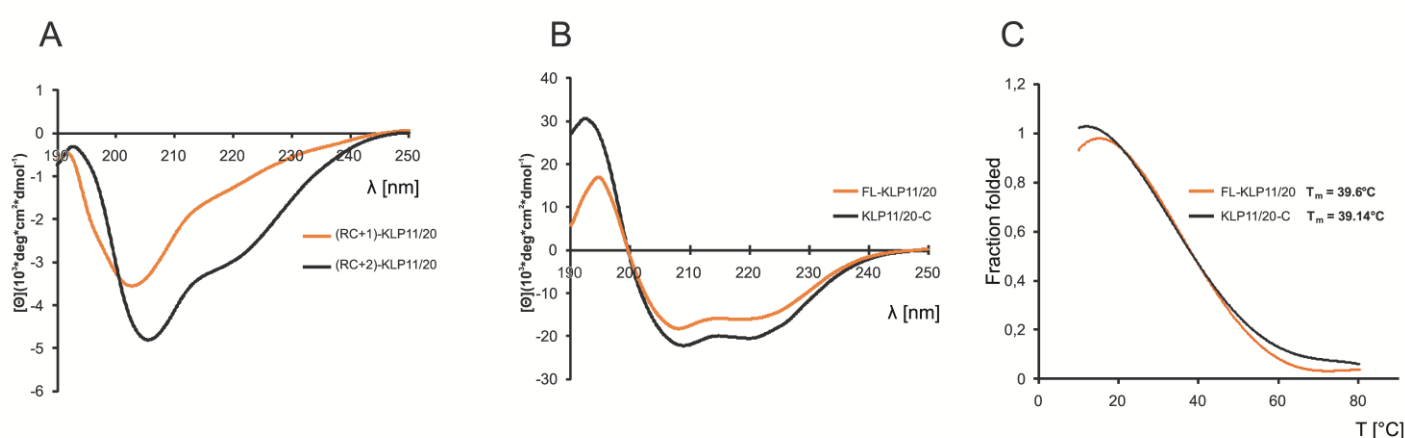


Figure 29: CD spectroscopy indicates an increasing coiled-coil fraction with growing chain length under native conditions. (A) Spectra of (RC+1)-KLP11/20 and (RC+2)-KLP11/20 are dominated by a random coil morphology (minimum at 195 nm) due to a low α -helical content. Note the increase in coiled-coil stability from RC+1 to RC+2 achieved with only eight more amino acids. Not only the first minimum shifts towards 208 nm, but also the minimum at 222 nm becomes more prominent, both signatures indicative of increasing secondary structure. (B) KLP11/20-C and FL-KLP11/20 show typical spectra of α -helical coiled-coil with double minima at 208 nm and 222 nm and a maximum at 190 nm. (C) Melting curves were recorded by following the change of ellipticity at 222 nm between 10 °C and 80 °C. The fraction of folded protein was calculated as $f_f = ([\theta] - [\theta]_u) / ([\theta]_n - [\theta]_u)$, where $[\theta]_n$ and $[\theta]_u$ represent the ellipticity values for the fully folded and fully unfolded species, respectively, and $[\theta]$ the observed ellipticity at 222 nm at any temperature. The comparable melting temperatures for KLP11/20-C and FL-KLP11/20 indicate low stability of the coiled coil in the N-terminal half of the stalk.

2.4.3 KLP11 and KLP20 do not homodimerize

The stalks of KLP11 and KLP20 are coiled-coil forming α -helices, so the question arises whether the motor subunits also homodimerize. To test this, FL-KLP11, FL-KLP20, KLP11-C and KLP20-C were expressed separately and their far UV-spectra analyzed and compared to those of corresponding dimers.

Figure 30 shows that both heterodimers deliver typical coiled-coil spectra with almost equal minima at 208 and 222 nm with $[\theta]_{222}/[\theta]_{208}$ ratios being almost 1 (Table 3). $[\theta]_{222}/[\theta]_{208} = 1$ is characteristic for dimers, which contain 100 % coiled-

Results

coil (Zhou *et al.*, 1992; Muhle-Goll *et al.*, 1994). Deeper minimum at 208 nm than at 222 nm, which leads to $[\theta]_{222}/[\theta]_{208}$ ratio significantly lower than 1 is indicative of a monomeric α -helix population. The latter is the case for the single expressions of the polypeptide chains (Figure 30). Whereas the spectra of heterodimers show $[\theta]_{222}/[\theta]_{208}$ ratios of 0.97 for KLP11/20-C and 0.89 for FL-KLP11/20, those of single expressions are 0.68 for KLP11-C, 0.79 for KLP20-C, 0.69 FL-KLP11 and 0.74 for FL-KLP20. These results indicate that heterodimerization is favoured and that single motor chains stay monomeric in the absence of their dimerization partner.

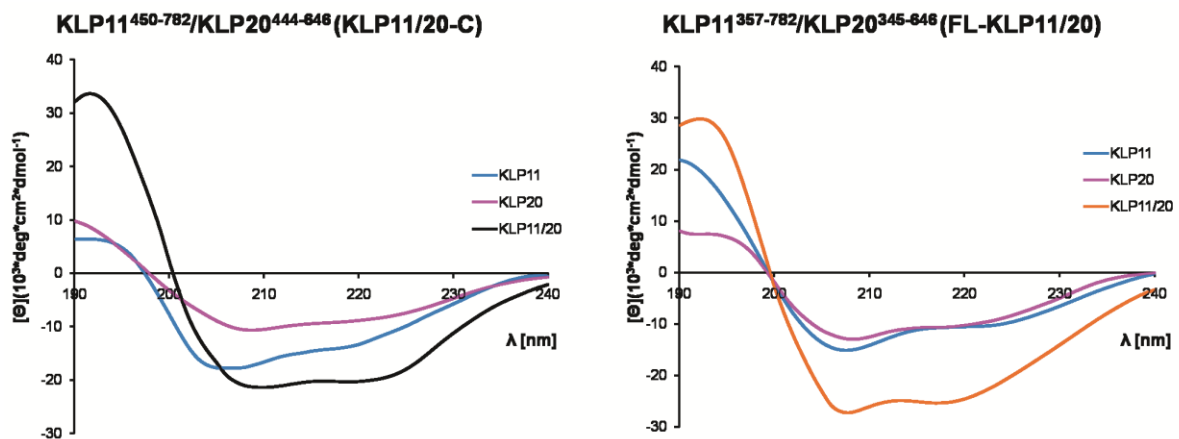


Figure 30: KLP11 and KLP20 prefer hetero- to homodimer formation under native conditions. For both KLP11/20-C and FL-KLP11/20, the spectra show significantly more secondary structure for the heterodimers (higher absorption at 208 nm and 222 nm and higher maximum at 190 nm). In support of spectra, the $[\theta]_{222}/[\theta]_{208}$ ratio, index for coiled-coil content is higher for the heterodimers (0.97 for KLP11/20-C; 0.89 FL-KLP11/20, see Table 3), indicating that motor domains indeed do not form homodimers but remain in monomeric state.

Short monomeric RC+1-3 constructs were unfortunately not stable after the purification and during the measurement, thus it was not possible to obtain spectra that could deliver information on the oligomerization state. But this again demonstrates greater stability of the dimers when co-expressed versus monomers. To exclude that potential KLP11/11 and KLP20/20 homodimers do exist but contain less coiled-coil, resulting in spectra typical of a monomeric α -helix, temperature-dependent CD measurements were performed with dimers and monomers of both lengths, C-terminal half and full length constructs (Figure 28). The denaturation process was followed as described in Methods section 2.4.3. The spectra reveal

Results

one isodichroic point for all the monomers/homodimers but two isodichroic points for both heterodimers (Figure 31), indicating that heterodimers unfold in a 3-state process, while monomers do this in a 2-state process. In monomers the two states are the α -helix and the unfolded protein. The three states in the case of heterodimers are coiled-coil, α -helix and unfolded protein.

Table 3. Summary of circular dichroism analysis

Peptide dimers	Chain length ^a	[θ] ₂₂₂		# of α -helical residues		% of α -helical content		[θ] ₂₂₂ /[θ] ₂₀₈ ^f	
		observed	predicted ^b	included ^c	calculated ^d	included	calculated ^e		
(RC+1)-KLP11/20	253	-1,124	-39,275	10	8	4	3	KLP11-C KLP20-C	0.68 0.79
(RC+2)-KLP11/20	261	-2,790	-39,298	18	18	7	7	KLP11/20-C	0.97
KLP11/20-C	341	-19,885	-39,459	107	172	32	50	FL-KLP11 FL-KLP20	0.69 0.74
FL-KLP11/20	434	-15,727	-39,575	205	172	48	40	FL-KLP11/20	0.89

^a Number of amino acids in KLP11 peptide including tag-residues

^b The predicted molar ellipticity was calculated from the equation [θ]₂₂₂ = -40 x 10³ x (1-4.6/n) (Chen *et al.*, 1974; Gans *et al.*, 1991), where n is the number of residues in the peptide.

^c n = chain length – random coil tail - tag

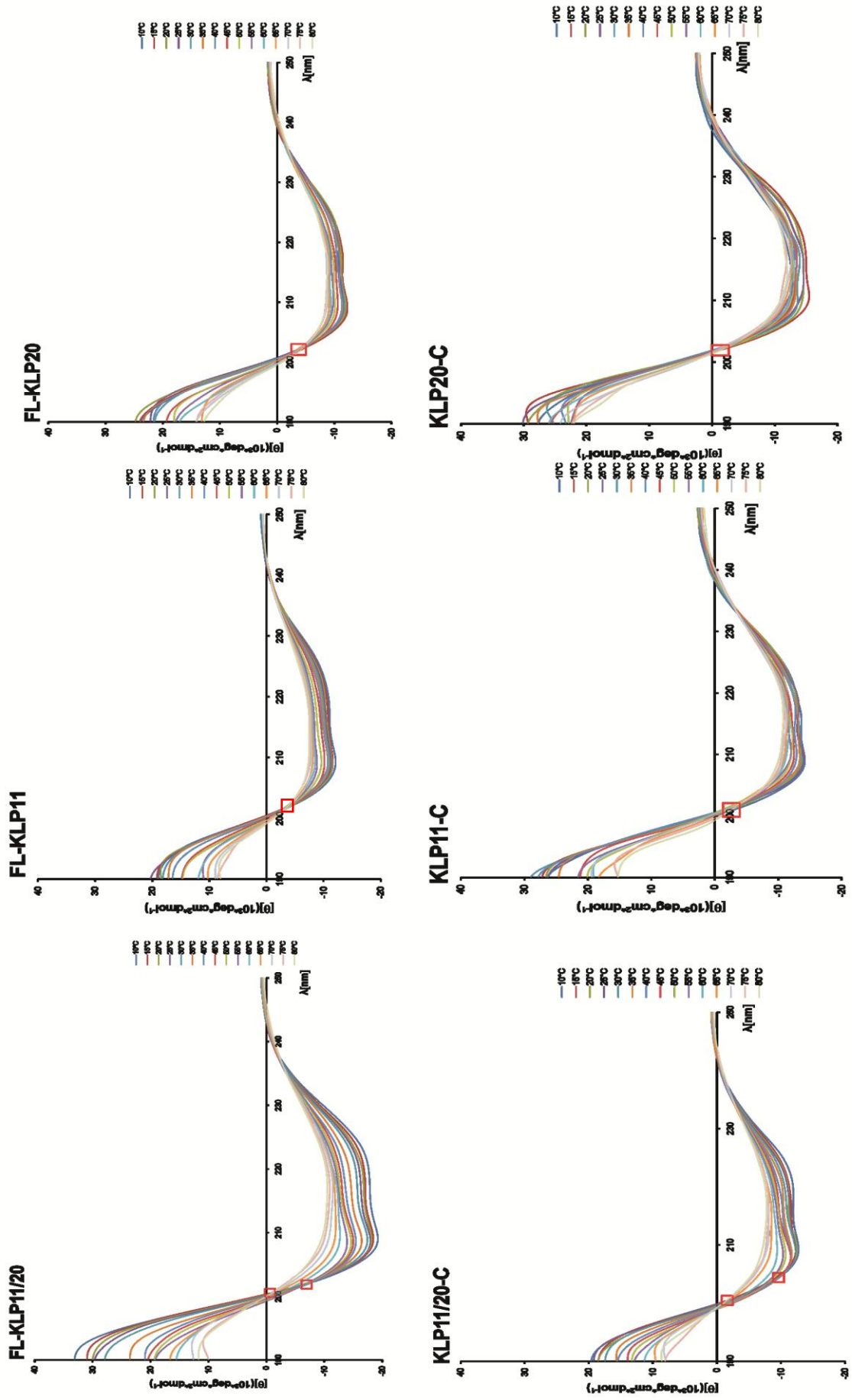
^d The number of helical residues was calculated by multiplying the % of helical content with chain length.

^e The (%) helical content was calculated from the ration of the observed [θ]₂₂₂ value divided by the predicted molar ellipticity(^b) x 100.

^f [θ]₂₂₂/[θ]₂₀₈ ratio >1 is used as an index of coiled-coil formation; the lower the ratio the more single stranded α -helices are contained (Zhou *et al.*, 1992; Muhle-Goll *et al.*, 1994)

Figure 31: Temperature dependent CD measurements of monomeric and dimeric KLP11/20-C and FL-KLP11/20. The samples were heated from 10 °C to 80 °C and spectra recorded every 5°C 5 min after the temperature was reached. While denaturation of monomeric constructs is a 2-state process (one isodichroic point (red square)), heterodimers denaturate in a 3-state process (two isodichroic points). The two states are α -helix and unfolded state; the three states are coiled-coil, α -helix and unfolded state.

Results



Discussion

Heteromeric kinesin-2 is an essential player in a variety of transport processes in the eukaryotic cell, especially in elongated structures. It is a unique member of the kinesin superfamily because it is the only motor to combine three distinct subunits into a functional entity.

One goal of this thesis was to elucidate the regulation mechanism of kinesin-2 catalytic activity. Michaelis-Menten kinetics of different motor truncations show that kinesin-2 can be autoinhibited and that its heteromeric structure is crucial for this process.

Furthermore, the principles of heterodimerization in this unique kinesin were successfully determined providing a more complete understanding of its submolecular structure. The importance of the C-terminal end of the stalk domain came into light, as it is necessary for triggering specific heterodimerization between KLP11 and KLP20.

Dimerization of KLP11 and 20 is, however, not necessary for the binding of the third subunit, KAP. The cargo-binding domain interacts only with a short and somewhat conserved sequence in KLP11 random coil tail via its Armadillo-like domain.

1 Heterodimeric structure is required for autoinhibition

The catalytic activity has to be regulated to avoid futile ATP hydrolysis when the motor is not bound to its cargo. Autoinhibition has been shown to be the regulation mechanism of kinesin-1 (Coy *et al.*, 1999; Stock *et al.*, 1999; Yonekura *et al.*, 2006; Cai *et al.*, 2007; Dietrich *et al.*, 2008; Hackney and Stock, 2008; Hackney *et al.*, 2009; Wong *et al.*, 2009) and kinesin-3 (Lee *et al.*, 2004; Yamada *et al.*, 2007; Hammond *et al.*, 2009). During this process the motor folds, allowing interaction between the tail domain and N-terminal regions, which abolishes ATPase activity. Molecular details of autoinhibition are best studied in kinesin-1. Here one tail domain interacts with both heads after folding at the hinge region in the middle of the stalk domain (Hackney *et al.*, 2009). The tail interacts with both heads and acts as a lock-down that prevents head movement (Kaan *et al.*, 2011).

Discussion

Although there is still no evidence for direct interaction of head and tail domains in kinesin-2, it has been shown that the tail domain is crucial for the regulation of homodimeric kinesin-2 from *C. elegans* and mouse (Imanishi *et al.*, 2006; Hammond *et al.*, 2010). Both, deletion and mutation of the hinge region led to a robustly active motor (Imanishi *et al.*, 2006). The same results were obtained by deletion of the tail domain (Hammond *et al.*, 2010).

This work confirms the role of protein folding in catalytic regulation of heteromeric kinesin-2 indicated by Brunnbauer *et al.* (2010). Furthermore, results here provide an insight into molecular details of the regulation process.

While the wild-type motor is constantly inactive, mutation of its hinge region from G⁴⁵⁰S⁴⁵¹ in KLP11 and G⁴⁴⁴G⁴⁴⁵ in KLP20 to EE in both chains resulted in robust motor activity (Figure 12). Because of its size and negative charge, the glutamate side chain hinders the folding of the heterodimer at the hinge region, thus preventing the head-tail interaction, which explains motor activation. Robust activity was also achieved by deletion of both tail domains in the motor dimer with the wild-type hinge (Figure 12). From these results it can be concluded that heteromeric kinesin-2 is also autoinhibited by its tail by a similar or the same mechanism as in homodimeric kinesin-2.

In contrast to other kinesins in heteromeric kinesin-2 there are two different catalytic units and two different potential inhibitors. Here it could be shown that both tails play a role during inhibition (Results 1.3 and 1.4) but which tail affects which head still remains elusive.

Monomeric heads could not be inhibited by any of the tails (Figure 14, Table 1). This is in accordance with findings in kinesin-1 whose tail binds only weakly to a monomeric head (Hackney *et al.*, 2009). Apparently, the dimeric state of the kinesin-1 heads is necessary for tail binding but the heads need not dimerize via the native neck coiled-coil since any artificial coiled-coil would lead to the same result. The same was found here to be true for kinesin-2. While monomeric heads remained unaffected, artificially homodimerized heads and the EE-mutant were successfully inhibited by addition of the tails (Figure 14, Table 2) albeit the artificially dimerized heads were significantly less prone to inhibition *in trans* by the tails. The reason for this might be a suboptimal tail-to-motor ratio or more probably the absence of the native neck region. Different than Hackney *et al.* (2009), Friedman and Vale (1999)

Discussion

postulated that the inactivation of kinesin-1 requires the native neck region. The neck coiled-coil contains conserved charged residues positioned asymmetrically on its surface, which could serve as a platform for the tail binding. The neck of kinesin-1 also contains conserved residues that destabilize the coiled-coil, indicating that partial melting of this structure may be required for tail-mediated repression of motor activity (Friedman and Vale, 1999). This finding fits the CD analysis of kinesin-2 in this work, which points to lower coiled-coil stability in the neck and the N-terminal half of the stalk, a feature that will be discussed in more detail later on.

That the EE-mutant was most effectively inhibited supports the possible importance of the native neck in this process but its concrete role remains to be determined. On the other hand, the success of EE-mutant inhibition can also be due to the heterodimeric state of the heads. The heterodimer provides an asymmetric conformation for tail binding, which might be essential not only for the head-tail interaction but also for the inhibition outcome. Thus, probably the overall conformation of the folded heterodimer is an important feature of the autoinhibition mechanism.

Taken together, both heads and both tails are required for catalytic regulation. However, the head of KLP11 appears to be the key target, as the KLP11 homodimer successfully pulled down co-expressed tails in the co-IP assay (Figure 15). The two different heads of kinesin-2 were already shown by Brunnbauer *et al.* (2010) to display different characteristics. While full-length kinesin-2 with two KLP20 heads is a processive motor, two KLP11 heads make it unprocessive. Combination of the two heads results in a processive motor. The evolutionary advantage of combining two different motors can thus be the task splitting: while KLP20 accomplishes processivity, KLP11 mediates catalytic regulation.

The same can be concluded for the tails: although both tails are important for inhibition, the key player appears to be the KLP20 tail because it co-precipitated with KLP11 GCN4 head homodimer (Figure 15). The KLP11 tail, on the other hand, was identified here as the KAP binding site, which might be its primary role. Nevertheless, KLP11 tail also clearly plays a role during inhibition. *In trans*, the KLP11 tail alone significantly inhibits the EE-mutant. Thus, KLP20 tail might be essential for the initial binding of the tails to the heads and for the initial steps of inhibition, while KLP11 tail plays a complementary role.

2 Co-factors in kinesin-2 kinetics

The purity of wild type motor dimer purifications indicates that no co-factors, including KAP, are needed for inhibition. Yamazaki *et al.* (1996) showed that KAP does not influence the kinetics of the active kinesin-2. Further, this work demonstrates that effective autoinhibition of the motor is achieved without the KAP subunit (Figure 12).

Whether KAP is still associated with the inhibited motor is not clear but it is intriguing that *in vivo* only 70 % of the KAP were found in complex with kinesin-2 (Yamazaki *et al.*, 1995, 1996). It is thus tempting to speculate that the remaining 30 % dissociated from the inhibited motor and that KAP binding might activate the motor. This effect, however, could not be observed in *in vitro* experiments during this thesis (data not shown) but it cannot be excluded that such activation happens only under *in vivo* conditions because it might require other co-factors or even KAP and/or motor modifications. Supportive findings revealed KAP as a phosphorylation target for different kinases, such as Src tyrosine kinase (Shimizu *et al.*, 1996) and breast tumor kinase, BRK (Lukong and Richard, 2008) during different cell stages (Haraguchi *et al.*, 2006). The phosphorylation takes place in the C-terminal region and is important for cargo binding (Nagata *et al.*, 1998; Haraguchi *et al.*, 2006). It can be speculated that KAP phosphorylation and subsequent cargo binding are required for motor activation.

Phosphorylation was also shown to directly regulate the catalytic activity of other kinesins (Verhey and Hammond, 2009). In the concrete case of heteromeric kinesin-2, a MAP kinase was found to affect motor's behaviour *in vivo*. In *C. elegans*' sensory cilia, dye-filling kinase 5 (Dyf-5) restricts kinesin-2 activity to the middle segment of the cilium, i. e. to the part with the microtubule doublet (Figure 1), (Burghoorn *et al.*, 2007). During this PhD thesis no direct phosphorylation of either of the kinesin-2 subunits by Dyf-5 could be detected (data not shown). It was further speculated that Dyf-5 may phosphorylate tubulin subunits, thus marking the path for kinesin-2 but no tubulin phosphorylation could be detected neither. Since Dyf-5 is a MAP-kinase (Burghoorn *et al.*, 2007) it is probable that the target lies further upstream in the cascade and that this whole cascade rather than Dyf-5 alone influences the kinesin-2 behaviour.

Nevertheless, Dyf-5 seems to inactivate kinesin-2 because the Dyf-5 knockout leads to increased kinesin-2 activity, i. e., the motor then moves along the distal segment of the cilium as well (Burghoorn *et al.*, 2007). An inhibitory effect of MAP-kinase cascade was also observed for kinesin-1 (Verhey and Hammond, 2009).

But how is the autoinhibition released? Is the motor activated simply by cargo binding (Coy *et al.*, 1999), or are there co-factors, that mediate activation after cargo binding to the tail? In kinesin-1 the tail does not bind directly to the cargo but involves co-factors. The binding of such co-factors is sufficient to release the autoinhibition of kinesin-1 (Blasius *et al.*, 2007; Hackney and Stock, 2008). In contrast, when the co-factor of human kinesin-3 binds to the tail, the motor is still inactive. It requires cargo binding for activation to take place (Yamada *et al.*, 2007). How the activation is accomplished in heteromeric kinesin-2, whether KAP binding is sufficient, or whether interaction with cargo must be provided as well, remains to be determined in future experiments and will be best studied *in vivo*.

Since autoinhibition was found to regulate catalytic activity already in three kinesin families (kinesin-1 to 3), it is conceivable that this mechanism has co-evolved with kinesin motors. However, it remains to be seen whether autoinhibition can be found in other kinesin families as well.

3 KAP on top of it

Though the cargo-binding subunit of kinesin-2, KAP, does not influence the motor's catalytic activity (Yamazaki *et al.*, 1996; Zhang and Hancock, 2004), it is indispensable for the proper function of the motor *in vivo* (Sarpal *et al.*, 2003; Mueller *et al.*, 2005; Ou *et al.*, 2007). KAP knockdown leads to severe cell dysfunctions, including aberrant progression of mitosis or elimination of ciliary axonemes from certain neuron types (Sarpal *et al.*, 2003; Haraguchi *et al.*, 2006), and intact KAP protein is essential for kinesin-2 localization to the basal bodies of *Chlamydomonas* flagellae (Mueller *et al.*, 2005).

Here the interaction site of KAP from *C. elegans* with the motor was identified. KAP binds only to the random coil tail of KLP11 via its Armadillo-like domain. Studies on *Drosophila* KAP showed interaction with the stalk for which stabilizing properties were suggested. Further, the importance of the N-terminal end of the KAP sequence

Discussion

for the interaction was demonstrated (Doodhi *et al.*, 2009). Neither of these findings could be confirmed for *C. elegans* KAP. The N- and C-terminally truncated KAP¹⁰³⁻⁶⁷¹ construct containing only Armadillo repeats bound successfully to the middle segment of the KLP11 random coil tail, thus excluding the necessity of both, the N-terminal end of KAP and the stalk domain of the motor. KAP orthologues from sea urchin and mouse also bind only to the tail region (Wedaman *et al.*, 1996; Yamazaki *et al.*, 1996) and there are some indications of the general importance of the C-terminal region (Nagata *et al.*, 1998; Jimbo *et al.*, 2002; Deacon *et al.*, 2003; Lukong and Richard, 2008) rather than the N-terminal end. The C-terminal region of KAP contains conserved sequences and in some orthologues it is tyrosine-rich with consensus sequences for different kinases (Shimizu *et al.*, 1996; Sarpal and Ray, 2002). Beside high tyrosine content, the C-terminal region also contains a conserved phenylalanine, which is critical for KAP function but the exact role is still unknown (Mueller *et al.*, 2005).

However, as shown here the very last 25 amino acids downstream of the Armadillo repeats (Figure 6) in the CeKAP are not required for motor interaction (Figure 24). The interaction with the middle segment of the KLP11 random coil tail is probably facilitated by one of the 9 Armadillo repeats. Whether this region is important for cargo interaction and whether it is modified still has to be determined.

Brunnbauer *et al.* (2010) failed to co-precipitate KAP with KLP11 wild type monomer but were successful in pulling down KAP with KLP11 EE-mutant. This suggests that KAP gets released upon motor folding just like the finding that approximately 30 % of the KAP protein is not bound to the motor dimer under *in vivo* conditions (Yamazaki *et al.*, 1995, 1996). Whether KAP indeed dissociates from the complex upon motor inhibition still needs to be experimentally shown. In general, little is known on how KAP fulfils its function and whether KAP also has a role as dissociated monomer.

As seen so far, random coil tails of KLP11 and 20 are important for the interaction with the cargo binding domain, KAP, and for the autoregulation of catalytic activity. However, the random coil tails do not contribute to dimerization of KLP11 and KLP20 (Figures 19B and 20). Heterodimerization of the two motor chains is carried out merely by their stalk domains.

4 From seed to stalk

This work provides a molecular understanding of how heterodimerization of the motor chains is accomplished in *C. elegans* kinesin-2 (Figure 32).

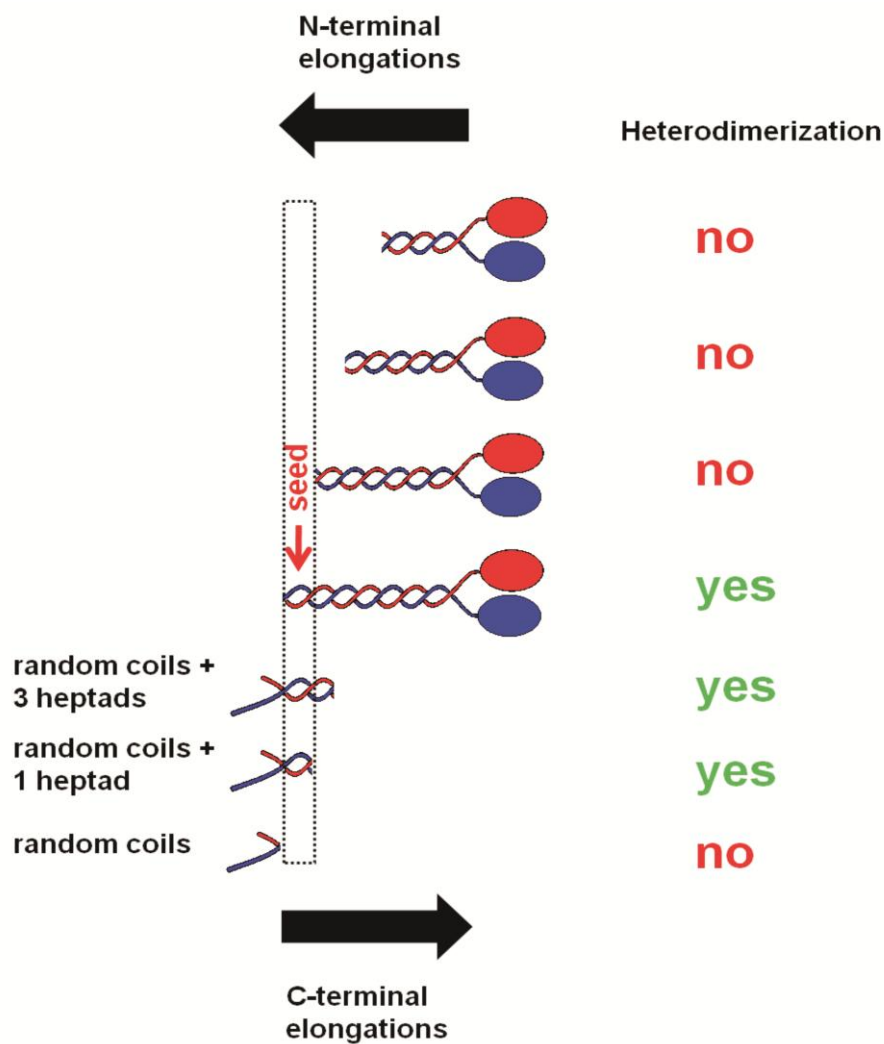


Figure 32: Identification of the dimerization seed by systematic N- and C-terminal elongations of truncated KLP11 and KLP20 polypeptide chains. No dimerization occurs unless the C-terminal end of the stalk is present. C-terminally truncated constructs must thus be elongated to include the entire stalk, whereas elongation of random coil tails by only 10 amino acids already leads to dimerization.

Discussion

According to coiled-coil predictions (Figure 16) the whole stalk domain of both motors is able to form a coiled coil. The same is true for the well-studied kinesin-1 in which the neck domain or fusion to any part of the stalk is sufficient for stable dimer formation (Grummt *et al.*, 1998; Kallipolitou *et al.*, 2001; Verbrugge *et al.*, 2009). Surprisingly, C-terminally truncated KLP11 and KLP20 were unable to dimerize (Figures 17A and 19A), unless both contained the entire stalk domain (Figure 19B). Dimerization requires a small seed at the C-terminal end of the stalk (Figure 19C). Without it, heterodimerization does not take place even though the rest of the stalk is predicted to form a sufficiently stable coiled-coil (Figure 16). The mere number of heptad repeats is apparently not sufficient for dimerization of the two motor domains (Figures 17A and 19A). The short sequence of about two heptads at the C-terminal end of the stalk can be considered a genuine trigger that dictates the overall structure of the entire stalk.

Such trigger sites have been found also in other proteins (Steinmetz *et al.*, 1998; Burkhard *et al.*, 2000; Araya *et al.*, 2002), though coiled-coils may fold also in their absence (Lee *et al.*, 2001). In *C. elegans* kinesin-2, however, the trigger is strictly required; its presence provokes an all-or-none response in stalk formation (Figures 19B, 19C and 32). Once triggered, the entire stalk domain forms a coiled-coil structure starting at the stalk's C-terminus that brings the two motor domains in close proximity to each other (Figures 25 and 26). Thus, although sufficient for stable dimerization (Fig 19C) the seed does not represent the entire dimerization site. Such direct evidence for extensive coiled-coils in kinesins' stalks existed until now only for kinesin-1 whose stalk forms an α -helical coiled coil when expressed without the head and tail domains (de Cuevas *et al.*, 1992). Moreover, even portions excised from the stalk can form stable dimers. These include the neck (Morii *et al.*, 1997; Romberg *et al.*, 1998; Rashid *et al.*, 2005), the N-terminal and C-terminal halves of the stalk (de Cuevas *et al.*, 1992), and the C-terminal ~80 amino acids of the stalk (Dietrich *et al.*, 2008). These findings argue against the requirement for a general trigger sequence and against a directed coiled-coil formation in kinesin-1 as it was shown here for kinesin-2.

5 Only with the right partner

What might be the reason for the different modes of dimer formation of the closely related kinesin-1 (no specific or a single trigger) and kinesin-2 (clearly specified seed)? Structurally, the major difference is that kinesin-1 forms homodimers whereas kinesin-2 is heterodimer. Therefore, a mechanism must exist to prefer heterodimerization over homodimerization. The latter is also possible in kinesin-2, though exceptional (De Marco *et al.*, 2003). An ideal way indeed would be to specify a site where the two different chains have to come together first, analogous to the bottom stop and slider of a mechanical zipper that must be brought in contact before the zipper can be closed.

Studies of another representative of the kinesin-2 family, Xklp3A/B of *Xenopus laevis*, hinted at the importance of the C-terminal half of the stalk for dimerization (De Marco *et al.*, 2001). Neither the neck nor the highly charged stretch next to the neck region, which is typical for many kinesin-2 motors (but not KLP11/20), are required for heterodimer formation. The exact region was not specified but was believed to encompass ~100 amino acids at the C-terminal end of the stalk (De Marco *et al.*, 2001). A trigger site was not identified, however.

A preference for heterodimer formation was suggested for sea urchin (Rashid *et al.*, 1995), *X. laevis* (De Marco *et al.*, 2001) and mouse (Chana *et al.*, 2005) kinesin-2. If the same is true for Fla8/10, kinesin-2 from *Chlamydomonas reinhardtii*, and if all orthologues heterodimerize by triggered coiled-coil formation, this means that the seeded mode of dimerization is evolutionarily conserved (ranging from unicellular algae to mouse) and probably essential for favouring hetero- over homodimerization. In mouse, there is even a third kinesin-2 motor chain. Besides Kif3A (corresponds to KLP11) and Kif3B (corresponds to KLP20) there is also Kif3C, which is more related to Kif3B than to Kif3A (Muresan *et al.*, 1998). Kif3C displays tissue-specific expression pattern. It is enriched in brain, retina and lung where it shows specific cellular localization. Although Kif3C can act as an independent motor it also forms heterodimers with Kif3A, but never with Kif3B. This exquisite specificity emphasizes once more how nature can fine-tune interactions within the kinesin-2 class.

This work confirms this specificity and preference of heterodimerization for the *C. elegans* orthologue, not only by the co-precipitation analysis delivering protein bands

in 1:1 molar ratio (Figure 17B, 19B and 19C), but also by CD measurements delivering higher ellipticity of dimers (Figure 30) and also higher ratios of $[\theta_{222}]/[\theta_{208}]$ than of monomers (Table 3). Furthermore, temperature-dependent CD measurements of monomeric and dimeric KLP11/20-C and FL-KLP11/20 result in one isodichroic point for monomers and two isodichroic points for dimers (Figure 31), indicating a 2-state denaturing process for monomers and a 3-state process for dimers. The two states are α -helix and unfolded protein and the three states are coiled-coil, α -helix and unfolded protein, which again indicates a preference of heterodimerization.

The difference between KLP11/20 and the other orthologues is that it lacks the charged regions following the neck, which are present in sea urchin KRP85/95, *X. laevis* Xklp3A/B, and mouse Kif3A/3B. Fla8/10, the orthologue from *Chlamydomonas reinhardtii*, also lacks charged stretches. Since Fla8/10 and KLP11/20 diverged much earlier in evolution than the orthologues from frog and mouse, the charged region does not seem to be a prerequisite for heterodimerization, though it was shown to play a role in the stabilization of the neck of mouse Kif3A/3B (Chana *et al.*, 2005). Thus a contribution of the charged region to overall dimer stability cannot be generally excluded.

6 The stability issue

Concerning the dimer stability, the CD data implicate that the coiled-coil stability of the N-terminal half differs from that of the rest of the stalk as indicated by the lack of a significant increase in ellipticity of full-length KLP11/20 compared to KLP11/20-C. Moreover, the calculated number of α -helical residues is lower by 30 amino acids than the actual number contained between the neck and the C-terminal random coil (Table 3). Because the 30 amino acids are approximately half of the N-terminal part of the stalk, it can be speculated that the discrepancy hints at an interconversion of coiled and uncoiled states of this region. The option that these 30 amino acids are permanently uncoiled can be excluded regarding the positive FRET result. Thus, the neck and the N-terminal end of the stalk must at least transiently form a coiled-coil. Another possibility is that the coiled-coil of the N-terminal half of the stalk is not as tightly coiled as the C-terminal half though it is able to maintain a dimerized state. A

lower stability of the N-terminal part of the stalk was already suggested for kinesin-1 (de Cuevas *et al.*, 1992). In general, the ends of coiled-coils were shown to be more flexible (Zhou *et al.*, 1992). Moreover, small disruptions in the flow of heptads, the so called stutters and stammers, may lead to either overwinding or underwinding of the coiled coil (Brown *et al.*, 1996), resulting in either an increase or a decrease in helicity. Overwinding in the C-terminal half of the stalk would not only account for its higher stability, it may also explain that its calculated number of amino acids exceeds the actual number by 70. Conversely, underwinding of the N-terminal half of the stalk may account for the calculated 30 amino acids less than actually present in full-length KLP11/20. Support for the overwinding/underwinding suggestion comes from the melting profiles of FL-KLP11/20 and KLP11/20-C (Figure 29C). The FRET signal and the calculated distance of 4.95 nm in the FL-KLP11-20 indicate that the N-terminal half of the stalk also forms a coiled coil but the lack of gain in thermal stability between KLP11/20-C and FL-KLP11/20 suggests that this part of the coiled-coil is either less stable or undergoes coiling/uncoiling.

Evidence for higher flexibility of the N-terminal half of the stalk has now been provided for two dimeric processive kinesins, kinesin-1 and kinesin-2. This suggests that this feature may be important for force generation, processivity, supertwist release or autoregulation of kinesin's catalytic activity and may be common for dimeric processive kinesins. Whether this part of the stalk is indeed capable of switching conformations remains to be determined.

7 The seed as a common good

Finally, one aspect of the work described here deserves particular consideration because it points to applications beyond the study of heterodimeric coiled-coils. Because of its short length and high specificity, the nucleation seed identified here holds the promise of serving as a useful tool to induce specific heterodimerization of any two proteins. A protein sequence containing the seed can simply be fused to any pair of polypeptides by appropriate primer design. The use of such seeds for specific heterodimerization would further avoid chemical interference, such as introducing disulfide bonds, and the need for oxidizing or reducing environments, leaving the proteins in their native state and enabling protein analysis under physiological conditions.

Outlook

This work provides the first molecular insights in regulation of the subunit assembly and catalytic activity in kinesin-2 from *C. elegans*. It is further a solid basis for detailed investigation of these processes, such as revealing the molecular mechanism of favouring hetero- over homodimerization. This requires a detailed study of the amino acid composition of the stalk and especially of the seed sequence. Since some obvious features like complementary charges in the two motor chains, which would lead to repulsion in the homodimer, are not provided and thus not the reason for heterodimerization, a closer inspection of the heptad composition should be performed. Here the sequences of Kif3A, 3B and 3C, kinesin-2 orthologues from mouse, should be taken into consideration. Given the fact that Kif3B and 3C are both KLP20 homologues and that both heterodimerize with Kif3A, but never with each other (Muresan *et al.*, 1998), the comparison of the sequences might provide an idea about heterodimerization background. This analysis would provide a basis for mutation experiments, which could lead to homodimerization, thus revealing the importance of specific amino acids for heterodimerization.

Because of its small size the detailed structure of the seed sequence can be analyzed by nuclear magnetic resonance (NMR) spectroscopy along with the nature of binding forces in the two peptides. The seed's potential as a biochemical zipper of molecules should be tested by fusing it to peptides other than kinesin-2 and subsequent co-IP assays.

As to the opposite end of the motor, this work indicates that the coiled-coil in the N-terminal half of the stalk displays lower stability than the C-terminal half and that it may be able to transiently uncoil. Whether the N-terminal part of the stalk is indeed capable of switching conformations remains to be determined by future experiments such as measuring and comparing the forces needed to pull the peptide chains apart from both stalk ends.

Possible implications of this feature should also be explored, including the potential role in autoinhibition. Ideally, the *in trans* inhibition by tails of the EE-mutant, KLP11/20 GCN4 head heterodimer, and the GCN4 heterodimer of motors including the N-terminal half of the stalk should be compared. This comparison would provide

Outlook

information on whether any region further C-terminal from the heads is required for efficient inhibition by tails.

The importance of the helix breaker or the hinge region for this process was demonstrated by mutation into glutamates. To confirm this position as the folding point of the motor, the helix breaker can simply be deleted and then the motor activity analyzed. In general, the conformation of the folded protein is completely unknown. Where are the exact interaction sites between the tails and the heads/necks? Some idea on this can be given by cross-link experiments. It is further still elusive which tail influences which head. Light can be shed on this by an ATPase assay with asymmetric dimers consisting of one full-length wild type partner and with one motor chain lacking the random coil tail. Moreover, the tails' influence can be tested in a gliding assay in which motors are C-terminally attached to the glass surface, while the motor domains are free in solution and cause gliding of bound microtubules. By comparing motilities of unaffected motors and after flowing the tail constructs into the chamber, the effect of the tails can be elucidated in more detail using different motor constellations mentioned in this work. Do they just hinder or slow down the filament movement or their attachment to the motors as well?

Last but not least, the interaction site of KAP with KLP11 can be narrowed down by further truncations of KAP. Finding the region of the Armadillo-like domain that interacts with KLP11 would reveal regions of this domain responsible for cargo binding and provide a basis for investigations of how kinesin-2 binds cargo and possible regulation of this process.

References

Adio, S., Jaud, J., Ebbing, B., Rief, M., and Woehlke, G. (2009). Dissection of kinesin's processivity. *PLoS One* 4, e4612.

Araya, E., Berthier, C., Kim, E., Yeung, T., Wang, X., and Helfman, D.M. (2002). Regulation of coiled-coil assembly in tropomyosins. *J Struct Biol* 137, 176-183.

Blasius, T.L., Cai, D., Jih, G.T., Toret, C.P., and Verhey, K.J. (2007). Two binding partners cooperate to activate the molecular motor Kinesin-1. *J Cell Biol* 176, 11-17.

Brady, S.T. (1985). A novel brain ATPase with properties expected for the fast axonal transport motor. *Nature* 317, 73-75.

Brown, J.H., Cohen, C., and Parry, D.A. (1996). Heptad breaks in alpha-helical coiled coils: stutters and stammers. *Proteins* 26, 134-145.

Brown, J.M., Marsala, C., Kosoy, R., and Gaertig, J. (1999). Kinesin-II is preferentially targeted to assembling cilia and is required for ciliogenesis and normal cytokinesis in *Tetrahymena*. *Mol Biol Cell* 10, 3081-3096.

Brunnbauer, M., Mueller-Planitz, F., Kosem, S., Ho, T.H., Dombi, R., Gebhardt, J.C., Rief, M., and Okten, Z. (2010). Regulation of a heterodimeric kinesin-2 through an unprocessive motor domain that is turned processive by its partner. *Proc Natl Acad Sci U S A* 107, 10460-10465.

Burghoorn, J., Dekkers, M.P., Rademakers, S., de Jong, T., Willemsen, R., and Jansen, G. (2007). Mutation of the MAP kinase DYF-5 affects docking and undocking of kinesin-2 motors and reduces their speed in the cilia of *Caenorhabditis elegans*. *Proc Natl Acad Sci U S A* 104, 7157-7162.

Burkhard, P., Kammerer, R.A., Steinmetz, M.O., Bourenkov, G.P., and Aebi, U. (2000). The coiled-coil trigger site of the rod domain of cortexillin I unveils a distinct network of interhelical and intrahelical salt bridges. *Structure* 8, 223-230.

Cai, D., Hoppe, A.D., Swanson, J.A., and Verhey, K.J. (2007). Kinesin-1 structural organization and conformational changes revealed by FRET stoichiometry in live cells. *J Cell Biol* 176, 51-63.

Chana, M., Tripet, B.P., Mant, C.T., and Hodges, R.S. (2002). The role of unstructured highly charged regions on the stability and specificity of dimerization of two-stranded alpha-helical coiled-coils: analysis of the neck-hinge region of the kinesin-like motor protein Kif3A. *J Struct Biol* 137, 206-219.

Chana, M.S., Tripet, B.P., Mant, C.T., and Hodges, R. (2005). Stability and specificity of heterodimer formation for the coiled-coil neck regions of the motor proteins Kif3A

References

- and Kif3B: the role of unstructured oppositely charged regions. *J Pept Res* 65, 209-220.
- Chen, Y.H., Yang, J.T., and Chau, K.H. (1974). Determination of the helix and beta form of proteins in aqueous solution by circular dichroism. *Biochemistry* 13, 3350-3359.
- Chen, Y.H., Yang, J.T., and Martinez, H.M. (1972). Determination of the secondary structures of proteins by circular dichroism and optical rotatory dispersion. *Biochemistry* 11, 4120-4131.
- Cole, D.G. (1999). Kinesin-II, the heteromeric kinesin. *Cell Mol Life Sci* 56, 217-226.
- Cole, D.G., Chinn, S.W., Wedaman, K.P., Hall, K., Vuong, T., and Scholey, J.M. (1993). Novel heterotrimeric kinesin-related protein purified from sea urchin eggs. *Nature* 366, 268-270.
- Cole, D.G., Diener, D.R., Himelblau, A.L., Beech, P.L., Fuster, J.C., and Rosenbaum, J.L. (1998). Chlamydomonas kinesin-II-dependent intraflagellar transport (IFT): IFT particles contain proteins required for ciliary assembly in *Caenorhabditis elegans* sensory neurons. *J Cell Biol* 141, 993-1008.
- Cooper, T.M., and Woody, R.W. (1990). The effect of conformation on the CD of interacting helices: a theoretical study of tropomyosin. *Biopolymers* 30, 657-676.
- Corbit, K.C., Shyer, A.E., Dowdle, W.E., Gaulden, J., Singla, V., Chen, M.H., Chuang, P.T., and Reiter, J.F. (2008). Kif3a constrains beta-catenin-dependent Wnt signalling through dual ciliary and non-ciliary mechanisms. *Nat Cell Biol* 10, 70-76.
- Coy, D.L., Hancock, W.O., Wagenbach, M., and Howard, J. (1999). Kinesin's tail domain is an inhibitory regulator of the motor domain. *Nat Cell Biol* 1, 288-292.
- Coy, D.L., and Howard, J. (1994). Organelle transport and sorting in axons. *Curr Opin Neurobiol* 4, 662-667.
- de Cuevas, M., Tao, T., and Goldstein, L.S. (1992). Evidence that the stalk of *Drosophila* kinesin heavy chain is an alpha-helical coiled coil. *J Cell Biol* 116, 957-965.
- De Marco, V., Burkhard, P., Le Bot, N., Vernos, I., and Hoenger, A. (2001). Analysis of heterodimer formation by Xklp3A/B, a newly cloned kinesin-II from *Xenopus laevis*. *Embo J* 20, 3370-3379.
- De Marco, V., De Marco, A., Goldie, K.N., Correia, J.J., and Hoenger, A. (2003). Dimerization properties of a *Xenopus laevis* kinesin-II carboxy-terminal stalk fragment. *EMBO Rep* 4, 717-722.
- Deacon, S.W., Serpinskaya, A.S., Vaughan, P.S., Lopez Fanarraga, M., Vernos, I., Vaughan, K.T., and Gelfand, V.I. (2003). Dynactin is required for bidirectional organelle transport. *J Cell Biol* 160, 297-301.

References

- Dietrich, K.A., Sindelar, C.V., Brewer, P.D., Downing, K.H., Cremo, C.R., and Rice, S.E. (2008). The kinesin-1 motor protein is regulated by a direct interaction of its head and tail. *Proc Natl Acad Sci U S A* *105*, 8938-8943.
- Doodhi, H., Ghosal, D., Krishnamurthy, M., Jana, S.C., Shamala, D., Bhaduri, A., Sowdhamini, R., and Ray, K. (2009). KAP, the accessory subunit of kinesin-2, binds the predicted coiled-coil stalk of the motor subunits. *Biochemistry* *48*, 2248-2260.
- Endow, S.A., and Waligora, K.W. (1998). Determinants of kinesin motor polarity. *Science* *281*, 1200-1202.
- Fan, J., and Beck, K.A. (2004). A role for the spectrin superfamily member Syne-1 and kinesin II in cytokinesis. *J Cell Sci* *117*, 619-629.
- Farrell, C.M., Mackey, A.T., Klumpp, L.M., and Gilbert, S.P. (2002). The role of ATP hydrolysis for kinesin processivity. *J Biol Chem* *277*, 17079-17087.
- Förster, T. (1946). *Naturwissenschaften* *6*.
- Förster, T. (1948). *Ann. Phys.* *2*, 57-65.
- Friedman, D.S., and Vale, R.D. (1999). Single-molecule analysis of kinesin motility reveals regulation by the cargo-binding tail domain. *Nat Cell Biol* *1*, 293-297.
- Gans, P.J., Lyu, P.C., Manning, M.C., Woody, R.W., and Kallenbach, N.R. (1991). The helix-coil transition in heterogeneous peptides with specific side-chain interactions: theory and comparison with CD spectral data. *Biopolymers* *31*, 1605-1614.
- Gilbert, S.P., Moyer, M.L., and Johnson, K.A. (1998). Alternating site mechanism of the kinesin ATPase. *Biochemistry* *37*, 792-799.
- Gilbert, S.P., Webb, M.R., Brune, M., and Johnson, K.A. (1995). Pathway of processive ATP hydrolysis by kinesin. *Nature* *373*, 671-676.
- Greenfield, N.J. (2006). Using circular dichroism collected as a function of temperature to determine the thermodynamics of protein unfolding and binding interactions. *Nat Protoc* *1*, 2527-2535.
- Grummt, M., Woehlke, G., Henningsen, U., Fuchs, S., Schleicher, M., and Schliwa, M. (1998). Importance of a flexible hinge near the motor domain in kinesin-driven motility. *EMBO J* *17*, 5536-5542.
- Hackney, D.D. (1994). Evidence for alternating head catalysis by kinesin during microtubule-stimulated ATP hydrolysis. *Proc Natl Acad Sci U S A* *91*, 6865-6869.
- Hackney, D.D., Baek, N., and Snyder, A.C. (2009). Half-site inhibition of dimeric kinesin head domains by monomeric tail domains. *Biochemistry* *48*, 3448-3456.
- Hackney, D.D., Levitt, J.D., and Suhan, J. (1992). Kinesin undergoes a 9 S to 6 S conformational transition. *J Biol Chem* *267*, 8696-8701.

References

- Hackney, D.D., and Stock, M.F. (2000). Kinesin's IAK tail domain inhibits initial microtubule-stimulated ADP release. *Nat Cell Biol* 2, 257-260.
- Hackney, D.D., and Stock, M.F. (2008). Kinesin tail domains and Mg²⁺ directly inhibit release of ADP from head domains in the absence of microtubules. *Biochemistry* 47, 7770-7778.
- Hammond, J.W., Blasius, T.L., Soppina, V., Cai, D., and Verhey, K.J. Autoinhibition of the kinesin-2 motor KIF17 via dual intramolecular mechanisms. *J Cell Biol* 189, 1013-1025.
- Hammond, J.W., Blasius, T.L., Soppina, V., Cai, D., and Verhey, K.J. (2010). Autoinhibition of the kinesin-2 motor KIF17 via dual intramolecular mechanisms. *J Cell Biol* 189, 1013-1025.
- Hammond, J.W., Cai, D., Blasius, T.L., Li, Z., Jiang, Y., Jih, G.T., Meyhofer, E., and Verhey, K.J. (2009). Mammalian Kinesin-3 motors are dimeric in vivo and move by processive motility upon release of autoinhibition. *PLoS Biol* 7, e72.
- Hancock, W.O., and Howard, J. (1998). Processivity of the motor protein kinesin requires two heads. *J Cell Biol* 140, 1395-1405.
- Haraguchi, K., Hayashi, T., Jimbo, T., Yamamoto, T., and Akiyama, T. (2006). Role of the kinesin-2 family protein, KIF3, during mitosis. *J Biol Chem* 281, 4094-4099.
- Heinrich, B., and Deshler, J.O. (2009). RNA localization to the Balbiani body in *Xenopus* oocytes is regulated by the energy state of the cell and is facilitated by kinesin II. *RNA* 15, 524-536.
- Hirokawa, N., Noda, Y., and Okada, Y. (1998). Kinesin and dynein superfamily proteins in organelle transport and cell division. *Curr Opin Cell Biol* 10, 60-73.
- Hirokawa, N., Pfister, K.K., Yorifuji, H., Wagner, M.C., Brady, S.T., and Bloom, G.S. (1989). Submolecular domains of bovine brain kinesin identified by electron microscopy and monoclonal antibody decoration. *Cell* 56, 867-878.
- Huang, T.G., and Hackney, D.D. (1994). *Drosophila* kinesin minimal motor domain expressed in *Escherichia coli*. Purification and kinetic characterization. *J Biol Chem* 269, 16493-16501.
- Imanishi, M., Endres, N.F., Gennerich, A., and Vale, R.D. (2006). Autoinhibition regulates the motility of the *C. elegans* intraflagellar transport motor OSM-3. *J Cell Biol* 174, 931-937.
- Inglis, P.N., Ou, G., Leroux, M.R., and Scholey, J.M. (2007). The sensory cilia of *Caenorhabditis elegans*. *WormBook*, 1-22.
- Jimbo, T., Kawasaki, Y., Koyama, R., Sato, R., Takada, S., Haraguchi, K., and Akiyama, T. (2002). Identification of a link between the tumour suppressor APC and the kinesin superfamily. *Nat Cell Biol* 4, 323-327.

References

- Johnson, K.A., and Gilbert, S.P. (1995). Pathway of the microtubule-kinesin ATPase. *Bioophys J* 68, 173S-176S; discussion 176S-179S.
- Kaan, H.Y., Hackney, D.D., and Kozielski, F. (2011). The structure of the kinesin-1 motor-tail complex reveals the mechanism of autoinhibition. *Science* 333, 883-885.
- Kalab, P., and Soderholm, J. The design of Forster (fluorescence) resonance energy transfer (FRET)-based molecular sensors for Ran GTPase. *Methods* 51, 220-232.
- Kallipolitou, A., Deluca, D., Majdic, U., Lakamper, S., Cross, R., Meyhofer, E., Moroder, L., Schliwa, M., and Woehlke, G. (2001). Unusual properties of the fungal conventional kinesin neck domain from *Neurospora crassa*. *EMBO J* 20, 6226-6235.
- Kolpakova-Hart, E., Jinnin, M., Hou, B., Fukai, N., and Olsen, B.R. (2007). Kinesin-2 controls development and patterning of the vertebrate skeleton by Hedgehog- and Gli3-dependent mechanisms. *Dev Biol* 309, 273-284.
- Kondo, S., Sato-Yoshitake, R., Noda, Y., Aizawa, H., Nakata, T., Matsuura, Y., and Hirokawa, N. (1994). KIF3A is a new microtubule-based anterograde motor in the nerve axon. *J Cell Biol* 125, 1095-1107.
- Lakowicz, J.R. (1999). Principles of fluorescence spectroscopy. Kluwer Academic/Plenum: New York.
- Le Bot, N., Antony, C., White, J., Karsenti, E., and Vernos, I. (1998). Role of xklp3, a subunit of the *Xenopus* kinesin II heterotrimeric complex, in membrane transport between the endoplasmic reticulum and the Golgi apparatus. *J Cell Biol* 143, 1559-1573.
- Lee, D.L., Lavigne, P., and Hodges, R.S. (2001). Are trigger sequences essential in the folding of two-stranded alpha-helical coiled-coils? *J Mol Biol* 306, 539-553.
- Lee, J.R., Shin, H., Choi, J., Ko, J., Kim, S., Lee, H.W., Kim, K., Rho, S.H., Lee, J.H., Song, H.E., Eom, S.H., and Kim, E. (2004). An intramolecular interaction between the FHA domain and a coiled coil negatively regulates the kinesin motor KIF1A. *EMBO J* 23, 1506-1515.
- Lin, F., Hiesberger, T., Cordes, K., Sinclair, A.M., Goldstein, L.S., Somlo, S., and Igarashi, P. (2003). Kidney-specific inactivation of the KIF3A subunit of kinesin-II inhibits renal ciliogenesis and produces polycystic kidney disease. *Proc Natl Acad Sci U S A* 100, 5286-5291.
- Lukong, K.E., and Richard, S. (2008). Breast tumor kinase BRK requires kinesin-2 subunit KAP3A in modulation of cell migration. *Cell Signal* 20, 432-442.
- Lupas, A., Van Dyke, M., and Stock, J. (1991). Predicting coiled coils from protein sequences. *Science* 252, 1162-1164.
- Ma, Y.Z., and Taylor, E.W. (1997). Interacting head mechanism of microtubule-kinesin ATPase. *J Biol Chem* 272, 724-730.

References

- Mandelkow, E.M., Herrmann, M., and Ruhl, U. (1985). Tubulin domains probed by limited proteolysis and subunit-specific antibodies. *J Mol Biol* 185, 311-327.
- Mans, D.A., Lolkema, M.P., van Beest, M., Daenen, L.G., Voest, E.E., and Giles, R.H. (2008). Mobility of the von Hippel-Lindau tumour suppressor protein is regulated by kinesin-2. *Exp Cell Res* 314, 1229-1236.
- Marshall, W.F., and Nonaka, S. (2006). Cilia: tuning in to the cell's antenna. *Curr Biol* 16, R604-614.
- Marszalek, J.R., Ruiz-Lozano, P., Roberts, E., Chien, K.R., and Goldstein, L.S. (1999). Situs inversus and embryonic ciliary morphogenesis defects in mouse mutants lacking the KIF3A subunit of kinesin-II. *Proc Natl Acad Sci U S A* 96, 5043-5048.
- Miki, H., Okada, Y., and Hirokawa, N. (2005). Analysis of the kinesin superfamily: insights into structure and function. *Trends Cell Biol* 15, 467-476.
- Miki, H., Setou, M., Kaneshiro, K., and Hirokawa, N. (2001). All kinesin superfamily protein, KIF, genes in mouse and human. *Proc Natl Acad Sci U S A* 98, 7004-7011.
- Miller, M.G., Mulholland, D.J., and Vogl, A.W. (1999). Rat testis motor proteins associated with spermatid translocation (dynein) and spermatid flagella (kinesin-II). *Biol Reprod* 60, 1047-1056.
- Miller, M.S., Esparza, J.M., Lippa, A.M., Lux, F.G., 3rd, Cole, D.G., and Dutcher, S.K. (2005). Mutant kinesin-2 motor subunits increase chromosome loss. *Mol Biol Cell* 16, 3810-3820.
- Morii, H., Takenawa, T., Arisaka, F., and Shimizu, T. (1997). Identification of kinesin neck region as a stable alpha-helical coiled coil and its thermodynamic characterization. *Biochemistry* 36, 1933-1942.
- Morris, R.L., and Scholey, J.M. (1997). Heterotrimeric kinesin-II is required for the assembly of motile 9+2 ciliary axonemes on sea urchin embryos. *J Cell Biol* 138, 1009-1022.
- Mueller, J., Perrone, C.A., Bower, R., Cole, D.G., and Porter, M.E. (2005). The FLA3 KAP subunit is required for localization of kinesin-2 to the site of flagellar assembly and processive anterograde intraflagellar transport. *Mol Biol Cell* 16, 1341-1354.
- Muhle-Goll, C., Gibson, T., Schuck, P., Schubert, D., Nalis, D., Nilges, M., and Pastore, A. (1994). The dimerization stability of the HLH-LZ transcription protein family is modulated by the leucine zippers: a CD and NMR study of TFEB and c-Myc. *Biochemistry* 33, 11296-11306.
- Mukhopadhyay, B., Nam, S.C., and Choi, K.W. (2010). Kinesin II is required for cell survival and adherens junction positioning in *Drosophila* photoreceptors. *Genesis* 48, 522-530.

References

- Muresan, V., Abramson, T., Lyass, A., Winter, D., Porro, E., Hong, F., Chamberlin, N.L., and Schnapp, B.J. (1998). KIF3C and KIF3A form a novel neuronal heteromeric kinesin that associates with membrane vesicles. *Mol Biol Cell* 9, 637-652.
- Nagata, K., Puls, A., Futter, C., Aspenstrom, P., Schaefer, E., Nakata, T., Hirokawa, N., and Hall, A. (1998). The MAP kinase kinase kinase MLK2 co-localizes with activated JNK along microtubules and associates with kinesin superfamily motor KIF3. *EMBO J* 17, 149-158.
- Nonaka, S., Tanaka, Y., Okada, Y., Takeda, S., Harada, A., Kanai, Y., Kido, M., and Hirokawa, N. (1998). Randomization of left-right asymmetry due to loss of nodal cilia generating leftward flow of extraembryonic fluid in mice lacking KIF3B motor protein. *Cell* 95, 829-837.
- O'Reilly, D.R., Miller, L.K. and Luckow, V.A. . (1992). *Baculovirus Expression Vectors: A Laboratory Manual*. W.H. Freeman and Company, New York.
- Ocbina, P.J., and Anderson, K.V. (2008). Intraflagellar transport, cilia, and mammalian Hedgehog signaling: analysis in mouse embryonic fibroblasts. *Dev Dyn* 237, 2030-2038.
- Ogawa, T., Nitta, R., Okada, Y., and Hirokawa, N. (2004). A common mechanism for microtubule destabilizers-M type kinesins stabilize curling of the protofilament using the class-specific neck and loops. *Cell* 116, 591-602.
- Okada, Y., and Hirokawa, N. (1999). A processive single-headed motor: kinesin superfamily protein KIF1A. *Science* 283, 1152-1157.
- Orozco, J.T., Wedaman, K.P., Signor, D., Brown, H., Rose, L., and Scholey, J.M. (1999). Movement of motor and cargo along cilia. *Nature* 398, 674.
- Ou, G., Koga, M., Blacque, O.E., Murayama, T., Ohshima, Y., Schafer, J.C., Li, C., Yoder, B.K., Leroux, M.R., and Scholey, J.M. (2007). Sensory ciliogenesis in *Caenorhabditis elegans*: assignment of IFT components into distinct modules based on transport and phenotypic profiles. *Mol Biol Cell* 18, 1554-1569.
- Pan, J., and Snell, W.J. (2002). Kinesin-II is required for flagellar sensory transduction during fertilization in *Chlamydomonas*. *Mol Biol Cell* 13, 1417-1426.
- Patterson, G.H., Piston, D.W., and Barisas, B.G. (2000). Forster distances between green fluorescent protein pairs. *Anal Biochem* 284, 438-440.
- Pazour, G.J., Baker, S.A., Deane, J.A., Cole, D.G., Dickert, B.L., Rosenbaum, J.L., Witman, G.B., and Besharse, J.C. (2002). The intraflagellar transport protein, IFT88, is essential for vertebrate photoreceptor assembly and maintenance. *J Cell Biol* 157, 103-113.
- Perkins, L.A., Hedgecock, E.M., Thomson, J.N., and Culotti, J.G. (1986). Mutant sensory cilia in the nematode *Caenorhabditis elegans*. *Dev Biol* 117, 456-487.

References

- Provencher, S.W., and Glockner, J. (1981). Estimation of globular protein secondary structure from circular dichroism. *Biochemistry* 20, 33-37.
- Rashid, D.J., Bononi, J., Tripet, B.P., Hodges, R.S., and Pierce, D.W. (2005). Monomeric and dimeric states exhibited by the kinesin-related motor protein KIF1A. *J Pept Res* 65, 538-549.
- Rashid, D.J., Wedaman, K.P., and Scholey, J.M. (1995). Heterodimerization of the two motor subunits of the heterotrimeric kinesin, KRP85/95. *J Mol Biol* 252, 157-162.
- Romberg, L., Pierce, D.W., and Vale, R.D. (1998). Role of the kinesin neck region in processive microtubule-based motility. *J Cell Biol* 140, 1407-1416.
- Rosenbaum, J.L., and Witman, G.B. (2002). Intraflagellar transport. *Nat Rev Mol Cell Biol* 3, 813-825.
- Sablin, E.P., Case, R.B., Dai, S.C., Hart, C.L., Ruby, A., Vale, R.D., and Fletterick, R.J. (1998). Direction determination in the minus-end-directed kinesin motor ncd. *Nature* 395, 813-816.
- Sarpal, R., and Ray, K. (2002). Dynamic expression pattern of kinesin accessory protein in *Drosophila*. *J Biosci* 27, 479-487.
- Sarpal, R., Todi, S.V., Sivan-Loukianova, E., Shirolkar, S., Subramanian, N., Raff, E.C., Erickson, J.W., Ray, K., and Eberl, D.F. (2003). *Drosophila* KAP interacts with the kinesin II motor subunit KLP64D to assemble chordotonal sensory cilia, but not sperm tails. *Curr Biol* 13, 1687-1696.
- Scholey, J.M. (2008). Intraflagellar transport motors in cilia: moving along the cell's antenna. *J Cell Biol* 180, 23-29.
- Scholey, J.M., and Anderson, K.V. (2006). Intraflagellar transport and cilium-based signaling. *Cell* 125, 439-442.
- Scholey, J.M., Porter, M.E., Grissom, P.M., and McIntosh, J.R. (1985). Identification of kinesin in sea urchin eggs, and evidence for its localization in the mitotic spindle. *Nature* 318, 483-486.
- Seiler, S., Kirchner, J., Horn, C., Kallipolitou, A., Woehlke, G., and Schliwa, M. (2000). Cargo binding and regulatory sites in the tail of fungal conventional kinesin. *Nat Cell Biol* 2, 333-338.
- Shaner, N.C., Patterson, G.H., and Davidson, M.W. (2007). Advances in fluorescent protein technology. *J Cell Sci* 120, 4247-4260.
- Shaner, N.C., Steinbach, P.A., and Tsien, R.Y. (2005). A guide to choosing fluorescent proteins. *Nat Methods* 2, 905-909.
- Shimizu, K., Kawabe, H., Minami, S., Honda, T., Takaishi, K., Shirataki, H., and Takai, Y. (1996). SMAP, an Smg GDS-associating protein having arm repeats and phosphorylated by Src tyrosine kinase. *J Biol Chem* 271, 27013-27017.

References

- Signor, D., Wedaman, K.P., Rose, L.S., and Scholey, J.M. (1999). Two heteromeric kinesin complexes in chemosensory neurons and sensory cilia of *Caenorhabditis elegans*. *Mol Biol Cell* 10, 345-360.
- Singla, V., and Reiter, J.F. (2006). The primary cilium as the cell's antenna: signaling at a sensory organelle. *Science* 313, 629-633.
- Starich, T.A., Herman, R.K., Kari, C.K., Yeh, W.H., Schackwitz, W.S., Schuyler, M.W., Collet, J., Thomas, J.H., and Riddle, D.L. (1995). Mutations affecting the chemosensory neurons of *Caenorhabditis elegans*. *Genetics* 139, 171-188.
- Steinmetz, M.O., Stock, A., Schulthess, T., Landwehr, R., Lustig, A., Faix, J., Gerisch, G., Aebi, U., and Kammerer, R.A. (1998). A distinct 14 residue site triggers coiled-coil formation in cortexillin I. *Embo J* 17, 1883-1891.
- Stock, M.F., Guerrero, J., Cobb, B., Eggers, C.T., Huang, T.G., Li, X., and Hackney, D.D. (1999). Formation of the compact conformation of kinesin requires a COOH-terminal heavy chain domain and inhibits microtubule-stimulated ATPase activity. *J Biol Chem* 274, 14617-14623.
- Svoboda, K., Schmidt, C.F., Schnapp, B.J., and Block, S.M. (1993). Direct observation of kinesin stepping by optical trapping interferometry. *Nature* 365, 721-727.
- Takeda, S., Yamazaki, H., Seog, D.H., Kanai, Y., Terada, S., and Hirokawa, N. (2000). Kinesin superfamily protein 3 (KIF3) motor transports fodrin-associating vesicles important for neurite building. *J Cell Biol* 148, 1255-1265.
- Takeda, S., Yonekawa, Y., Tanaka, Y., Okada, Y., Nonaka, S., and Hirokawa, N. (1999). Left-right asymmetry and kinesin superfamily protein KIF3A: new insights in determination of laterality and mesoderm induction by *kif3A*^{-/-} mice analysis. *J Cell Biol* 145, 825-836.
- Tripet, B., Wagschal, K., Lavigne, P., Mant, C.T., and Hodges, R.S. (2000). Effects of side-chain characteristics on stability and oligomerization state of a de novo-designed model coiled-coil: 20 amino acid substitutions in position "d". *J Mol Biol* 300, 377-402.
- Tuma, M.C., Zill, A., Le Bot, N., Vernos, I., and Gelfand, V. (1998). Heterotrimeric kinesin II is the microtubule motor protein responsible for pigment dispersion in *Xenopus melanophores*. *J Cell Biol* 143, 1547-1558.
- Vale, R.D., and Fletterick, R.J. (1997). The design plan of kinesin motors. *Annu Rev Cell Dev Biol* 13, 745-777.
- Vale, R.D., Reese, T.S., and Sheetz, M.P. (1985). Identification of a novel force-generating protein, kinesin, involved in microtubule-based motility. *Cell* 42, 39-50.
- van Stokkum, I.H., Spoelder, H.J., Bloemendal, M., van Grondelle, R., and Groen, F.C. (1990). Estimation of protein secondary structure and error analysis from circular dichroism spectra. *Anal Biochem* 191, 110-118.

References

- Vaughn, J.L., Goodwin, R.H., Tompkins, G.J., and McCawley, P. (1977). The establishment of two cell lines from the insect *Spodoptera frugiperda* (Lepidoptera; Noctuidae). *In Vitro* 13, 213-217.
- Verbrugge, S., van den Wildenberg, S.M., and Peterman, E.J. (2009). Novel ways to determine kinesin-1's run length and randomness using fluorescence microscopy. *Biophys J* 97, 2287-2294.
- Verhey, K.J., and Hammond, J.W. (2009). Traffic control: regulation of kinesin motors. *Nat Rev Mol Cell Biol* 10, 765-777.
- Wang, W., Dang, R., Zhu, J.Q., and Yang, W.X. (2010). Identification and dynamic transcription of KIF3A homologue gene in spermiogenesis of *Octopus tankahkeei*. *Comp Biochem Physiol A Mol Integr Physiol* 157, 237-245.
- Wedaman, K.P., Meyer, D.W., Rashid, D.J., Cole, D.G., and Scholey, J.M. (1996). Sequence and submolecular localization of the 115-kD accessory subunit of the heterotrimeric kinesin-II (KRP85/95) complex. *J Cell Biol* 132, 371-380.
- Whitmore, L., and Wallace, B.A. (2004). DICHROWEB, an online server for protein secondary structure analyses from circular dichroism spectroscopic data. *Nucleic Acids Res* 32, W668-673.
- Whitmore, L., and Wallace, B.A. (2008). Protein secondary structure analyses from circular dichroism spectroscopy: methods and reference databases. *Biopolymers* 89, 392-400.
- Woehlke, G., and Schliwa, M. (2000). Walking on two heads: the many talents of kinesin. *Nat Rev Mol Cell Biol* 1, 50-58.
- Wong, Y.L., Dietrich, K.A., Naber, N., Cooke, R., and Rice, S.E. (2009). The Kinesin-1 tail conformationally restricts the nucleotide pocket. *Biophys J* 96, 2799-2807.
- Wu, P., and Brand, L. (1994). Resonance energy transfer: methods and applications. *Anal Biochem* 218, 1-13.
- Yamada, K.H., Hanada, T., and Chishti, A.H. (2007). The effector domain of human Dlg tumor suppressor acts as a switch that relieves autoinhibition of kinesin-3 motor GAKIN/KIF13B. *Biochemistry* 46, 10039-10045.
- Yamazaki, H., Nakata, T., Okada, Y., and Hirokawa, N. (1995). KIF3A/B: a heterodimeric kinesin superfamily protein that works as a microtubule plus end-directed motor for membrane organelle transport. *J Cell Biol* 130, 1387-1399.
- Yamazaki, H., Nakata, T., Okada, Y., and Hirokawa, N. (1996). Cloning and characterization of KAP3: a novel kinesin superfamily-associated protein of KIF3A/3B. *Proc Natl Acad Sci U S A* 93, 8443-8448.
- Yildiz, A., Tomishige, M., Vale, R.D., and Selvin, P.R. (2004). Kinesin walks hand-over-hand. *Science* 303, 676-678.


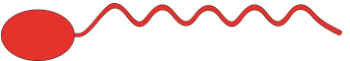

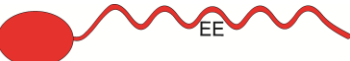

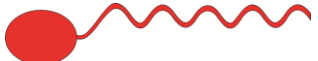

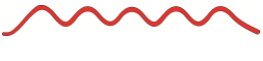





References

Yonekura, H., Nomura, A., Ozawa, H., Tatsu, Y., Yumoto, N., and Uyeda, T.Q. (2006). Mechanism of tail-mediated inhibition of kinesin activities studied using synthetic peptides. *Biochem Biophys Res Commun* 343, 420-427.




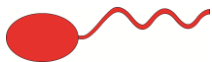
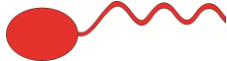
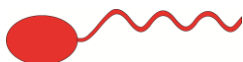








Zhang, Y., and Hancock, W.O. (2004). The two motor domains of KIF3A/B coordinate for processive motility and move at different speeds. *Biophys J* 87, 1795-1804.

Zhou, N.E., Kay, C.M., and Hodges, R.S. (1992). Synthetic model proteins. Positional effects of interchain hydrophobic interactions on stability of two-stranded alpha-helical coiled-coils. *J Biol Chem* 267, 2664-2670.


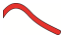







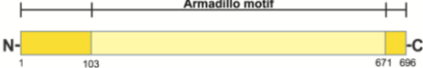
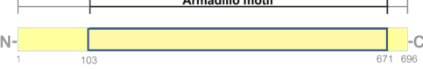

List of constructs

<i>Construct nr. and name</i>	<i>Amino acid stretch</i>	<i>Size in kDa</i>	<i>illustration</i>
1. KLP11 wt	1-782	88.1	
2. KLP20 wt	1-646	73.5	
3. KLP11 EE	1-782 G ⁴⁵⁰ S ⁴⁵¹ -> EE	88.1	
4. KLP20 EE	1-646 G ⁴⁴⁴ S ⁴⁴⁵ -> EE	73.5	
5. KLP11 noRC	1-548	62.9	
6. KLP20 noRC	1-550	62.5	
7. KLP11 no head	425-782	48.7	
8. KLP20 no head	301-646	35.4	
9. KLP11-N	1-449	51.3	
10. KLP20-N	1-443	49.9	
11. KLP11-N+1	1-463	52.7	
12. KLP11-N+2	1-475	54.2	
13. KLP11-N+3	1-487	55.8	

Lists

<i>Construct nr. and name</i>	<i>Amino acid stretch</i>	<i>Size in kDa</i>	<i>illustration</i>
14. KLP11-N+4	1-498	57	
15. KLP11-N+5	1-511	58.6	
16. KLP11-N+6	1-530	60.9	
17. KLP20-N+1	1-457	51.5	
18. KLP20-N+2	1-468	52.8	
19. KLP20-N+3	1-480	54.2	
20. KLP20-N+4	1-491	55.6	
21. KLP20-N+5	1-504	57	
22. KLP20-N+6	1-525	59.5	
23. KLP11 RC	549-782	25.8	
24. KLP20 RC	551-646	11	
25. KLP11 RC+1	538-782	27	
26. KLP11 RC+2	530-782	27.8	
27. KLP11 RC+3	524-782	28.6	

Lists

<i>Construct nr. and name</i>	<i>Amino acid stretch</i>	<i>Size in kDa</i>	<i>illustration</i>
28. KLP20 RC+1	540-646	12.3	
29. KLP20 RC+2	535-646	12.9	
30. KLP20 RC+3	529-646	13.6	
31. KLP11-C	450-782	37.5	
32. KLP 20-C	444-646	23.6	
33. KLP11 mono	1-365	41	
34. KLP20 mono	1-353	39.1	
35. KLP11 GCN4	1- 365 plus GCN4	45.1	
36. KLP20 GCN4	1-353 plus GCN4	43.2	
37. KAP	1-696	78.6	
38. KAParm	103-672	64.3	
39. KLP11 RCcons	636-763	12	

Protein sequences

KLP11

MVEIMKKSSKQETVKVIVRCRPLSSQEIANNSKIVHMRPQRGQIELK
 NPKEQDEPSKDFTFDAIYDENSTQSDLYEETFRLDLDVSVLNGYNATIF
 AYGQTGTGKTHTEGKSSDPEQRGVYKCIDHIFEHMAASHNQEYLVR
 ASYLEIYQEELRDLLAEASNKLEIKERPDGGVYVKDLTSLKTRTVGEI
 HEVMIRGNGHRVGRNMMNEHSSRSHAFIITVECSRIGEDGESHTVG
 RLNLVDLAGSERQSKTGATGERFKEATKINLSLSALGNVISALVDAKSA
 HIPYRDSKLTRLLQDSLGGNSKTMVACIGPASYNFEETLGTLYANR
 AKNIKNQPKINEDPKDALLREFQEEIEMLREQLKQRKTRSRDGATQSF
 YDAERAKLEDDIEAIQKDDSLIKHEKDRLIREIQEKHDLLEKERIEQARV
 AERIANIQSRLIVGSEEDGRLESRTKEQHAQLEKKRRELAEQKRRE
 MVEALERQEEDTVDLKQTFSDLRTEVEAKTKKLLKMLIKLRQARNEIR
 DVSGAYSDERQDLDTIAEVSKELKLLKLLIVENFIPRDVSERIKERA
 EWNEDSFEWNVNAFQSTSSNSSTPLNNTIEVNEDEGDFTRSSGADSGVSV
 SGGNGT **PATS** QFLDKRLVATPGCRRP **MSMCERMLVETAREQFGAQR**
RPPISGSGSFVEATIPEETIRFCGENVVVFSALERFVPEVTDSDPSTFS
 NS **MMMSARRPSIENLTIDASKVLVPILNQSTMILKN** **SK**NGQARNDT **MP**
PNGSMRRSQN

Catalytic head

stalk

random coil tail

Borders of KLP11 RCcons

KLP20

MEGAEKVQVVRCPVISTTEKLQGHKIAVTCNDEEKAVNIKSLSQEDP
 PRTFFYFDAVFPNTDQMTVYNVAARPIVENVLKGYNGTIFAYGQTGTG
 KTFT **MAGDLEPVEMRGIIPNSFAHIFDHIACQHDTTFLVRVSYLEIYN**
EEIRDLLSKDHNGNLEIKERPDVGVYVRNLSNPTVENASKMQALMEFG
SKNRKVGATAMNLESSRSHAMFTVTIESCRNGLVTQGKLQLVDLAGS
ERQSKTGAQGERLKEAAKINLSLSTLGNVISSLDGKSTHPIYRNSKLT
RLQDSLGGNSKTMIANVGPATYNYDETLLSTLYANRAKNIQNVAKI
NEDPKDAQLRKFQLEIEALRKILDEENPGDDENQEEAWEAKMQEREV
EMEKKRKILEERVNSAVNDEETHRLVKEMMENEAELEKARSEHEKLR
KLEKIEKKLIVGGENLLEKVEEQAKLLEVNNKELEQSKFQEAHLRTQLE
ERTAVKVEIEERYSSLQEEAFVKS KIKKVSNELKDARAELKDLEEDH
QRQVEAMLDDIRQLRKELLLN **IAIIDEYIPVEHVELIEKYVSWSEEHG**
WQLKAIAYTGNNMRASAPPAKKEFSNNNQTVPMYYSYRADLGASTAE
HRPRTSSKKHRASIRLQQLLT

Catalytic head

stalk

random coil tail

Lists

KAP

MNQVSI DAHP SDQAIIVRFEQ SPTNVE SLGHQKIIHLKE MSLD VDIRAL
SNVILQKCLFIPATSR SQLEQVLFYIQKRG NQRISARSRSSSAVSFDRR
PIHSPTISAELGKIDEYIECFYGETSVEKNKGAVALYELSKNPQNLTQL
VNNETLMMALARVFREDWKKHFEVGTNIMNLFVNISKFSCLHGILLHH
KIGTLCVNAMEHETKRYDFWIAEMKKT DQETLRK LKTAIRKQAMLLAA
CVTFLT NLATDISVELKMVRRNLVALLVKCLQMSSESTSSLT TATIKFL
LKLSIFDENKIVMEQNGTIEKLLKLFPIQDPELRKAVIMLLFNFSFDSKN
LPKMVNGGLVPHMASLLDSDTKALNMMYLLSCNDDAKAMLAYTDAIKL
LMKDVLSGTGSEVTKAVLLNICLEKRNAQLVCGQRGQGLDLLMEMSIN
SRDLMLIKVVRAISSHEGATQNMFLKWIETLIGIAKNEGADNSEKSSF
GLECMGTVAELKVAPWAKIIQSENLPWMMKTQLQEGIDEESEVTVLRD
IKPLQLQIVACGTMARQLDAARLLAPLIDTFVQLLQSCQIDDEFVVQLL
YVFLQFLKHKELSARLMTQDSALGAHMIDLMHDANAVVREVC DNALLI
MGEHSKEWAKRIAGERFKWHNAQWLEMVERDDSEFVDYDDED FGD
LKFDHYDDGFD MNEPLF

Armadillo motif

GCN4:

RMKQLEDKVEELLSKNYHLENEVARLKKLVGE

List of figures

Figure 1: Intraflagellar transport (IFT) in <i>C. elegans</i>	6
Figure 2: Structural organization of kinesins.....	7
Figure 3: Diversity in the kinesin superfamily.....	8
Figure 4: Processive kinesins move head-over-head.....	10
Figure 5: Tail domain regulates the catalytic activity in some kinesin families.....	11
Figure 6: Kinesin-2 architecture.....	14
Figure 7: Plasmid map of pFastBac1.....	18
Figure 8: Bacmid generation in MAX Efficiency® DH10Bac™ <i>E. coli</i> cells.....	21
Figure 9: Enzymatic coupling during the ATPase assay.....	28
Figure 10: Donor-acceptor pairs and FRET efficiency.....	31
Figure 11: Far UV CD spectra of protein secondary structures.....	33
Figure 12: Influence of the tail domain and the helix breaker on the catalytic activity of kinesin-2.....	37
Figure 13: Both kinesin-2 tails bind to microtubules.....	38
Figure 14: Kinesin-2 motor heads must be in dimeric state to be inhibited.....	39
Figure 15: KLP20 tail stably binds to KLP11 head.....	42
Figure 16: Coiled-coil predictions for KLP11 and KLP20.....	44
Figure 17: The C-terminal half of the stalk is necessary and sufficient for motor dimerization.....	45
Figure 18: Size exclusion chromatography of KLP11/20-C reveals its heterodimeric state.....	47
Figure 19: The C-terminal end of the stalk is essential for KLP11/20 dimerization.....	49
Figure 20: Random coil tails do not dimerize.....	50

Lists

Figure 21: Asymmetric co-expressions of kinesin-2 variants.....	51
Figure 22: KAP binds to the C-terminal half of KLP11.....	53
Figure 23: KAP binds to the random coil tail of KLP11.....	53
Figure 24: Small conserved region in the random coil of KLP11 and the Armadillo-motif in KAP are sufficient for interaction.....	54
Figure 25: Transmission electron microscopy indicates a long stalk and motor heads in close proximity.....	55
Figure 26: Co-expression of the FRET constructs.....	56
Figure 27: FRET analysis confirms the close proximity of the motor heads in wild type kinesin-2.....	58
Figure 28: Constructs for CD analysis.....	59
Figure 29: CD spectroscopy indicates an increasing coiled-coil fraction with growing chain length under native conditions.....	61
Figure 30: KLP11 and KLP20 prefer hetero- to homodimer formation under native conditions.....	62
Figure 31: Temperature dependent CD measurements of monomeric and dimeric KLP11/20-C and FL-KLP11/20.....	64
Figure 32: Identification of the dimerization seed by systematic N- and C-terminal elongations of truncated KLP11 and KLP20 polypeptide chains.....	71

Acknowledgements

Last but not least, I want to express my deepest gratefulness to people who have supported me during the past years and who made this thesis possible.

I thank Prof. Manfred Schliwa for giving me the opportunity to work in the great environment of the Institute for Cell Biology and for the always open door and, more importantly, ears, also for non-scientific issues. Many, many thanks to Dr. Zeynep Ökten for her mentoring and supervision, great discussions and lots of constructive input. To both, Prof. Schliwa and Dr. Ökten, I deeply thank for giving me the freedom and autonomy, as well as for their unconditional understanding during a tough period I had to cope with.

Dennis Zimmermann, Süleyman Kösem, Katharina von Roman and Angela Oberhofer turned our tiny “Doktorandenzimmer” into an entire universe of joy, tears, brain storming sessions and gossip and herewith to a place hard to leave and impossible to forget.

The good fairy of our group, Renate Dombi, I thank for her expert help with the cloning of the numerous constructs and accurate checking the sequenced DNA, and not to forget for making every, and I mean EVERY, PCR work. I am also indebted to Thi-Hieu Ho for her help in virus generation, test-expression of the truncated proteins and for being the mistress of the cell culture. Without Renate and Hieu this thesis would have taken a bit longer to be completed.

Prof. Michael Schleicher and his group I thank not only for providing the fluorimeter, but also for all the input and the great working atmosphere at the institute. My special thanks to Julia and Christoph Gallinger, whose friendship and support started even before they joined the group of Prof. Michael Schleicher.

I am also grateful to have experienced long-term joys of mentoring with Andrea Hohenauer, Knut Thiele and Ricarda Tiemeyer.

Ralf Biegil and Manfred Steiner are the secret heroes of the institute because, although not their responsibility, they, not only once, saved data from computers, which just decided to cease their duty.

Dr. Felix Müller-Planitz made the ATPase assays much easier by providing the ELISA reader and also helped out with the Äkta Purifier. Furthermore, he was always willing to be pierced with questions, to criticize and give input.

Acknowledgements

Dr. Stephane Roche and Prof. Dirk Niessing I thank for their co-work in trying to crystalize parts of kinesin-2.

I am further indebted to Prof. Hendrik Dietz for taking time despite a full schedule for hands-on support in making the amazing kinesin-2 TEM micrographs and to brainstorm the evaluation of the same.

Many thanks to Prof. Mathias Rief for financing the last six months of this thesis and the entire biophysical department E22 at the physics faculty of the TUM, especially Dr. Günther Woehlke for scientific discussions and Dr. Morten Bertz for introducing me to JASCO 815 spectrometer, my best friend for months.

The Elite Network of Bavaria I thank for giving me the chance to be a part of the pilot graduate program “Protein Dynamics in Health and Disease”, for financial support and for electing me as student attendee of the 61st Nobel laureates meeting in Lindau. I thank my fellow post-graduate members of the graduate program “Protein Dynamics in Health and Disease” for a great time during organizing and attending all our activities.

In the end, I thank my husband, Dejan, and my family for the unconditional support, patience and tolerance.

Curriculum vitae

Personal details

Name Marija Vukajlovic

Date of birth 1982, May 7th in Kragujevac, Serbia

University training

March 2009 - April 2012

Post-graduate studies at the Institute for Anatomy and Cell Biology, Ludwig-Maximilians-Universität München in the laboratory of Prof. Dr. Manfred Schliwa

Oct. 1999 - Feb. 2006

Studies in Biology at the Ludwig-Maximilians-Universität München with topics Zoology/Cell Biology, Genetics, Immunology and Anthropology and Human Genetics
Degree: Dipl. biol.

School training

Sept. 2000 - June 2003

Asam-Gymnasium, Munich
Degree: Abitur

Sept. 1997 - July 2000

Carl-von-Linde Realschule, Munich

Sept. 1996 - July 1997

Hauptschule Blumenau, Munich

Sept. 1989 – June 1996

Elementary school „Stanislav Sremcevic“, Kragujevac Serbien

Fellowships

Jan. 2010 – Sept. 2012

Active member of the graduate school “Protein Dynamics In Health And Disease“ in the “Elite Network of Bavaria” (ENB)

June 2011

Elected student attendee of the 61st Nobel laureates meeting in Lindau

Publications

Vukajlovic M., Dietz H., Schliwa M., Okten Z. How kinesin-2 forms a stalk, *Mol. Biol. Cell.* vol 22 (2011), p4279